Evaluation of the Need for Longitudinal Median Joints in Bridge Decks on Dual Structures

BRIDGE ENGINEERING CENTER

September 2015

IOWA STATE UNIVERSITY
Institute for Transportation

Sponsored by
Iowa Highway Research Board
(IHRB Project TR-661)
Iowa Department of Transportation
(InTrans Project 13-470)

About the BEC

The mission of the Bridge Engineering Center is to conduct research on bridge technologies to help bridge designers/owners design, build, and maintain long-lasting bridges.

Disclaimer Notice

The contents of this report reflect the views of the authors, who are responsible for the facts and the accuracy of the information presented herein. The opinions, findings and conclusions expressed in this publication are those of the authors and not necessarily those of the sponsors.

The sponsors assume no liability for the contents or use of the information contained in this document. This report does not constitute a standard, specification, or regulation.

The sponsors do not endorse products or manufacturers. Trademarks or manufacturers' names appear in this report only because they are considered essential to the objective of the document.

Non-Discrimination Statement

Iowa State University does not discriminate on the basis of race, color, age, religion, national origin, pregnancy, sexual orientation, gender identity, genetic information, sex, marital status, disability, or status as a U.S. veteran. Inquiries regarding non-discrimination policies may be directed to Office of Equal Opportunity, Title IX/ADA Coordinator and Affirmative Action Officer, 3350 Beardshear Hall, Ames, Iowa 50011, 515-294-7612, eooffice@iastate.edu.

Iowa Department of Transportation Statements

Federal and state laws prohibit employment and/or public accommodation discrimination on the basis of age, color, creed, disability, gender identity, national origin, pregnancy, race, religion, sex, sexual orientation or veteran's status. If you believe you have been discriminated against, please contact the Iowa Civil Rights Commission at 800-457-4416 or the Iowa Department of Transportation affirmative action officer. If you need accommodations because of a disability to access the Iowa Department of Transportation's services, contact the agency's affirmative action officer at 800-262-0003.

The preparation of this report was financed in part through funds provided by the Iowa Department of Transportation through its "Second Revised Agreement for the Management of Research Conducted by Iowa State University for the Iowa Department of Transportation" and its amendments.

The opinions, findings, and conclusions expressed in this publication are those of the authors and not necessarily those of the Iowa Department of Transportation.

Technical Report Documentation Page

1. Report No.	2. Government Accession No.	3. Recipient's Catalog No.
IHRB Project TR-661		

4. Title	5. Report Date
Evaluation of the Need for Longitudinal Median Joints in Bridge Decks on Dual Structures	September 2015
	6. Performing Organization Code

7. Author(s)	8. Performing Organization Report No.
Brent M. Phares, Lowell Greimann, and Zhengyu Liu	InTrans Project 13-470

9. Performing Organization Name and Address	10. Work Unit No. (TRAIS)
Bridge Engineering Center Iowa State University 2711 South Loop Drive, Suite 4700 Ames, IA 50010-8664	**11. Contract or Grant No.**

12. Sponsoring Organization Name and Address	13. Type of Report and Period Covered
Iowa Highway Research Board Iowa Department of Transportation 800 Lincoln Way Ames, Iowa 50010	Final Report
	14. Sponsoring Agency Code IHRB Project TR-661

15. Supplementary Notes

Visit www.intrans.iastate.edu for color pdfs of this and other research reports.

16. Abstract

The primary objective of this project was to determine the effect of bridge width on deck cracking in bridges. Other parameters, such as bridge skew, girder spacing and type, abutment type, pier type, and number of bridge spans, were also studied. To achieve the above objectives, one bridge was selected for live-load and long-term testing. The data obtained from both field tests were used to calibrate a three-dimensional (3D) finite element model (FEM). Three different types of loading—live loading, thermal loading, and shrinkage loading—were applied. The predicted crack pattern from the FEM was compared to the crack pattern from bridge inspection results. A parametric study was conducted using the calibrated FEM.

The general conclusions/recommendations are as follows:

- Longitudinal and diagonal cracking in the deck near the abutment on an integral abutment bridge is due to the temperature differences between the abutment and the deck. Although not likely to induce cracking, shrinkage of the deck concrete may further exacerbate cracks developed from thermal effects.
- Based upon a limited review of bridges in the Iowa DOT inventory, it appears that, regardless of bridge width, longitudinal and diagonal cracks are prevalent in integral abutment bridges but not in bridges with stub abutments.
- The parametric study results show that bridge width and skew have minimal effect on the strain in the deck bridge resulting from restrained thermal expansion.
- Pier type, girder type, girder spacing, and number of spans also appear to have no influence on the level of restrained thermal expansion strain in the deck near the abutment.

17. Key Words	18. Distribution Statement
continuous deck—deck cracks—diagonal cracks—field testing—finite element model—integral abutment—longitudinal cracks—thermal loading	**No restrictions.**

19. Security Classification (of this report)	20. Security Classification (of this page)	21. No. of Pages	22. Price
Unclassified.	Unclassified.	97	NA

Form DOT F 1700.7 (8-72) **Reproduction of completed page authorized**

EVALUATION OF THE NEED FOR LONGITUDINAL MEDIAN JOINTS IN BRIDGE DECKS ON DUAL STRUCTURES

Final Report
September 2015

Principal Investigator
Brent M. Phares, Director
Bridge Engineering Center, Iowa State University

Research Assistant
Zhengyu Liu

Authors
Brent M. Phares, Lowell Greimann, and Zhengyu Liu

Sponsored by
Iowa Highway Research Board
and Iowa Department of Transportation
(IHRB Project TR-661)

Preparation of this report was financed in part
through funds provided by the Iowa Department of Transportation
through its Research Management Agreement
with the Institute for Transportation
(InTrans Project 13-470)

A report from
Bridge Engineering Center
Iowa State University
2711 South Loop Drive, Suite 4700
Ames, IA 50010-8664
Phone: 515-294-8103 / Fax: 515-294-0467
www.instrans.iastate.edu

TABLE OF CONTENTS

LIST OF FIGURES

LIST OF TABLES

ACKNOWLEDGMENTS

The research team would like to acknowledge the Iowa Highway Research Board and the Iowa Department of Transportation (DOT) for sponsoring this research. In addition, the authors would like to acknowledge the support of the Iowa DOT Office of Bridges and Structures staff, who continually provide great insight, guidance, and motivation for practical and implementable research like this.

EXECUTIVE SUMMARY

The primary objective of this project was to determine the effect of bridge width on deck cracking in bridges. Other parameters, such as bridge skew, girder spacing and type, abutment type, pier type, and number of bridge spans, were also studied. To achieve the above objectives, one bridge was selected for live-load and long-term testing. The data obtained from both field tests were used to calibrate a three-dimensional (3D) finite element model (FEM). Three different types of loading—live loading, thermal loading, and shrinkage loading—were applied. The predicted crack pattern from the FEM was compared to the crack pattern from bridge inspection results. A parametric study was conducted using the calibrated FEM.

The general conclusions/recommendations are as follows:

- Longitudinal and diagonal cracking in the deck near the abutment on an integral abutment bridge is due to the temperature differences between the abutment and the deck. Although not likely to induce cracking, shrinkage of the deck concrete may further exacerbate cracks developed from thermal effects.

- Based upon a limited review of bridges in the Iowa DOT inventory, it appears that, regardless of bridge width, longitudinal and diagonal cracks are prevalent in integral abutment bridges but not in bridges with stub abutments.

- The parametric study results show that bridge width and skew have minimal effect on the strain in the deck bridge resulting from restrained thermal expansion.

- Pier type, girder type, girder spacing, and number of spans also appear to have no influence on the level of restrained thermal expansion strain in the deck near the abutment.

CHAPTER 1. INTRODUCTION

1.1 Background

Nationally, longitudinal joints are commonly used in dual structure bridge decks for the sake of ease of construction, staged construction, construction of wide bridges, etc. Among other reasons, the Iowa Department of Transportation (DOT) requires the use of longitudinal joints to reduce/eliminate deck cracking in wide bridges. This deck cracking can be induced by transverse contractions due to temperature change, shrinkage, and/or live loads. Longitudinal deck joints are thought to provide a relief point and to reduce the overall amount of shrinkage that must be accommodated. Unfortunately, these longitudinal joints have been known to begin leaking and allow chloride-contaminated water to reach the bottom of the deck overhang and the adjacent girders. This can be problematic when the joint is narrow and located between median barrier rails where chloride-contaminated snow and debris can be trapped for a long period. On weathering steel bridges, the constant exposure to moisture combined with limited air circulation prevents the natural formation of the protective patina. Thus, minimization or elimination of longitudinal joints may significantly lessen the aforementioned problems. A preliminary search of bridge design manuals from several state DOTs indicates that state DOTs are not in agreement with regard to the maximum width of the continuous deck, which ranges from 60 to 120 ft.

1.2 Objective and Scope

The main objective of this research is to determine the maximum width of a continuous deck that can be used without negatively impacting performance. To achieve this objective, analytical techniques including finite element analysis (FEA) were used to investigate the behavior of decks with various widths under typical loadings. Experimental field testing was also conducted principally to provide validation of the analytical models.

One bridge was selected based upon bridge inspection results to conduct live-load and long-term testing. The data obtained from the field tests were used to calibrate a three-dimensional (3D) finite element model (FEM). Three different types of loading—live loading, thermal loading and shrinkage loading—were applied. The crack pattern from the FEM was compared to the crack pattern observed from bridge inspection results to identify the primary crack-inducing loading. The validated model was then extrapolated to various other configurations to study the influence of those parameters.

1.3 Final Products

Based on the outcome of analytical and experimental investigations, the influence of various parameters, which include bridge width, bridge skew, abutment type, pier type, girder type, girder spacing, and number of spans, was studied. In addition to a summary of the results (including identification of structurally significant parameters), this report also includes recommendations for methods to potentially reduce the deck cracking due to thermal loads.

CHAPTER 2. LITERATURE REVIEW/SURVEY

2.1 Literature Review

2.1.1 Integral Abutment Bridge Advantage

Integral abutment bridges have been gaining popularity since the first integral abutment bridge was built in the state of New York in the late 1970s. The most prominent advantage of the integral abutment bridge is the elimination of expansion joints. Expansion joints typically leak chloride-contaminated water that can reach and degrade the bottom of the deck and the girders. Damaged and leaking bridge deck joints are a problem that effectively shortens the service life of many bridges (Kunin and Alampalli 2000). Purvis (2003) summarized performance data for commonly used expansion joint systems and also introduced examples of selection criteria and design guidelines in his synthesis report. The author concluded that there should be a high priority for state DOTs to reduce or eliminate deck joints whenever possible, although joints are sometimes unavoidable (Purvis 2003)

Beyond reduced initial costs and long-term maintenance expenses and the elimination of costly expansion joints and bearings, Kunin and Alampalli (2000) summarized that the benefits offered by integral abutment bridges also includes decreased impact loads, improved riding quality, simplified construction procedures, reduced substructure cost, and increased structure continuity to resist seismic events and overloading (Kunin and Alampalli 2000).

2.1.2 Cracking of Integral Abutment Bridge

Cracking in continuous bridge decks has been a concern of bridge designers and owners for decades. Various contributing factors have been identified, but their relationships are not fully understood (MnDOT 2011). Research has been conducted to study the cracks in continuous decks of integral abutment bridges, but most studies focus on transverse cracks rather than longitudinal and diagonal cracks.

Burke (1999) summarized the issues associated with integral abutment bridges, including early-age cracking of concrete; erosion of roadway shoulders, embankments, and backfill adjacent to bridge abutments; casting connections between moving members; and construction errors. They found that diagonal deck cracks located at acute corners of integral-type bridges are occasionally reported, and some uniformly spaced straight cracks are located over and perpendicular to the concrete diaphragms (Burke 1999).

2.1.3 Reasons for Cracks in Bridge Decks

Russell and Gerken (1994) reported that, rather than dead and live loadings, the major loadings that induce transverse cracks on a jointless bridge are temperature, creep, and shrinkage loadings. Temperature loading includes daily temperature changes and seasonal temperature changes. Daily temperature changes can induce a temperature gradient through the depth of the bridge,

while seasonal temperature changes cause changes in total structure length between summer and winter. Shrinkage and creep of concrete girders and the deck introduces forces into the structures and can also produce even greater effects depending upon the temperature and humidity conditions (Russell and Gerken 1994).

Frosch et al. (2003) completed an investigation to determine the factors affecting transverse and longitudinal bridge deck cracking. During laboratory work, the contribution of stay-in-place steel formwork was studied. Further, the effects of reinforcement bar spacing and epoxy thickness on crack width and spacing were evaluated. They concluded that longitudinal deck cracking was caused by a combination of factors, including restrained shrinkage and a construction detail associated with the stay-in-place formwork for the deck (Frosch et al. 2003).

Strainge and Burgueno (2012) used experimentally calibrated nonlinear FEMs to predict cracks in jointless bridge decks with integral abutments and semi-integral abutments. A parametric study was conducted using the calibrated FEM to study the influential factors on bridge deck cracking. During the bridge inspection phase, they found that few longitudinal cracks were observed on steel girder bridges. These results confirmed that the more restraint present in the bridge system, the greater the build-up of the restrained tensile forces, and, as a result, more cracking will occur. The results of the study indicated that longitudinal cracking can be attributed to bridge geometry and is not due to restrained concrete shrinkage. They also concluded that changing the amount of reinforcement and reinforcement distribution has no significant effect on deck cracking. Using larger shear studs at a larger spacing was found to slightly improve performance(Strainge and Burgueno 2012).

Paul et al. (2005) built 2D and 3D models to investigate forces and stresses induced by thermal loading in the superstructure of pre-stressed concrete integral abutment bridges. A preliminary study was conducted to compare the response of a central Pennsylvania bridge with numerical 2D and 3D model results. The results from this parametric study showed that (1) the largest thermally-induced superstructure force and stress occurred near the abutment, (2) the bridge length and abutment height can influence thermally-induced superstructure force, (3) the number of spans can affect thermally-induced superstructure forces, and (4) thermally-induced superstructure forces are comparable to those caused by live load. The research results also indicated that calculated thermally-induced stresses at the bottom of the beam and top of the deck slab exceeded the tensile strength of the beam and slab concrete near the abutment, which suggests that cracks would occur in those regions (Paul et al. 2005).

Fu et al. (2007) used a calibrated FEM to study corner cracking in the concrete decks of skewed bridges. Twenty straight and twenty skewed bridges were inspected with a specific focus on corner cracking of the deck, and the results show no obvious causal relationship. Two skewed decks were selected for field testing, and the results were used to calibrate FEMs. The results from the parametric study using the calibrated FEMs indicated that the main cause of skewed deck corner cracking is thermal and shrinkage load (Fu et al. 2007).

2.2 Survey of State DOTs

To investigate the current state-of-the-practice related to the objectives of this project, a search of state DOT design manuals related to bridge width limitations was conducted. A survey of state DOTs related to deck cracking performance was also conducted. The results of these information searches are summarized in the following sections.

2.2.1 Bridge Width Limitation

The bridge design manuals from several state DOTs indicate that state DOTs are not in agreement with regard to the maximum width of continuous decks in integral abutment bridges, which range from 60 to 120 ft. The Nevada DOT (2008) requires the use of longitudinal joints for the decks of multiple-span bridges with large skews. The Illinois DOT (2012) has different guidelines for non-staged and staged construction, as shown in Table 1.

Table 1. Bridge width limitations by state DOTs

Transportation Agency		Deck Width	Skew and Span Configuration
D.C. DOT (2009)		> 88 ft	…
Montana DOT (2002)		> 88 ft	…
Nevada DOT(2008)		> 120 ft	Multiple-span bridges with large skews
Illinois DOT (2012)	Non-staged construction	> 120 ft (center-to-center distance of exterior girders)	…
	Staged construction	> 120 ft (Total width of the staged pours)	
MnDOT (2012)		> 100 ft	…
Iowa DOT (2012)		> 60 ft	…

2.2.2 Deck Cracking Performance

A survey of the mid-central state DOTs was conducted to collect information regarding bridge width limitations and deck cracking performance. The questions in the survey and the responses from the eight states are listed in Table 2.

Table 2. Summary of survey

DOT	Q1. What, if any, limitations does your state have on bridge width?	Q2. Has there ever been observed deck cracking that was attributed to total bridge width? If so, please describe.	Q3. Besides limiting bridge width, have you used other techniques to control the development of deck cracking?	Q4. Are there other bridge components whose design and/or behavior are influenced by total bridge width?
North Dakota	No	I do not think anyone is looking	The rate that the deck is placed Wet cure	No
South Dakota	No	None of any significance	None specifically to control longitudinal cracking	Substructure components, especially columns in frame bents
Minnesota	No	Not that can be attributed mainly to width of the bridge	Transverse fixity is provided for only the interior 2/3 of the bearings Deck sequences are required for decks wider than 90 ft High performance concrete, night pours, and fibers have been used	Substructures and bearings
Illinois	No. When the distance between fascia girders is greater than 90 ft, a 1 in. open joint is required	Deck cracking issues do exist but can't be attributed to width alone	Pouring sequences Fibers, HPC, Type K cement, etc. Lower the maximum ambient temperature for deck casting Limiting LL deflection to something more restrictive than L/800.	Substructures, bearings, joints
Wisconsin	No	Not sure if we've seen cracking directly attributable to deck width	7 day wet cure for normal deck concrete 14 day wet cure for high-performance concrete decks	Longer piers
Kansas	No	Not width. The different shrinkage rate between the pile-lower abutment beam and upper abutment beam-deck.	Add additional transverse reinforcement.	Deck drainage design
Michigan	No. Bridge width greater than 100 ft 0 in. requires a longitudinal open/expansion joint.	Our deck cracking problems have been attributed to the acute corners on bridges with an excessive skew	Nighttime casting of superstructure concrete	Not that I can think of…
Nebraska	No	No	Using minimum placing and finishing rate to prevent setting before continuous spans are placed	Substructures (pile bearings) and bearings

In summary, the following was found:

- No limitations on bridge width were reported, although some states (Illinois, Michigan) do require the use of open joints or construction joints when bridges exceed a certain width.
- No DOT thinks that deck cracking can be attributed to bridge width.
- DOTs are using varying approaches to control the cracks in the deck in the early stages.
- Some DOTs think that the behavior of substructure elements such as columns, bearings or piles may be influenced by bridge width.

CHAPTER 3. FIELD TESTING

3.1 Introduction

The purpose of the field testing conducted as part of this research was to provide data to be used during the calibration of an FEM, , which will be subsequently described. During field testing, two types of tests were conducted on a bridge near Waterloo, Iowa: short-term and long-term. In this chapter, the process followed to select the bridge for field testing is described. Additionally, the instrumentation plans for the short-term live-load test and the long-term test are described and illustrated.

3.2 Bridge Inspection

To select the most suitable bridge for field testing, several factors including safety, structure type, structure geometry, traffic condition, and crack condition were considered. In total, five bridges were selected by the Iowa DOT for initial consideration and inspection because these bridges had varied locations, ages, element types, bridge geometries, and deck conditions. The cracking conditions in the decks from these five bridges were generically compared in terms of the effect from factors such as abutment type and bearing type. The key results of these inspections are summarized in Table 3.

Based upon the bridge inspection results and further discussion with the project technical advisory committee (TAC), Bridge #605220 was selected for the following reasons: (1) the crack pattern on its deck is typical, and (2) the traffic conditions on and under the bridge are suitable for live-load testing and instrumentation work can be conducted without completely stopping traffic on the bridge or under the bridge.

Table 3. Results of bridge inspection for selection of field testing bridge

Bridge FHWA No.	Bridge Location	Type*	Deck Width (ft)	No. of spans	Abutment type	Bearing type	Cracks		Traffic	Year built
							Inspection Report	Our Inspection (Cracks near abutment)		
012411	Mills Civic Parkway Over I-35	PPCB	196	2	Integral	Fixed	Noted cracking problem	Diagonal cracks near the corners and longitudinal cracks in the center region along deck width. 1/3 of bridge on each side Length: 3-6 ft Spacing: 8-10 ft	Heavy Complex traffic paths Curved lanes	2001
605220	Iowa-21 over US 20	PPCB	81	4	Integral	Fixed	Longitudinal cracks (especially near the abutments)	Diagonal cracks near the corners and longitudinal cracks in the center region along deck width. 1/3 of bridge on each side Length: 3-15 ft Spacing: 2-3 ft	State highway Straight lanes	1983
604730	Blairsferry road over I-380	PPCB	84	4	Integral	Fixed	Longitudinal cracks (especially near the abutments) Hollow areas on the bottom of crack	Diagonal cracks near the corners and longitudinal cracks in the center region along deck width. 1/3 of bridge on each side Length: 3-15ft Spacing: 2-4 ft	Complex traffic paths Curved lanes Far away	1980
042740	I-235 over the Des Moines River	CWPG	75.9	10	Stub	Expansion	Noted longitudinal cracking problem	None Found	Heavy Interstate highway Straight lanes	1964
042891	I-235 over East 15th Street	CWPG	71	3	Integral	Fixed	A few scattered hairline transverse cracks	One or two (6-8 ft)	Heavy Interstate highway Straight lanes	2004

* PPCB: precast, pre-stressed concrete beam; CWPG: continuous welded plate girder

Figure 1 shows the general configuration of Bridge #605220, which is a four-span bridge with a small 1.5 degree skew.

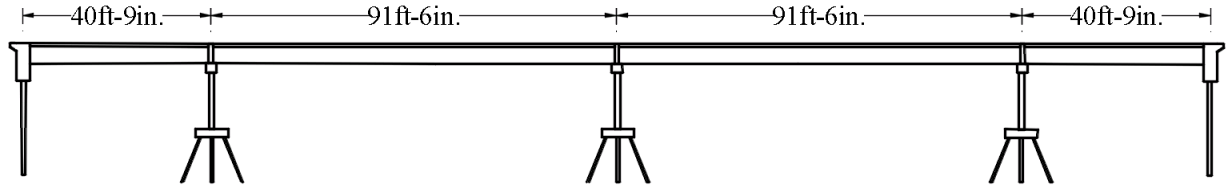

Figure 1. Side view of Bridge #605220

Figure 2 and Figure 3 show an overall cross-sectional view and the cross-section details in a typical bay.

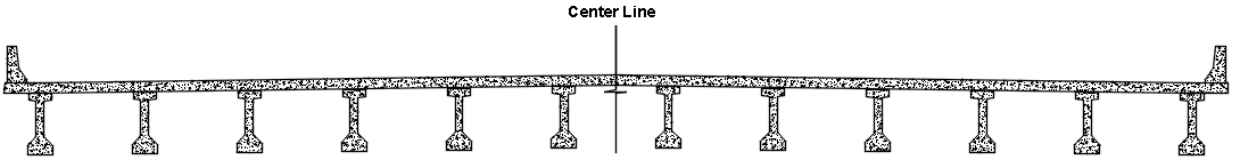

Figure 2. Cross-section view of Bridge #605220

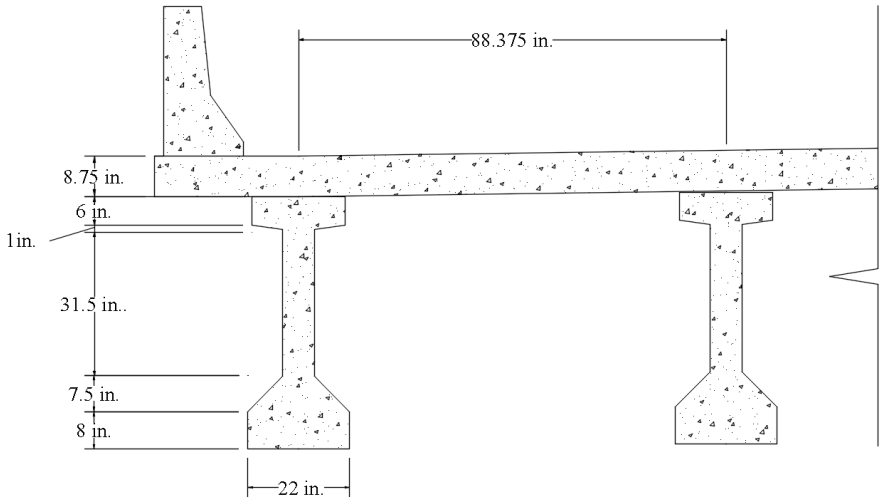

Figure 3. Cross-section details in a typical bay

The bridge consists of an integral abutment and 12 pre-stressed concrete girders. In general, the bridge is in very good condition. Figure 4 through Figure 6 illustrate the overall bridge geometry and crack conditions on the top of the deck.

Figure 4. Underside view of the bridge

Figure 5. Longitudinal cracks at the center of the south end

Figure 6. Diagonal cracks at the corner of the deck

With respect to degradation/damage that might be attributed to the width of the deck, the only observable evidence was cracking of the deck. The crack patterns on the top and bottom surface of the deck of Bridge #605220 are shown in Figure 7 and Figure 8, respectively.

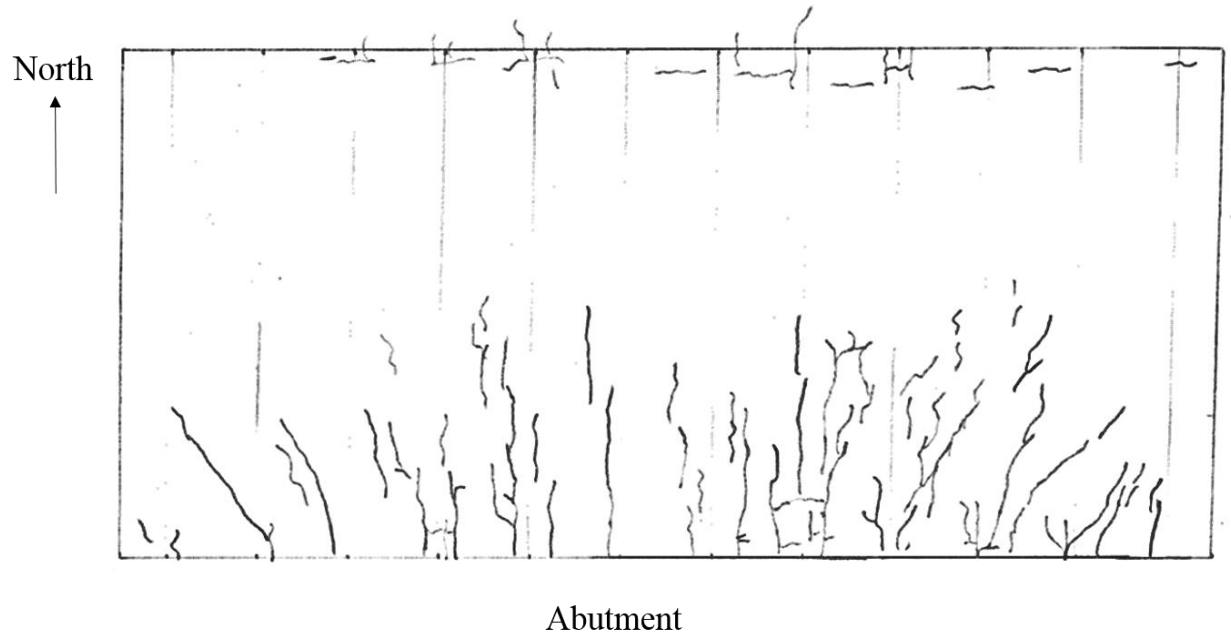

Figure 7. Crack map on the top of the deck on the top of the deck on the south end of Bridge #605220

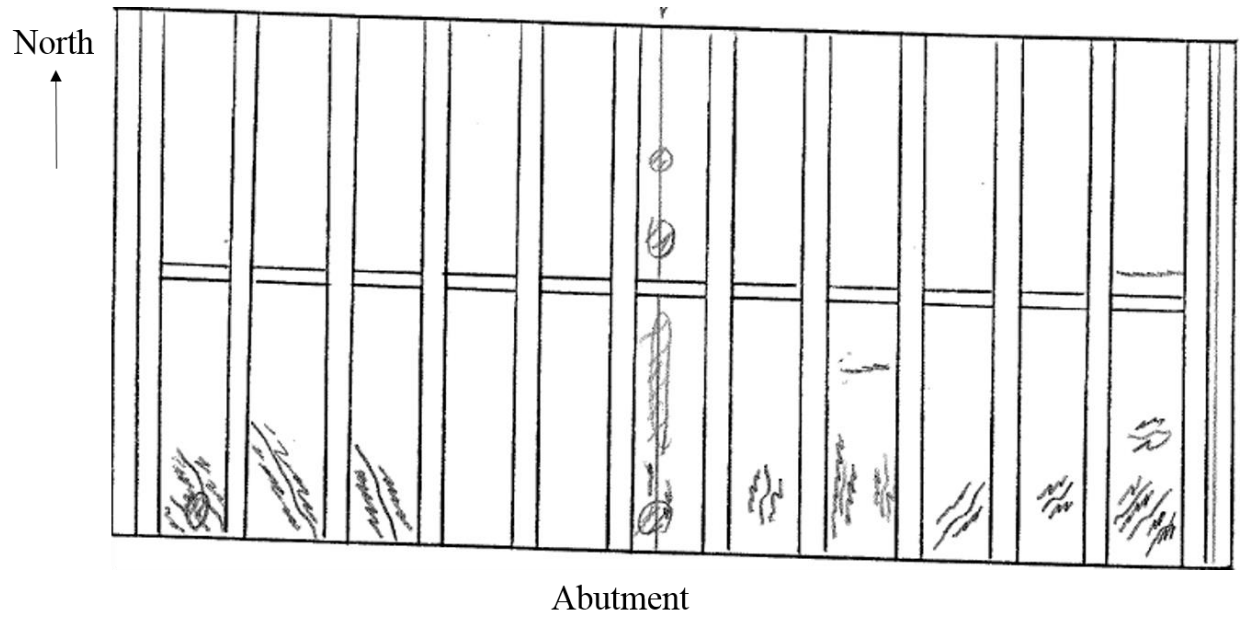

Figure 8. Crack map at the bottom of the deck on the south end of Bridge #605220

Of interest in these sketches is (1) the amount of cracking observed and (2) the orientation of the cracks. It was generally observed that cracks near the centerline of the bridge were less numerous than at the edges and that cracks near the centerline tended to be orientated longitudinally while those near the edges tended to be oriented at 45 degrees.

3.3 Live Load Testing Instrumentation Plan and Operation

3.3.1 Truck Information and Load Case Information

During live-load testing, a three-axle Iowa DOT snooper truck was driven across the bridge at a crawl speed to induce a pseudo-static load on the bridge. During passage of the truck, the bridge response was measured using a series of subsequently described strain transducers that had been strategically placed on the bridge. The gross vehicle weight of the truck was approximately 54,800 lb. The approximately weight supported by each wheel is illustrated in Figure 9.

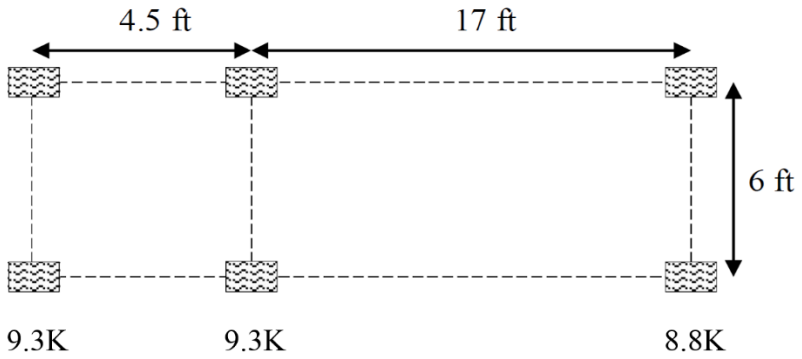

Figure 9. Snooper truck details

In total, five load cases (LCs) were utilized to obtain the needed strain data. The transverse location of the vehicle in each load case is shown in Figure 10. In each load case, the truck moved from south to north at approximately 3 mph.

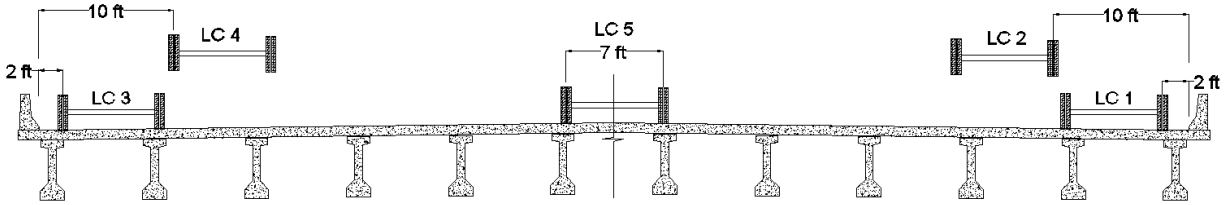

Figure 10. Transverse load position: vehicle traveling from south to north

3.3.2 Instrumentation Plan and Operation

During live-load testing, Bridge Diagnostic, Inc. (BDI) strain transducers were used to measure the load-induced strain at both the top and the bottom flanges of the girders. Three cross-sections were selected for instrumentation installation: near the abutment section (54 in. from the surface of the south abutment), the pier section (54 in. from the south side of the southernmost pier), and at mid-span of the second span from the south end of the bridge. The locations of these three instrumentation sections are shown in Figure 11.

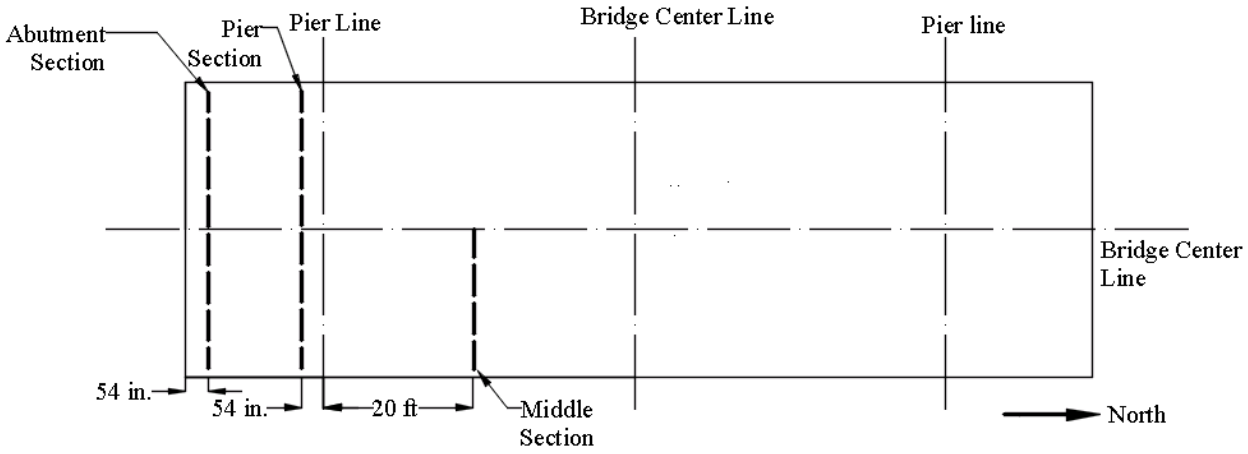

Figure 11. Locations of the three instrumentation sections

In total, 60 BDI transducers were installed and monitored as part of the live-load testing program. Twenty-four transducers were placed at each abutment and pier section, and twelve transducers were placed at the mid-span section. On each girder in each section, one transducer was attached on the side of the top flange, and a second transducer was attached at the bottom surface of the bottom flange. The strain gauge locations and associated gauge labels are shown in Figure 12.

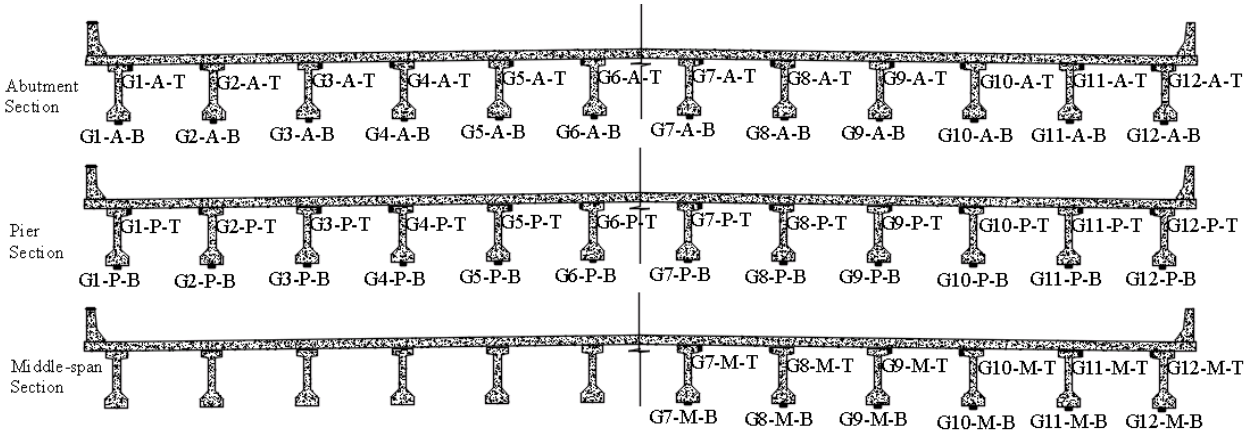

Figure 12. BDI transducer locations on cross-section

The gauge label, which consists of three parts, designates pertinent gauge location information in terms of girder number, cross-section section, and location on flange. For example, for gauge label “G1-A-T”, “G1” means the first girder on the west side of the bridge, “A” means the abutment section, and “T” means that the gauge is on the top flange of the girder.

After collecting the live-load test data, BDI WinGraf software was used to zero the data, convert the strain versus time data to strain versus truck position data, and plot the results.

3.4 Long-term Testing Instrumentation Plan and Operation

The objective of the long-term testing was to study the behavior of the bridge under temperature change and to provide strain, displacement, and temperature data for the calibration of the previously mentioned FEM. Since the bridge inspection results indicated that most cracks were observed on the deck near the abutment region, the long-term testing focused on studying the behavior of the bridge in that area.

3.4.1 Strain Data Measurement

During long-term testing, Geokon Model 4000 vibrating strain gauges were used to measure the load-induced strain on the bottom of the deck. For the strain gauge instrumentation, three sections—abutment section, middle-span section, and pier section—were selected to capture the needed strain data. The abutment section (Figure 13) is 54 in. from the surface of the south abutment.

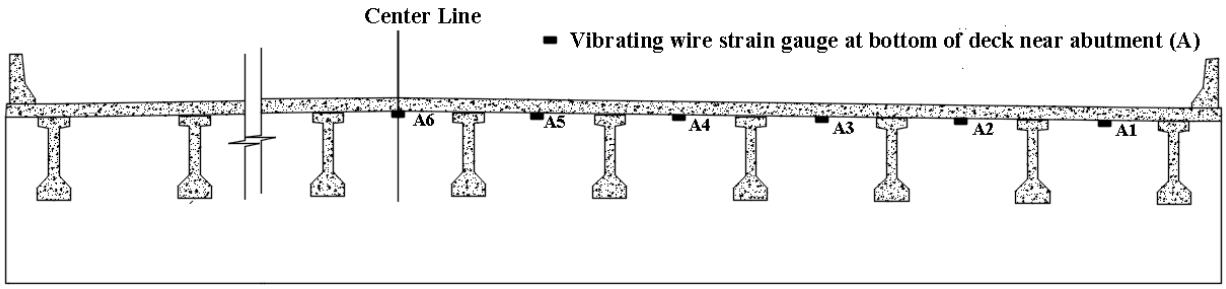

Figure 13. Instrumentation layout in abutment section for long-term testing

Six bays near the east side of the bridge were selected to install the strain gauges. In each bay the strain gauge was attached in the middle of the bay between the two girders. The middle-span section (Figure 14) is located in the middle of the first span on the south side of the bridge.

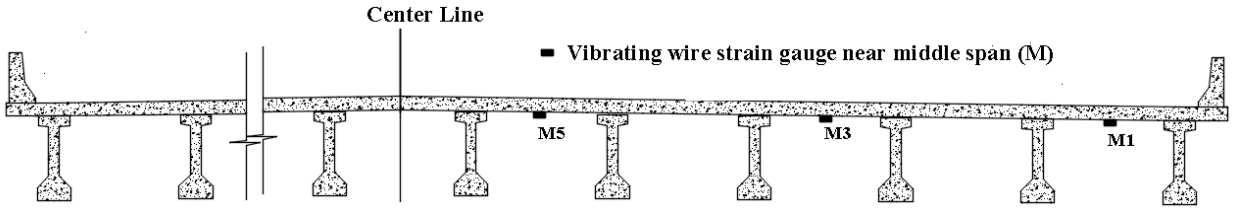

Figure 14. Instrumentation layout in middle-span section for long-term testing (first span)

The pier section (Figure 15) is 54 in. from the south side of the first pier in the south end of the bridge.

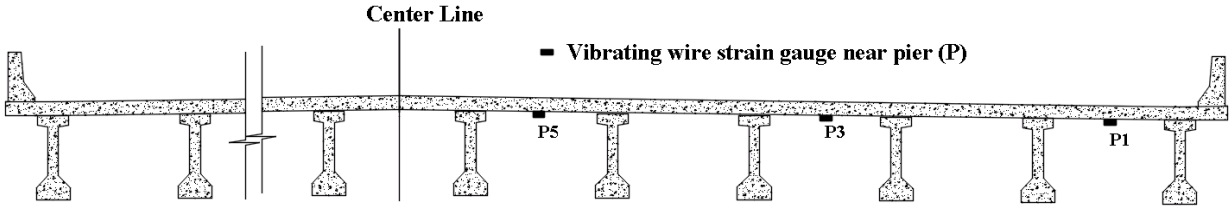

Figure 15. Instrumentation layout in pier section for long-term testing (first span)

In both the middle-span section and the pier section, the vibrating strain gauges were attached in the first bay, third bay, and fifth bay on the east side of the bridge.

Figure 16 shows a photograph of a vibrating strain gauge mounted to the bottom of the concrete deck prior to the installation of the protective cover.

Figure 16. Vibrating wire strain gauge at the bottom of the deck

3.4.2 Displacement Data Measurement

Four Geokon Model 4427 vibrating wire long-range displacement meters were used to measure relative displacement in the first span of the bridge due to the thermal effects in both longitudinal and transverse directions. The positions of these four displacement transducers are shown in Figure 17.

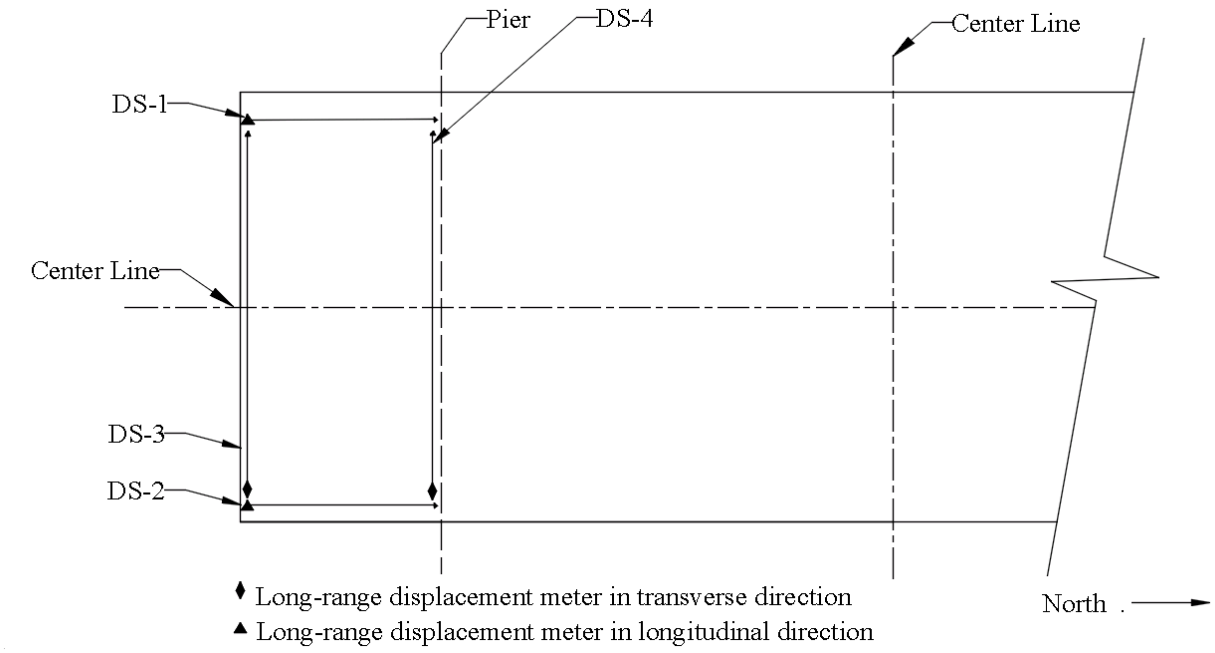

Figure 17. Instrumentation layout of long-range displacement meters (top view)

Two displacement meters were installed at the bottom of the deck in the two exterior bays near the first interior girder to measure the relative longitudinal displacement between the abutment and pier in the first span on the south side of the bridge. The other two displacement meters were used to measure relative displacement in the transverse direction. One of them was placed at the bottom of the girder near the surface of the abutment on the south side of the bridge. The other one was installed at the bottom of the girder near the surface of the pier in the first span on the south side. Figure 18 shows a vibrating wire long-range displacement meter attached to the bottom of the girder near the pier that measures the relative displacement in the transverse direction.

Figure 18. Vibrating wire long-range displacement meter

3.4.3 Temperature Data Measurement

For temperature measurement, two type of gauges were used during the long-term testing. Part of the temperature data were collected from the thermistor housed within each of the vibrating strain gauges (shown in Figure 13, Figure 14, and Figure 15). After installation of the vibrating strain gauge, a plastic cover (shown in Figure 19) was used to cover the vibrating strain gauge and create an isolated space so that the temperature data from the vibrating strain gauge very closely represents the temperature on the bottom surface of the deck.

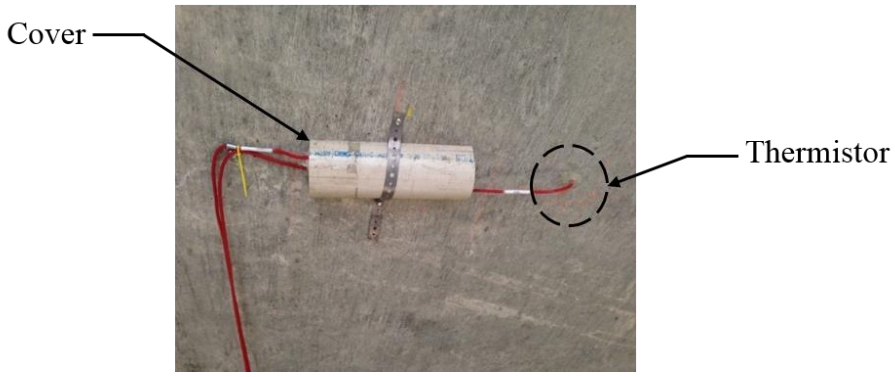

Figure 19. Relative positions of strain gauge and thermistor in one bay

In addition to the temperature at the bottom surface of the deck, the temperatures inside the deck and within the abutment were also measured using a Geokon 3800 thermistor placed at mid-depth of the deck and 3 in. below the surface of the abutment. The relative positions of the cover of the vibrating strain gauge and Geokon 3800 thermistors is shown in Figure 19. During long-term testing, five such thermistors were installed in the deck and 54 in. from the surface of the abutment (shown in Figure 20).

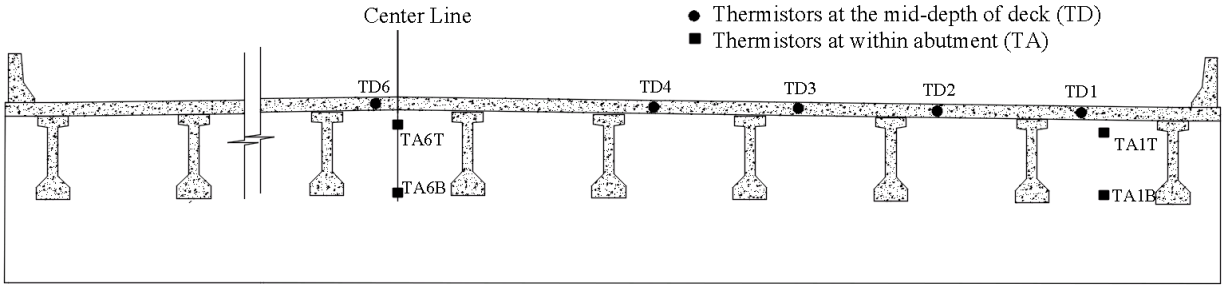

Figure 20. Thermistors in the middle depth of the deck and the abutment

Figure 21 shows a thermistor attached within the deck. The locations of the four thermistors installed in the abutment are shown in Figure 20.

Figure 21. Thermistor within deck

CHAPTER 4. FIELD TESTING RESULTS

4.1 Live-Load Testing Results

Because Bridge #605220 has a skew of only 1.5 degrees, and field testing demonstrated that the bridge effectively acted in a symmetric manner, only the results from LC1, LC2, and LC5 are presented in this section (see Section 3.3 for definitions of the LCs). Figure 22 shows how the girder strain varied with truck position when the truck was transversely positioned in LC1 (see Section 3.3 for the load case information and Figure 12 for the gauge locations).

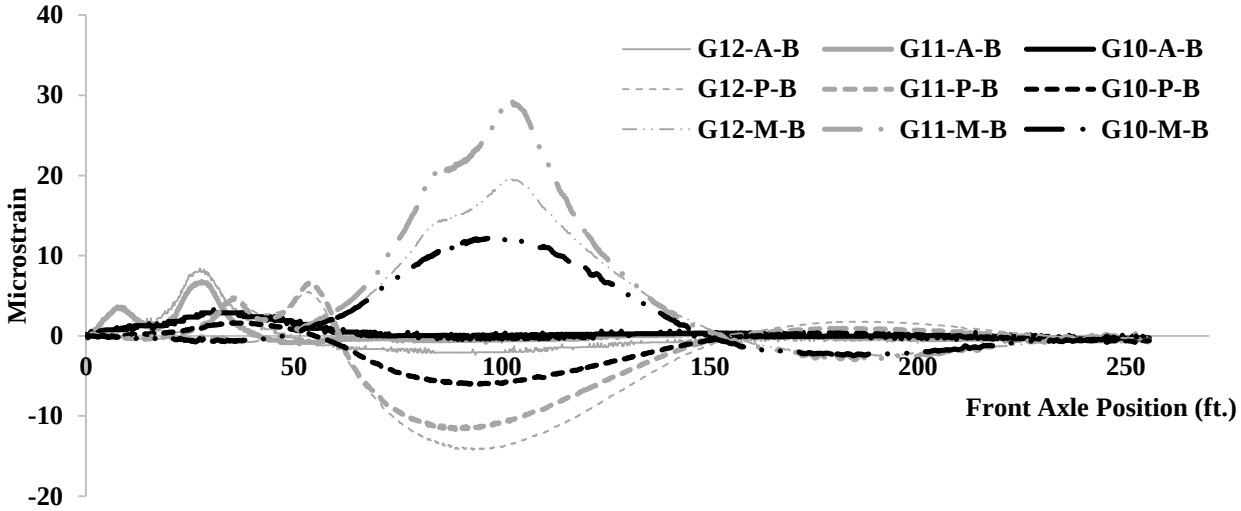

Figure 22. Strain vs. vehicle position from bottom gauges in LC1

The results from the first three girders on the east side of the bridge are presented, because only the gauges on those girders are close to the vehicle path and have significant readings (all other girders had minimal/negligible responses).

Figure 23 shows the live-load test results from LC2.

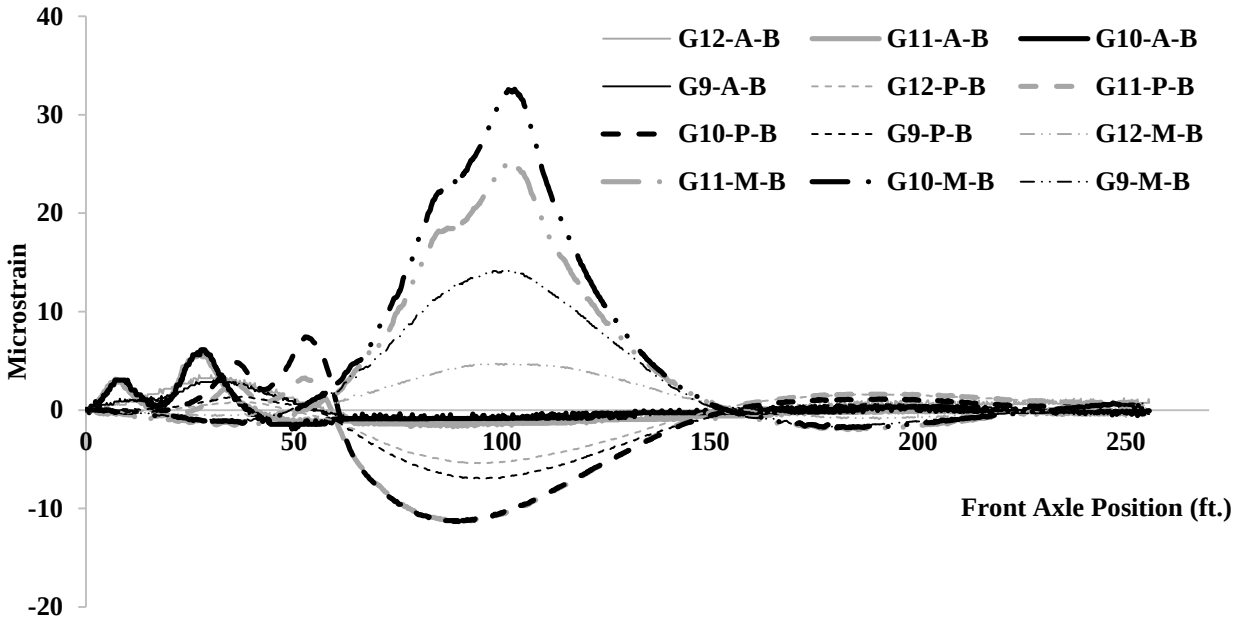

Figure 23. Strain vs. vehicle position from bottom gauges in LC2

Figure 24 shows the live-load test results from LC5. For both LC2 and LC5, only the strain values from the four girders that are close to the truck path are presented.

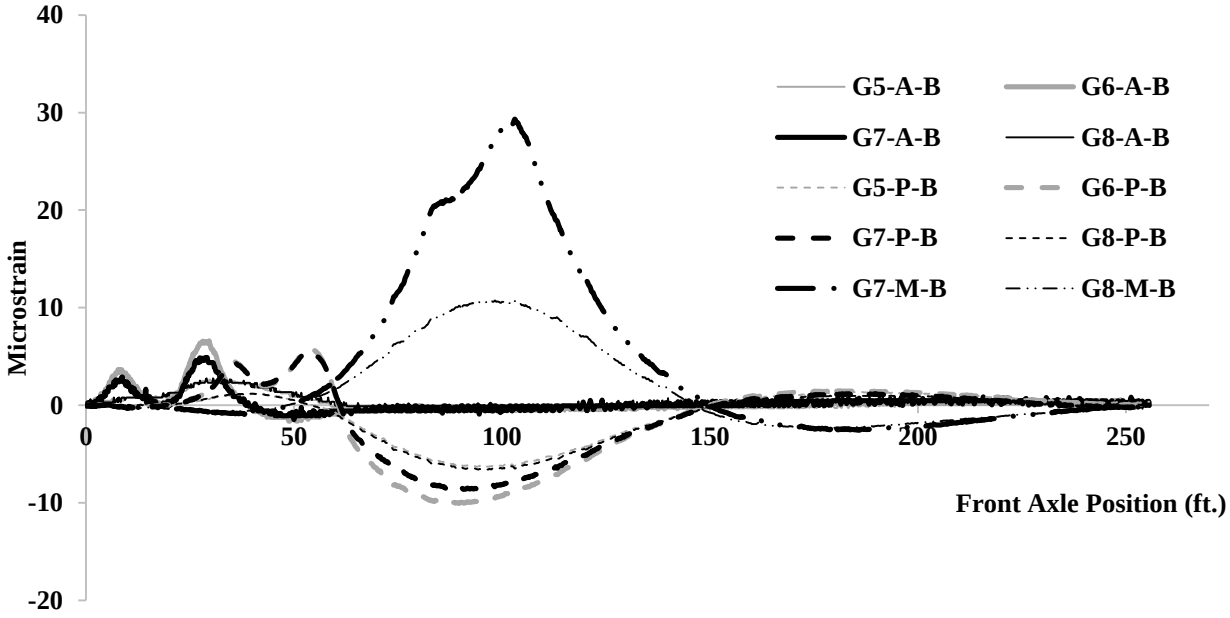

Figure 24. Strain vs. vehicle position from bottom gauges in LC5

Results are shown at three sections: abutment, pier, and middle sections (shown in Figure 12).

As shown in Figure 25, the strain values in the top flange gauges are very small, indicating that the cross-section neutral axis is very near the top flange. For future reference, during calibration of the FEM (Chapter 5), only the strain values from the bottom gauges in Figure 22 to Figure 24 were used, because only these gauges have significant readings (e.g., larger than 5 microstrain).

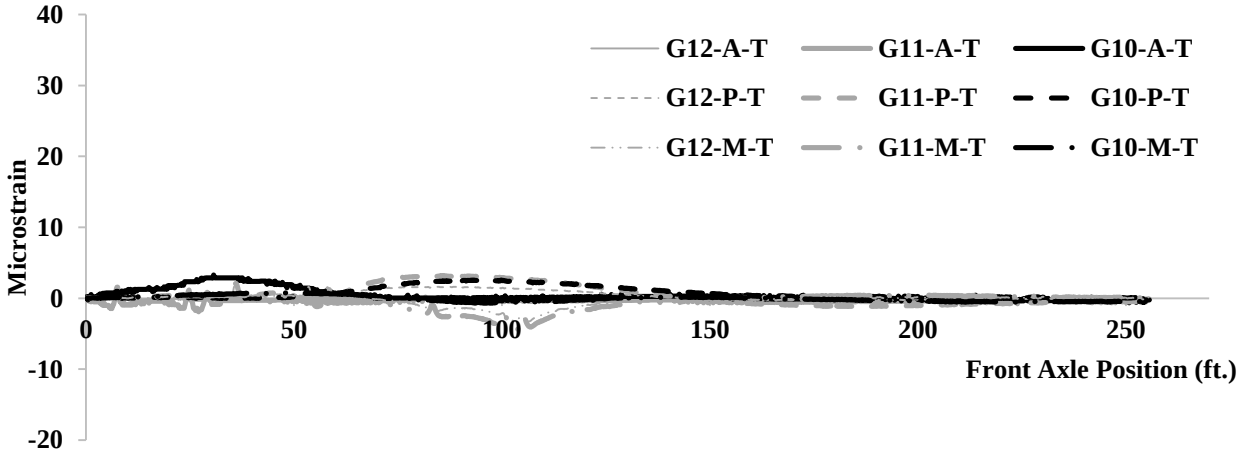

Figure 25. Strain vs. vehicle position from top gauges in LC1

4.2 Long-Term Testing Results

4.2.1 Temperature Data

In Figure 26 and Figure 27, the average temperature at the mid-span and pier section versus the average temperature at the abutment section are plotted, respectively.

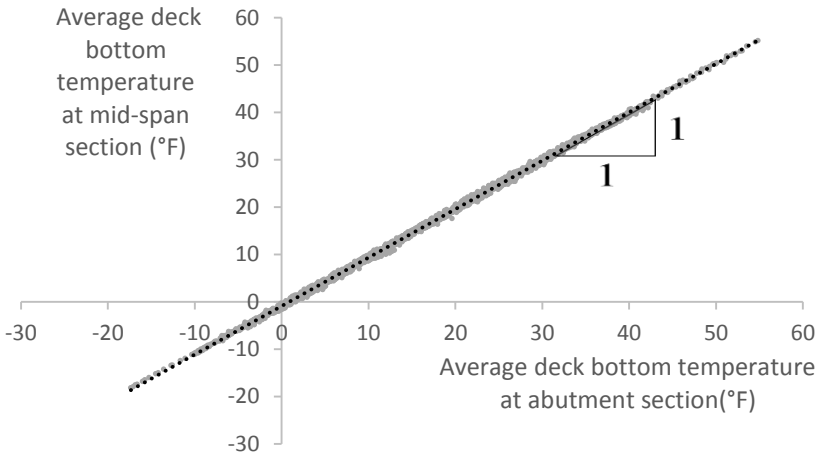

Figure 26. Average deck bottom temperature at mid-span section vs. average deck bottom temperature at abutment section

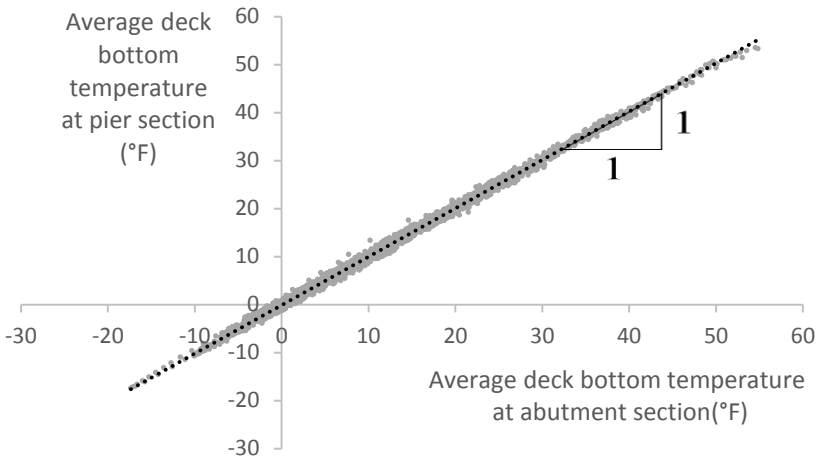

Figure 27. Average deck bottom temperature at pier section vs. average deck bottom temperature at abutment section

Figure 28 shows the relationship between the average temperature at the middle depth of the deck in the abutment section and the average temperature at the bottom of the deck in the abutment section.

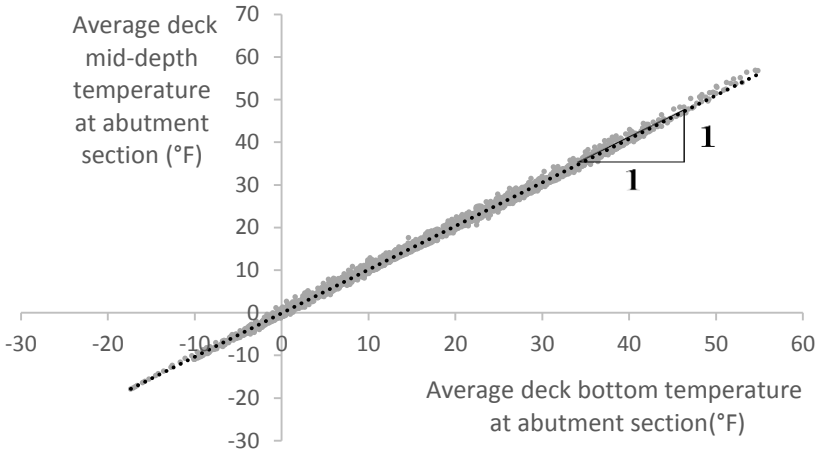

Figure 28. Average deck mid-depth temperature vs. average deck bottom temperature (abutment section)

Because the slopes in these figures are very close to one, it can be concluded that the temperature at the bottom of the deck can be regarded as uniform from the abutment section to the pier section and the temperature at the mid-depth of the deck can be assumed to be the same as at the bottom of the deck. The temperature at the bottom of the deck is very close to the temperature at the mid-depth of the deck at night, while during a sunny day the maximum temperature difference is just two degrees.

To study the relationship between temperature and strain and displacement, four one-day time periods were selected for more in-depth analysis. Figure 29 shows the temperature changes with time during these four time periods.

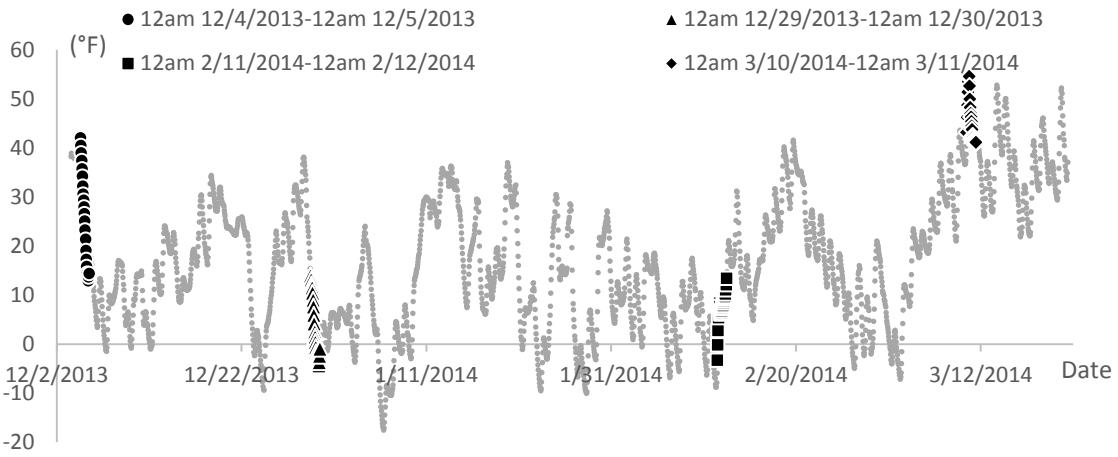

Figure 29. Average temperature at the bottom of the deck vs. time

Figure 30 shows the relationship between the temperatures in the abutment three inches below the bottom of the deck and the average temperature at the bottom of the deck.

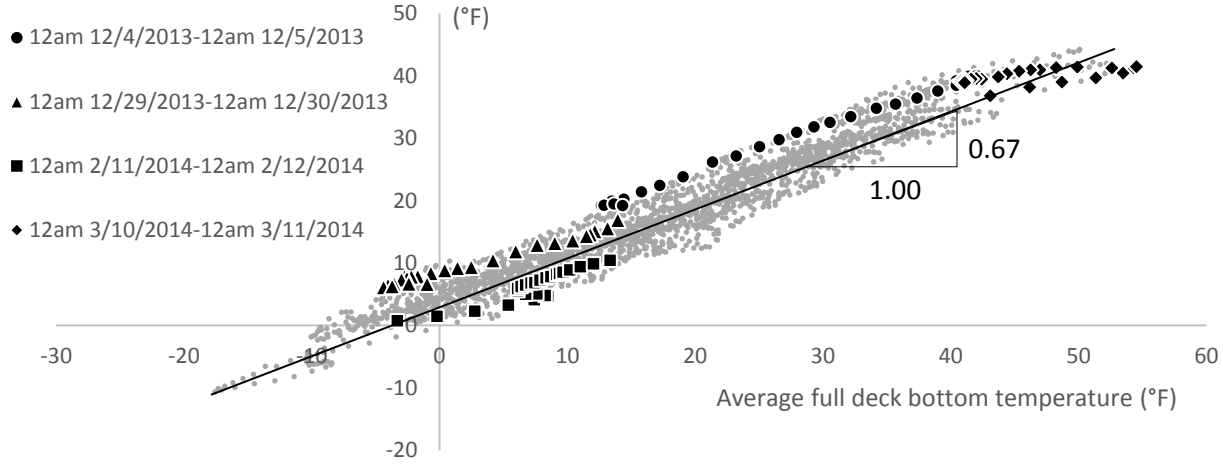

Figure 30. Average temperature in the abutment three inches below the deck (from TA1T and TA6T) vs. average temperature at the bottom of the deck

Figure 31 shows the relationship between the temperatures at the abutment 4 ft 3 in. below the bottom of the deck and the average temperature at the bottom of the deck.

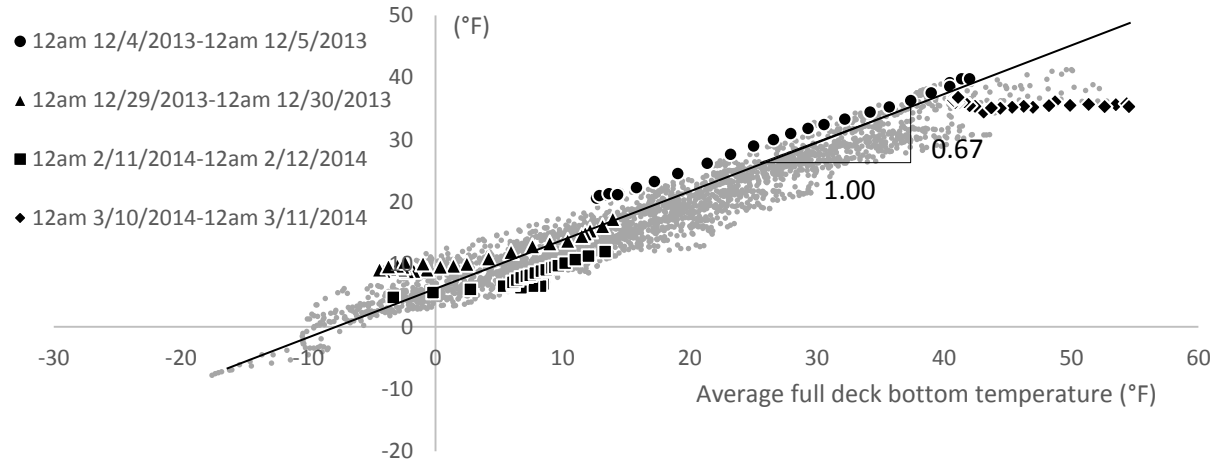

Figure 31. Average temperature in the abutment 4 ft 6 in. below the deck (from TA1B and TA6B) vs. average temperature at the bottom of the deck

In Figure 30 and Figure 31, the data are fitted by a line with a slope of 0.67, which indicates that the temperature change at the abutment is about 2/3 of the temperature change at the deck. In other words, when the temperature on the deck increases 30°F, the temperature on the abutment will increase around 20° F. As mentioned previously, this temperature relationship will be utilized during calibration of the FEM.

4.2.2 Strain Data

Figure 32 through Figure 43 show plots of strain versus average temperature at the bottom of the deck for all strain gauges installed on the bottom of the bridge deck. The temperature on the horizontal axes in the figures is the average temperature of all the strain gauges at the bottom of the deck.

From these strain versus temperature plots, it can be seen that, within most of the daily periods, a uniform slope between the strain changes and temperature changes is apparent. This slope can be used to calculate the strain value change for any temperature change. However, the strain corresponding to a certain temperature in a different time period is different.

For example, in Figure 32, when the average temperature at the bottom of the deck is zero, the corresponding strain in the second daily period is about 50 microstrain, while, in the third daily period, the strain is about -10 microstrain. One of the reasons for this difference could be the soil temperature changes at the back of the abutment during different seasons, because the temperature changes in soil will be smaller and slower than the air temperature change. The soil far below the ground maintains a relatively stable temperature during the whole year. The temperature change at the soil side of the abutment was not measured during long-term testing.

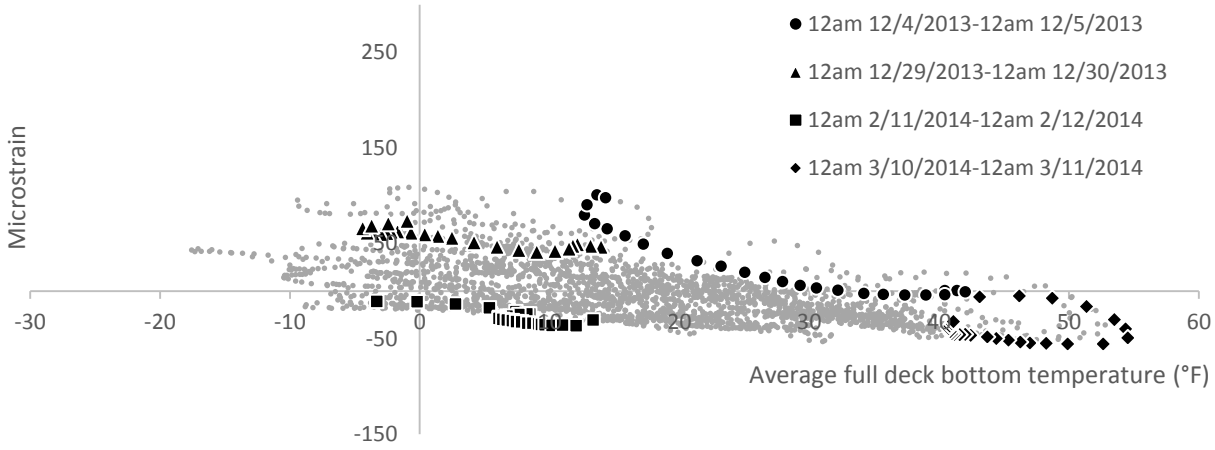

Figure 32. Strain from strain gauge A1 vs. average temperature at the bottom of the full deck

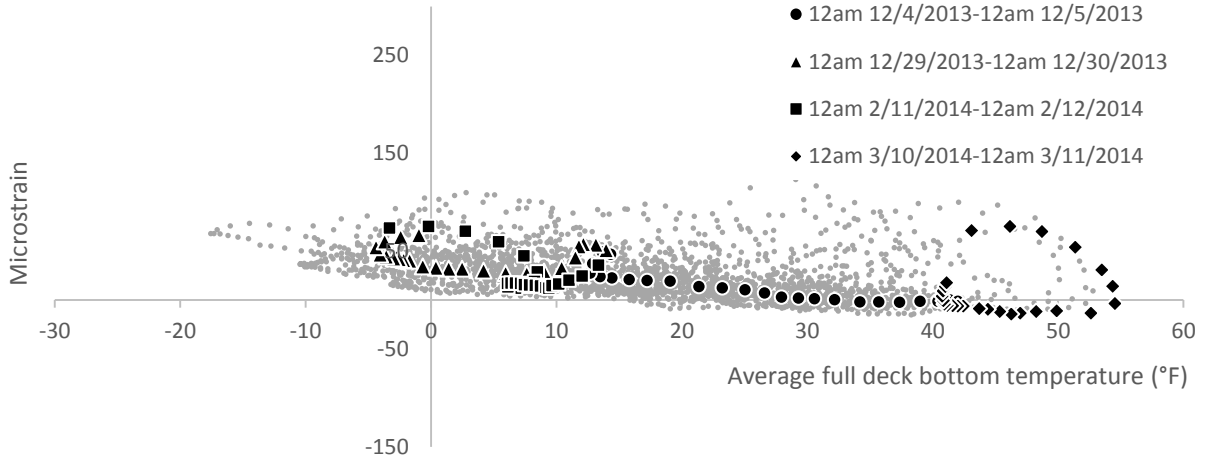

Figure 33. Strain from strain gauge A2 vs. average temperature at the bottom of the full deck

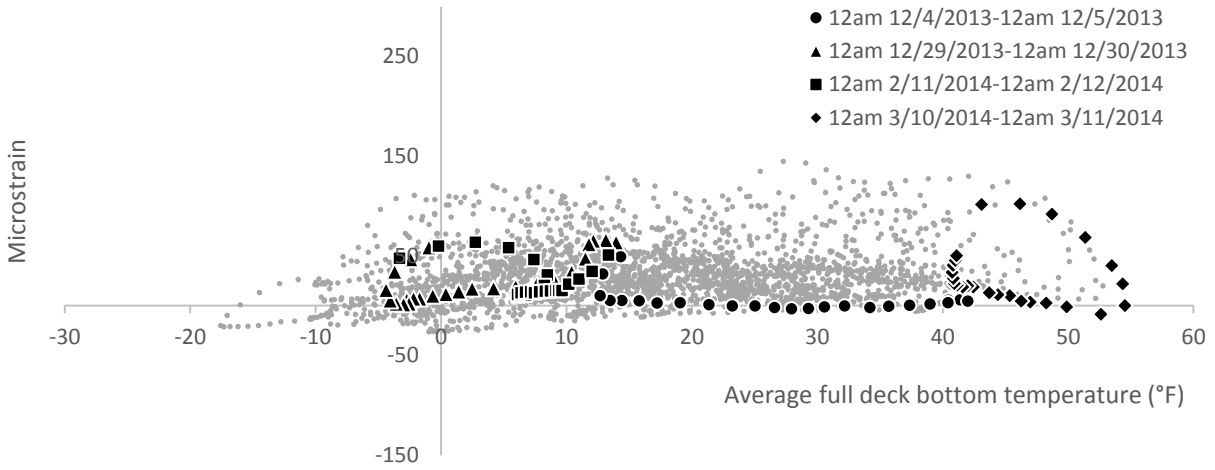

Figure 34. Strain from strain gauge A3 vs. average temperature at the bottom of the full deck

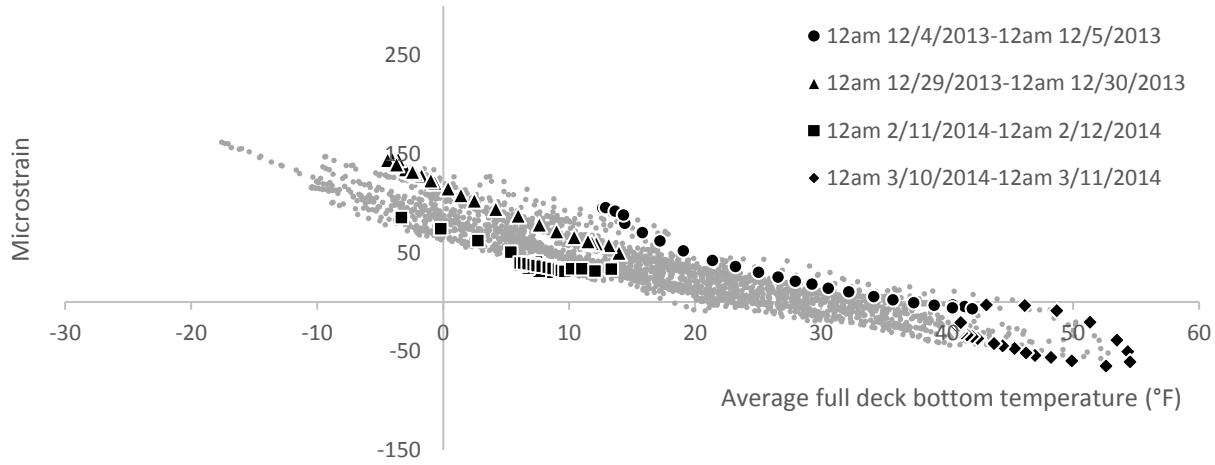

Figure 35. Strain from strain gauge A4 vs. average temperature at the bottom of the full deck

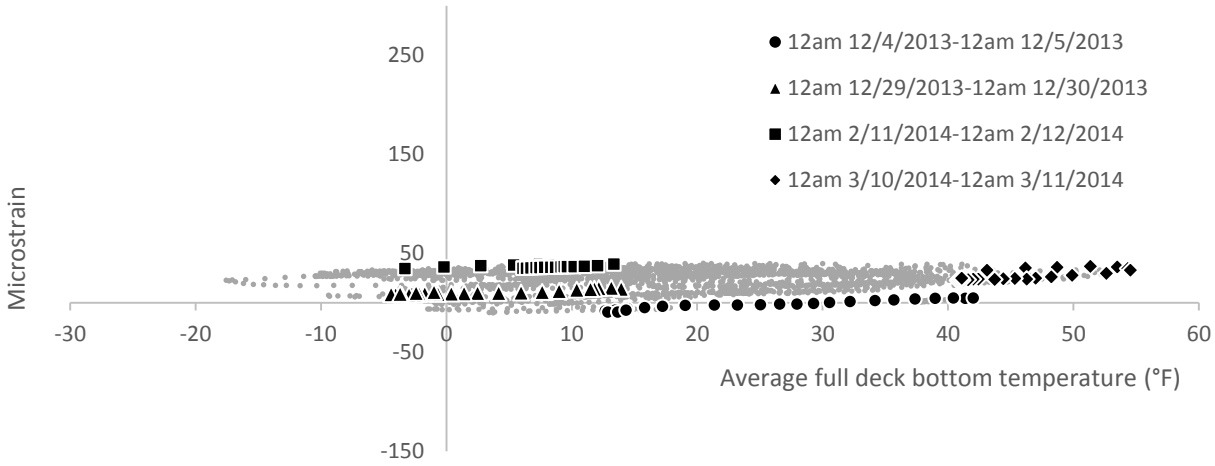

Figure 36. Strain from strain gauge A5 vs. average temperature at the bottom of the full deck

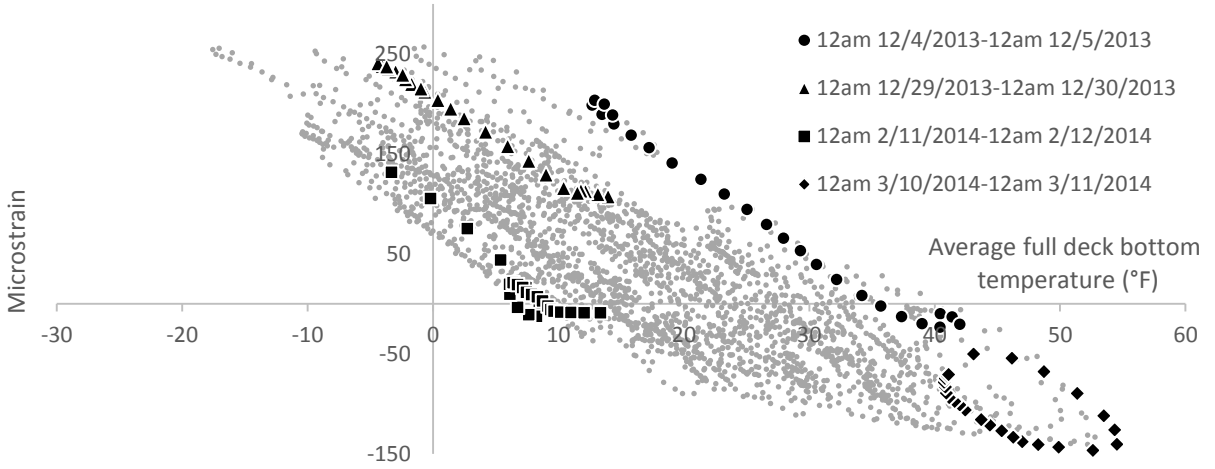

Figure 37. Strain from strain gauge A6 vs. average temperature at the bottom of the full deck

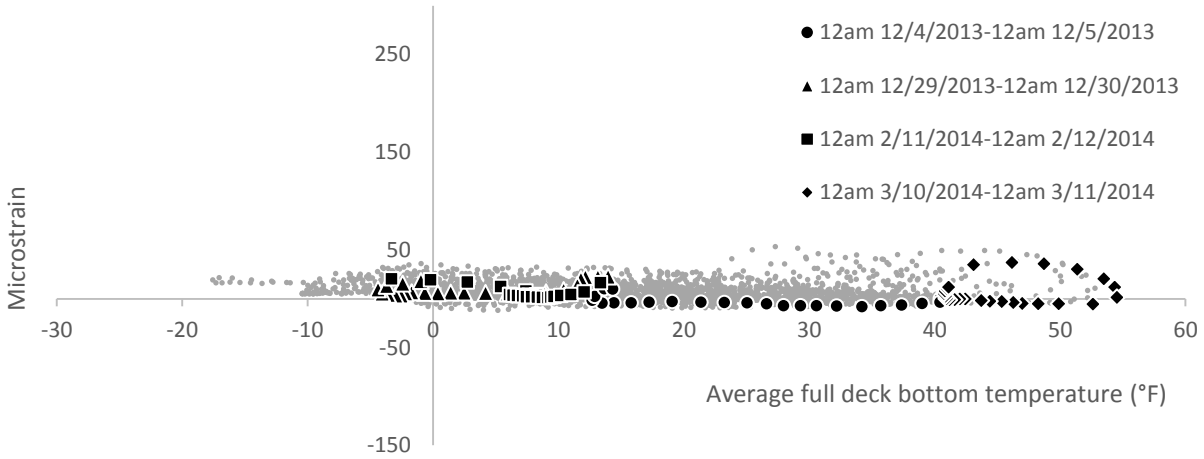

Figure 38. Strain from strain gauge M1 vs. average temperature at the bottom of the full deck

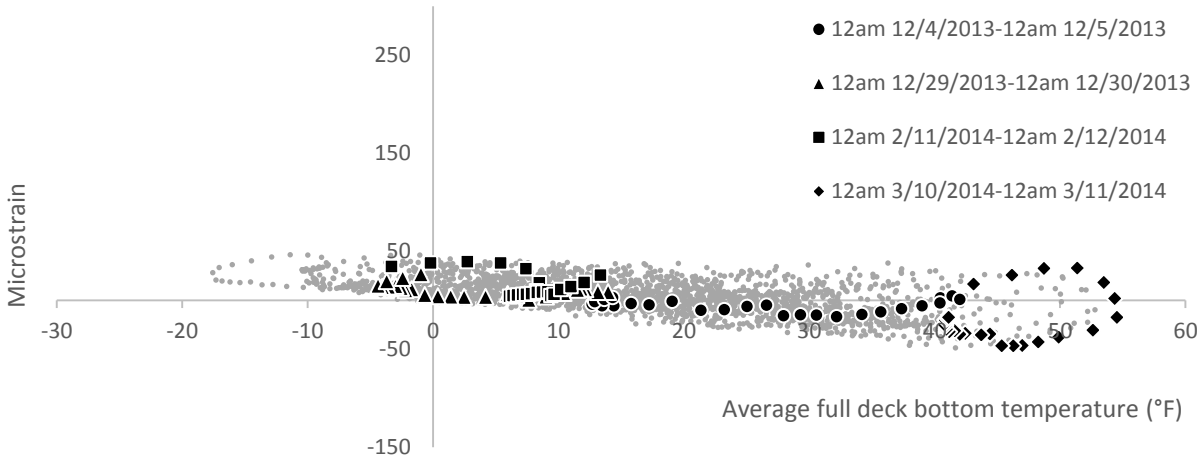

Figure 39. Strain from strain gauge M3 vs. average temperature at the bottom of the full deck

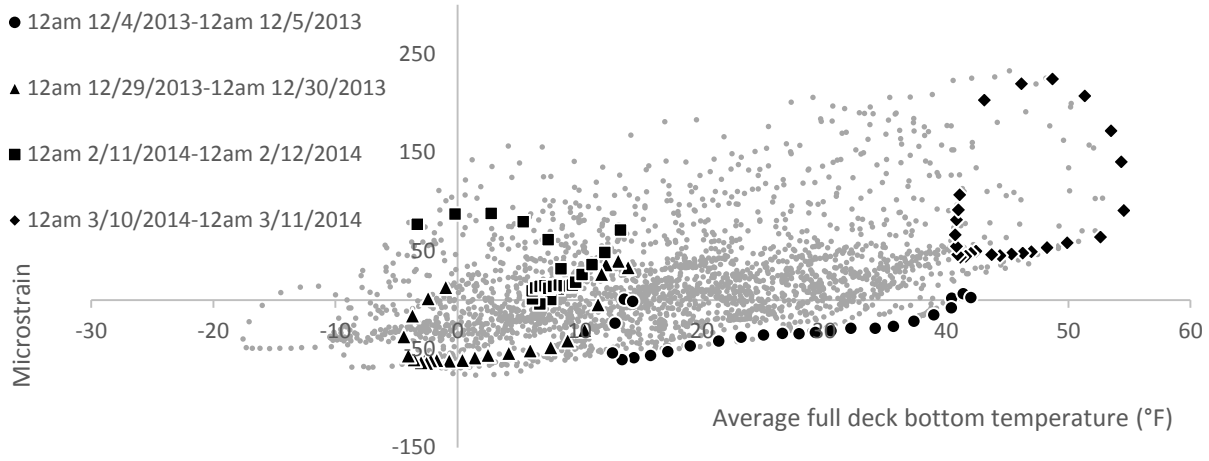

Figure 40. Strain from strain gauge M5 vs. average temperature at the bottom of the full deck

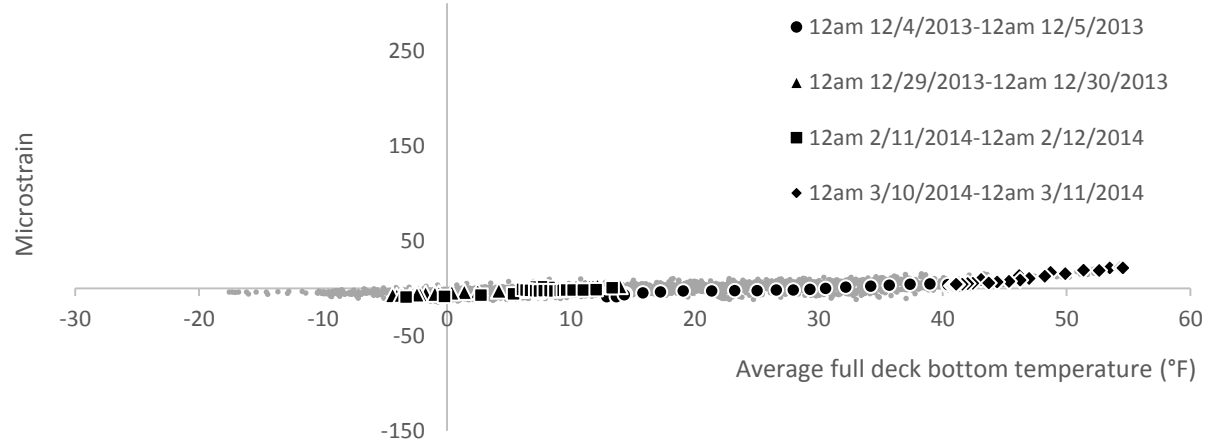

Figure 41. Strain from strain gauge P1 vs. average temperature at the bottom of the full deck

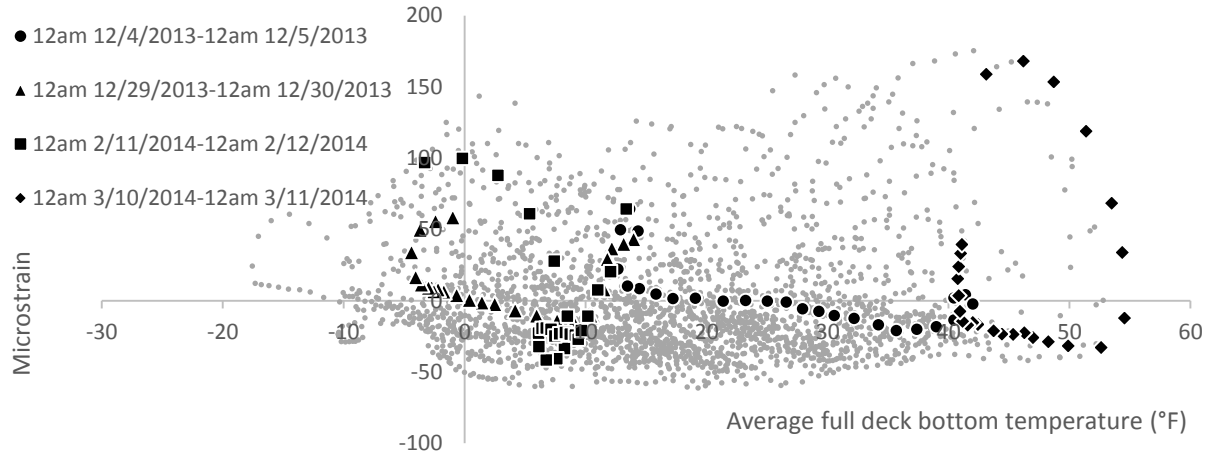

Figure 42. Strain from strain gauge P3 vs. average temperature at the bottom of the full deck

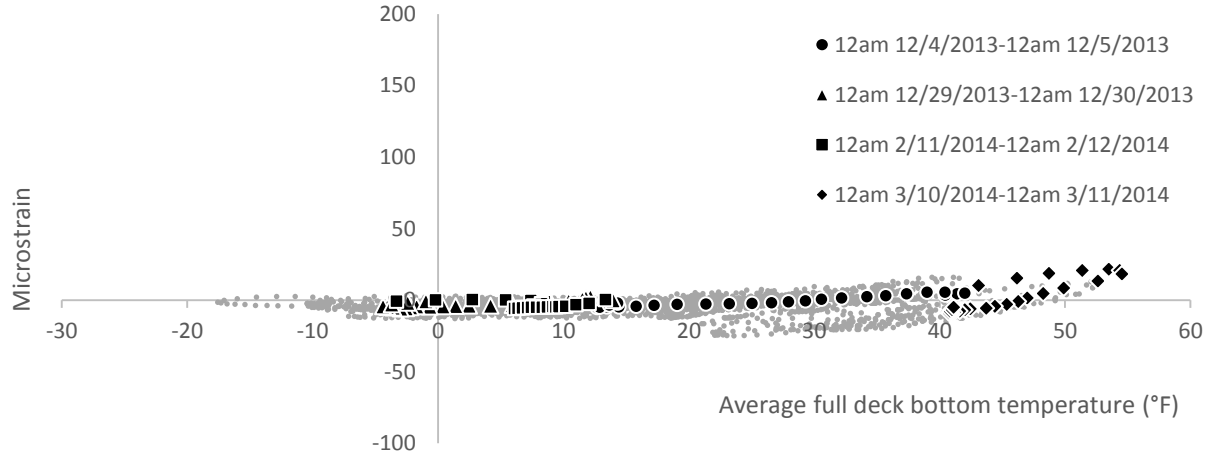

Figure 43. Strain from strain gauge P5 vs. average temperature at the bottom of the full deck

Although the long-term testing results show that the maximum difference between the average temperature at the bottom of the deck and the average temperature at the middle depth of the deck was just two degrees, the road surface temperature data from the Iowa DOT show that, in the Waterloo region, the road surface temperature can be 30° F higher than the air temperature on a sunny afternoon. A comparison between the bottom deck temperature and air temperature shows that the maximum difference between both temperatures was just two degrees (shown in Figure 44).

As a result of this phenomenon, the strain loop in the fourth time period (for example, in Figure 32) is due to the large temperature difference between the top and bottom surface of the deck in the afternoon. A further observation on the strain data reveals that the peak strain value in the fourth time period occurred between 12 p.m. and 4 p.m.

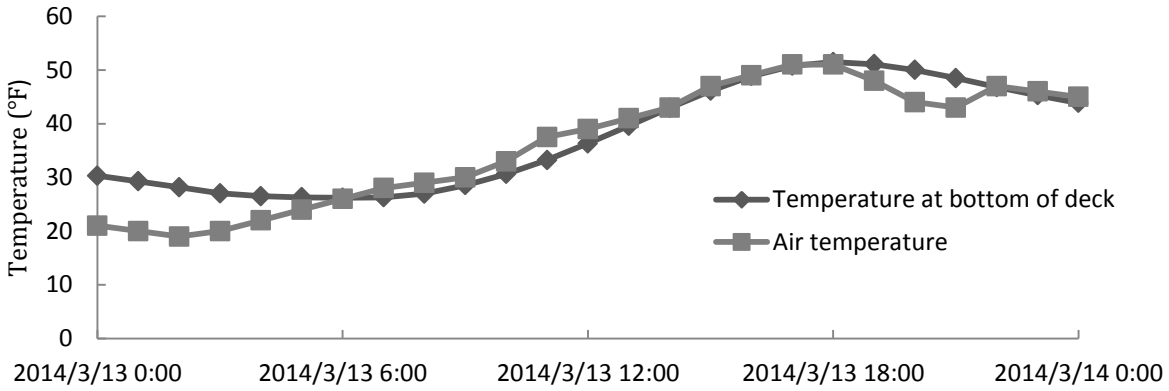

Figure 44. Comparison between the air temperature and the temperature at the bottom surface of deck

At the abutment section, the strain ranges in the first to fourth bays are around 150 microstrain (Figure 32 through Figure 35). The strain value versus temperature plot from the fifth bay (abutment section) shows a low strain range from -10 to 40 microstrain (Figure 36). The strain range in the sixth bay is as high as 400 microstrain (Figure 37). A visual inspection revealed that some deck cracks are near the strain gauges in these two bays. This is indicative that, among other items, high strains can be developed and then subsequently released once cracking occurs.

For the fifth bay, a crack parallel to the girders was found at the bottom of the deck within one inch from one side of the strain gauge (Figure 45).

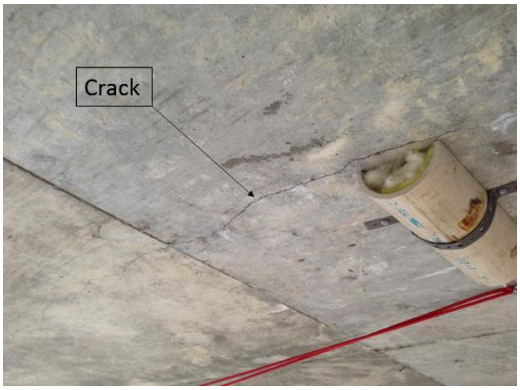

Figure 45. Relative positions of crack and strain gauge in the fifth bay

The strain gauge is near the edge of the crack and perpendicular to the crack; thus, the reading from the strain gauge is reduced due to the stress released near the edge of the crack. A similar situation was also observed in the third bay, where a crack developed close to the mounting block of the strain gauge, which resulted in an irregular strain versus temperature relationship.

In the sixth bay, a crack which ends eight inches from the strain gauge was found at the top surface of the deck. Figure 46 illustrates the relative positions of the vibrating wire strain gauge

(solid rectangle) and the crack. The high measured strain value in the sixth bay is probably due to the stress concentration at the end of the crack.

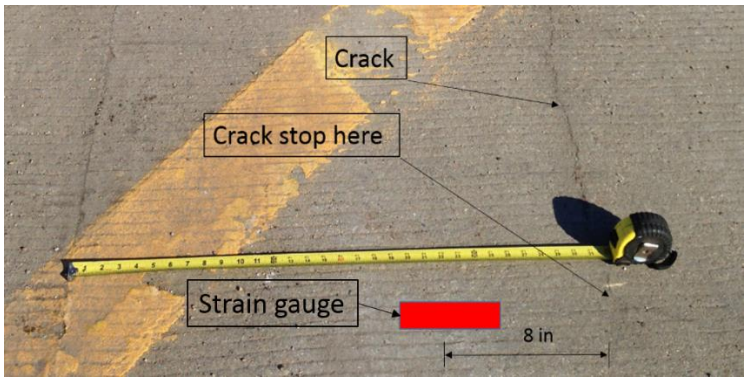

Figure 46. Relative positions of crack and strain gauge in the sixth bay

For the pier section and the middle section, the large strain readings and the small strain readings in some gauges can also be explained by the influence from nearby cracks. The gauges not near the cracks (such as A1, A2, and A4) show reasonable and consistent strain readings, which means the strain data obtained from long-term testing are valid for the calibration of the FEM.

4.2.3 Displacement Data

Figure 47 through Figure 50 show displacement versus temperature plots from the four displacement transducers.

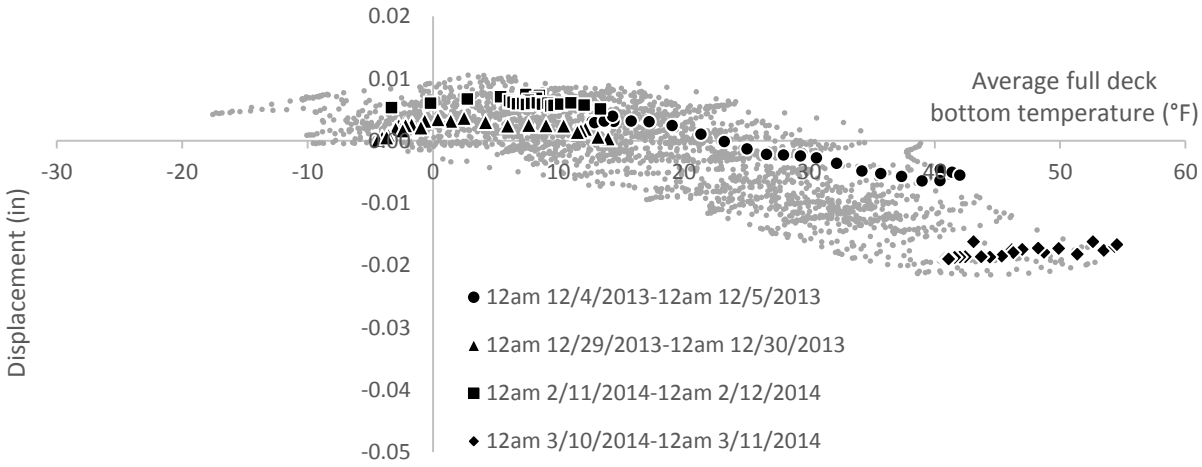

Figure 47. Displacement at DS-1 vs. average temperature at the bottom of the full deck

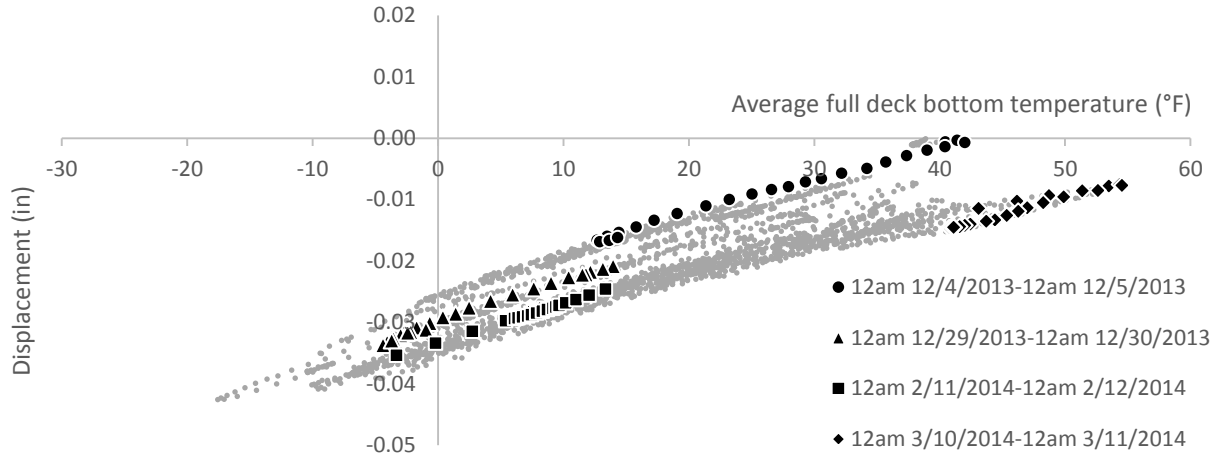

Figure 48. Displacement from DS-2 vs. average temperature at the bottom of the full deck

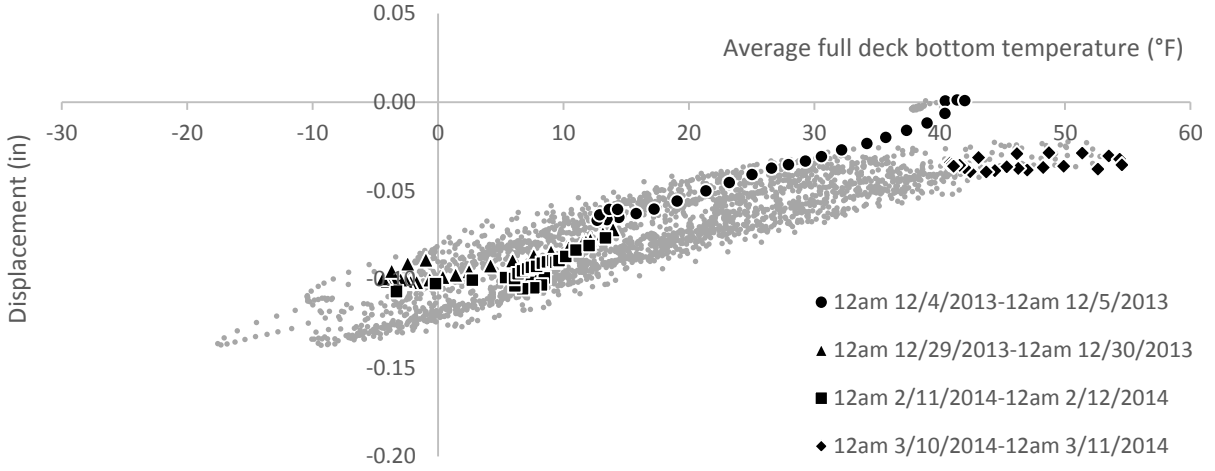

Figure 49. Displacement from DS-3 vs. average temperature at the bottom of the full deck

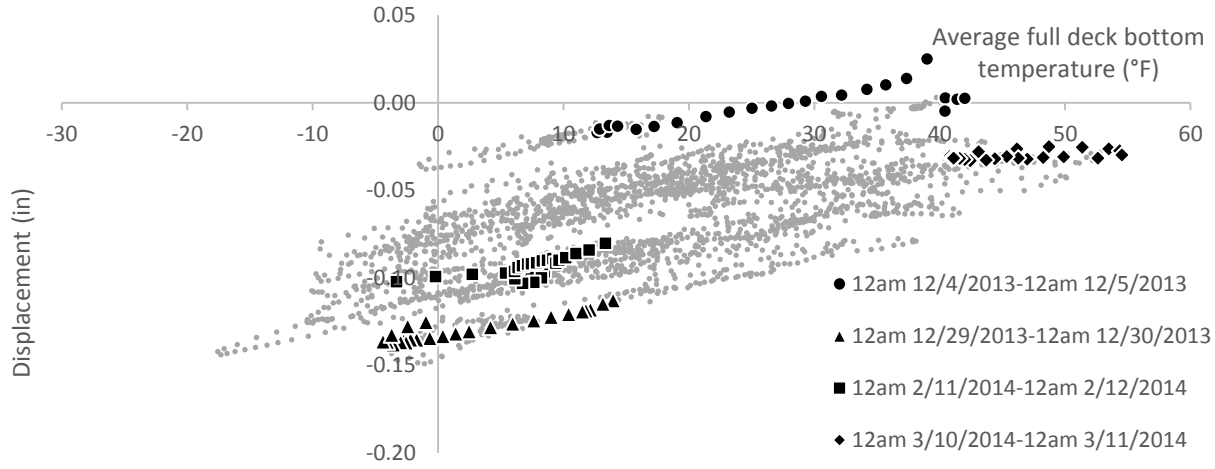

Figure 50. Displacement from DS-4 vs. average temperature at the bottom of the full deck

The locations of these four displacement transducers were shown in Figure 17. The temperature on the horizontal axis in Figure 47 through Figure 50 is the average temperature at the bottom of the deck. For DS-2, DS-3, and DS-4, a very similar slope can be observed from the data in the four daily periods. These slopes can be used to evaluate the displacement changes with temperature changes for each bay. The results from DS-1 (shown in Figure 47) are much different than those of the other displacement transducers. No similar slope can be extracted. Generally, the displacement value increases when the temperature drops, which is counter to basic engineering. Hence, the results from DS-1 were not used to calibrate the FEM. The results from DS-2 were used to calibrate for both the west and east side of the FEM.

CHAPTER 5. DEVELOPMENT OF BRIDGE MODEL

5.1 Introduction

In this chapter, a 3D FEM developed using the software ANSYS is described. Both live-load and long-term testing results were used to calibrate this FEM. This calibration involved incrementally altering various structural characteristics, such as the support conditions and material properties, until the FEM and the field test results matched reasonably well. The bridge model developed in this research includes the deck, girder, diaphragm, abutment, and pier cap. Piles under the abutment and pier columns were idealized by assuming proper support conditions.

5.2 Elements Used in This Study

Two element types were used to create the subsequently described FEM. The commercial software ANSYS was utilized, and the specific element types used are Shell 181 and Beam 4.

5.2.1 Shell 181 Element

Shell 181 is a four-node element with six degrees of freedom at each node: translations in the x, y, and z directions and rotations about the x, y, and z axes. The Shell 181 element is suitable for analyzing thin to moderately thick shell structures. In this bridge FEM, this element was used to simulate the deck, abutment, diaphragm, and the web of the girders. Both isotropic and orthotropic material properties can be used in association with this element. The thickness of the element is defined at the four nodes. Further, different temperature changes can be applied to the top and bottom of the element allowing for the study of thermal gradient induced behaviors. Figure 51 shows the geometry and coordinates of a Shell 181 element.

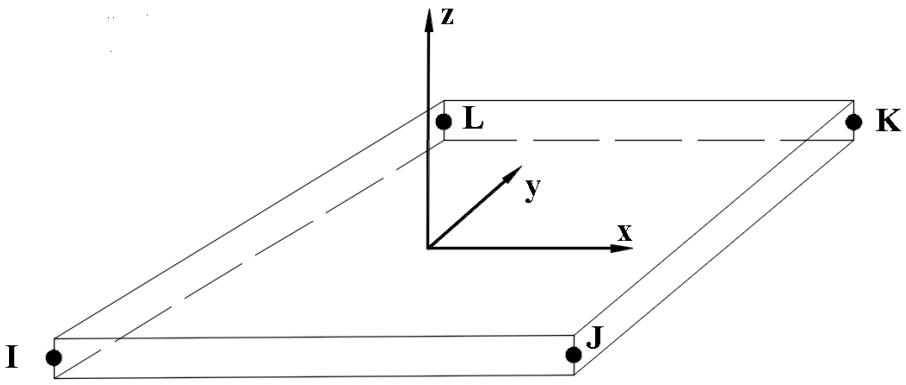

Figure 51. Shell 181 geometry

5.2.2 Beam 4 Element

The Beam 4 element is a two-node element with six degrees of freedom at each node: translations in the x, y, and z directions and rotations about the x, y, and z axes. It is a uniaxial element with tension, compression, torsion, and bending capability. In this FEM, the Beam 4 element was used to mesh the top and bottom flange of the girders, pier caps, and steel diaphragms. The section properties required for this element include area, two moments of inertia (IZZ and IYY), two thicknesses (TKY and TKZ), the torsional moment of inertia (IXX), and pertinent material properties. Temperature loading can be input on the node of the element. Figure 52 shows the geometry and coordinates of a Beam 4 element.

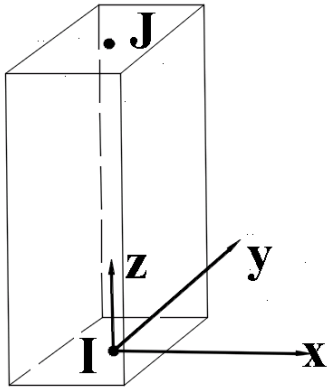

Figure 52. Beam 4 geometry

5.3 Material Properties

The bridge consists of high-strength, pre-stressed concrete for the girders and normal concrete for the other concrete components. Based on the original design plans for the bridge, the specified compressive strength (f_c') for the pre-stressed girder is 5 ksi, and for the concrete in the other bridge components it is 3.5 ksi. The Young's Modulus for concrete was calculated using $57000\sqrt{f_c'}$, yielding a Young's Modulus for concrete was calculated using $57000\sqrt{f_c'}$, yielding a Young's Modulus of 4,000 ksi for the pre-stressed girder and 3,400 ksi for the other concrete components.

The effect of steel reinforcement in the concrete was also taken into account by smearing the steel into the concrete. To simulate this orthotropic behavior of the bridge, an effective thermal expansion coefficient (α_{eff}) and an effective Young's Modulus (E_{eff}) were determined using Equation (1) and Equation (2) (Greimann et al. 2014):

$$\boldsymbol{E_{eff}} = \frac{\boldsymbol{A_c E_c + A_s E_s}}{\boldsymbol{A_c + A_s}} \quad (1)$$

$$\boldsymbol{\alpha_{eff}} = \frac{\boldsymbol{A_c E_c \alpha_c + A_s E_s \alpha_s}}{\boldsymbol{A_c E_c + A_s E_s}} \quad (2)$$

where,
E_{eff} = effective linear elastic modulus of combined steel and concrete,
α_{eff} = effective thermal expansion coefficient of combined steel and concrete,
A_c = area of concrete,
A_s = area of steel,
E_c = linear elastic modulus of concrete,
E_s = linear elastic modulus of steel,
α_c = thermal expansion coefficient of concrete, and
α_s = thermal expansion coefficient of steel.

Poisson's ratio (υ) for all the concrete members was taken as 0.2. For steel members, Poisson's ratio was specified as 0.3. The effective material properties of the FEM are listed in Table 4.

Table 4. Material properties input into the FEM

Bridge Component	Element Type	Direction	E (ksi)	α $(\times 10^{-6}\ in/in/F)$	υ
Deck	Shell 181	Transverse	3600	5.55	0.2
		Vertical	3370	5.50	0.2
		Longitudinal	2550	5.56	0.2
Girder-top flange	Beam 4	Isotropic	4 260	5.00	0.2
Girder-web	Shell 181	---	4 030	5.00	0.2
Girder-bottom flange (long span)	Beam 4	---	4 530	5.20	0.2
Girder-top flange (long span)	Beam 4	---	4 240	5.00	0.2
Abutment	Shell 181	---	3 370	5.50	0.2
Pier cap	Beam 4	---	3 530	5.55	0.2
Pier diaphragm	Shell 181	---	3 370	5.50	0.2
Steel diaphragm	Beam 4	---	29 000	6.50	0.3

5.4 Meshing and Idealized Support Conditions

5.4.1 Deck

Considering that the behavior of the bridge deck is the main focus of the FEM study, a fine mesh size was used to simulate the deck. Before finalizing the mesh pattern, several requirements, such as the location of the live load and the location of the girders, were taken into account. A convenient and acceptable element size was determined to be about six inches, with an aspect ratio near 1:1. Figure 53 shows the mesh geometry for the deck.

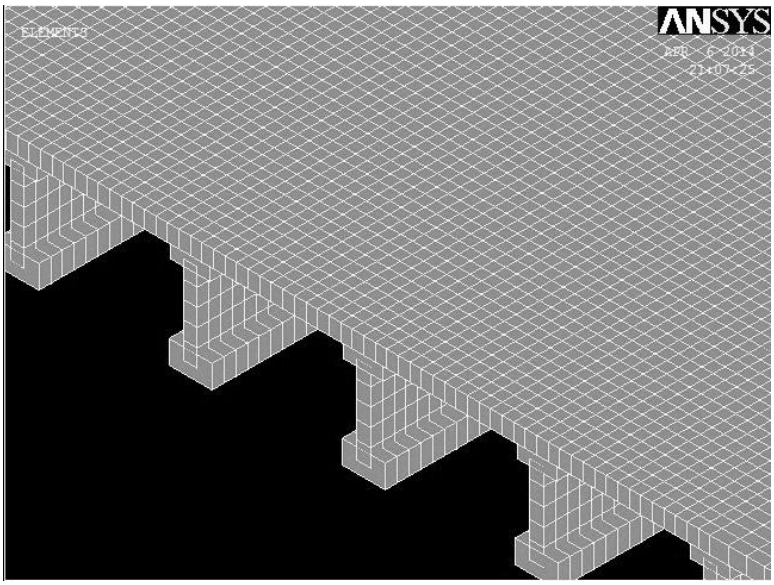

Figure 53. Meshed deck

5.4.2 Girder

In the FEM, two types of elements were used to model the pre-stressed concrete girder. The Shell 181 element was used to model the girder web, and the Beam 4 element was used to model both the top and bottom flanges. To simulate the shear connection between the girders and the deck, a four-inch long Beam 4 element with a very high stiffness was used.

5.4.3 Abutment - Deck, Girder

Both abutments were rigidly attached to the deck and girders. Note that the mesh geometry for the abutment is slightly irregular (shown in Figure 54), because at the top of the abutment a fine mesh was used to match the mesh pattern on the deck, while at the bottom of the abutment the element size was adjusted to match the pile locations.

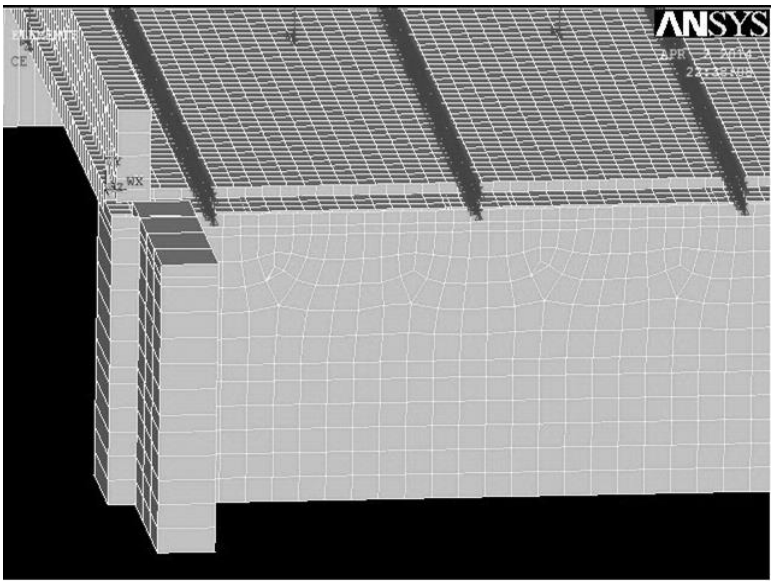

Figure 54. Meshed abutment

5.4.4 Girder - Pier Cap

Near the pier region, because both the bottom flange and the pier cap were simulated with beam elements, rigid links were used to connect the bottom flange of the girder and the pier cap. Because Bridge #605220 has an expansion pier, the connection between the superstructure and pier cap only constrains the translation in the vertical direction. Hence, in the FEM the rigid links (shown in Figure 55) that connect the girder and pier cap only transfer the translation in the vertical direction from the superstructure to the substructure.

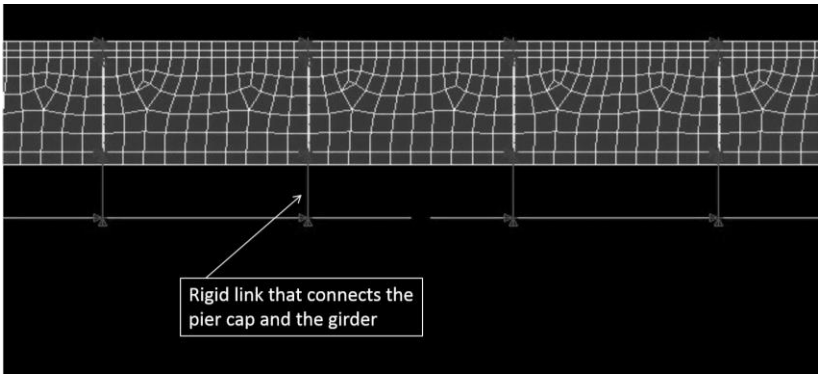

Figure 55. Rigid links that connect the bottom flange of the girder and the pier cap

5.4.5 Support Conditions

For the piles under the abutment, the bending stiffness of the pile is relatively small compared to that of the other structural elements. So, the rotation stiffness from those piles was ignored. For the same reason, the translation resistance from the pile in the transverse and longitudinal

directions of the bridge was also ignored. At each pile location under the abutment, a roller was used to simulate each pile and provided only vertical support (Figure 56).

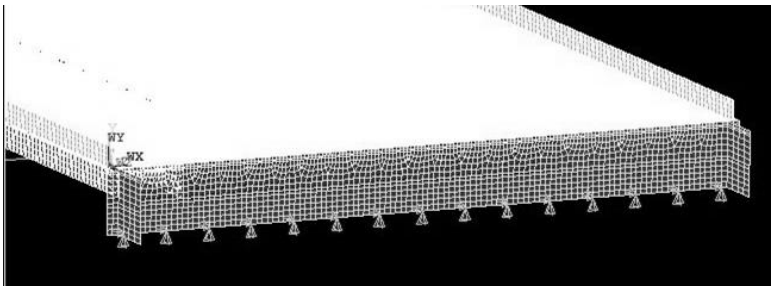

Figure 56. Roller supports used to replace the piles at the bottom of the abutment

The pier column was also incorporated into the model. Rollers were used to simulate the pier columns and provided only vertical support (Figure 57).

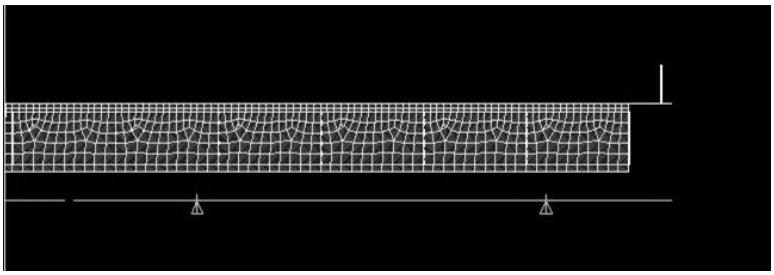

Figure 57. Roller support used to replace the pier column under the pier cap

Because the transverse stress in the deck induced by the soil pressure was relatively small compared to the stress induced by the thermal loading, the soil pressure behind the abutment was not included in the FEM.

5.5 Validation and Calibration of the Bridge Model

5.5.1 Calibration for Live-Load Behavior

5.5.1.1 Live Loading

In the FEM, the load generated by the three-axle Iowa DOT snooper truck was modeled with concentrated forces. The wheel spacing in the longitudinal direction and the weight carried by each wheel is shown in Figure 1 in Chapter 3.

For each load step, six concentrated forces were applied in the FEM to simulate the complete truck loading. In total, each load case consists of 58 load steps, and the spacing between each load step is five feet (shown in Figure 58).

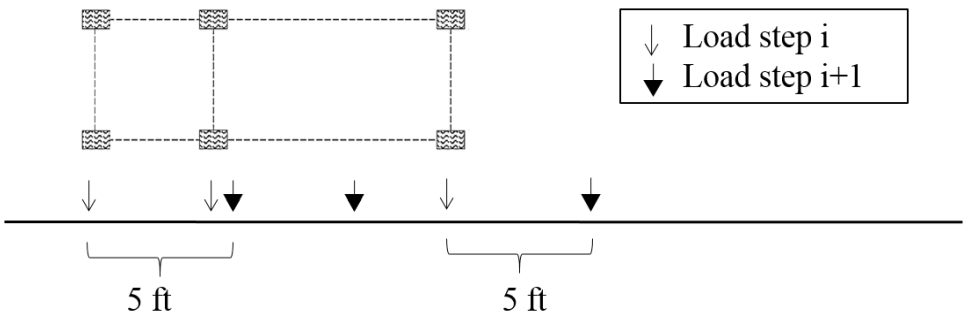

Figure 58. Load step spacing

5.5.1.2 Calibration

Bridge #605220 has a skew of only 1.5 degrees, and field testing results indicated a symmetric bridge response, so only the results from LC1, LC2, and LC5 are shown in this section. Comparisons between the field testing results and FEM results for LC1 for each strain gauge located on the bottom flange of the first interior girder and exterior girder on the east side of the bridge are shown in Figure 59 and Figure 60 (see Section 3.3 for detailed LC information).

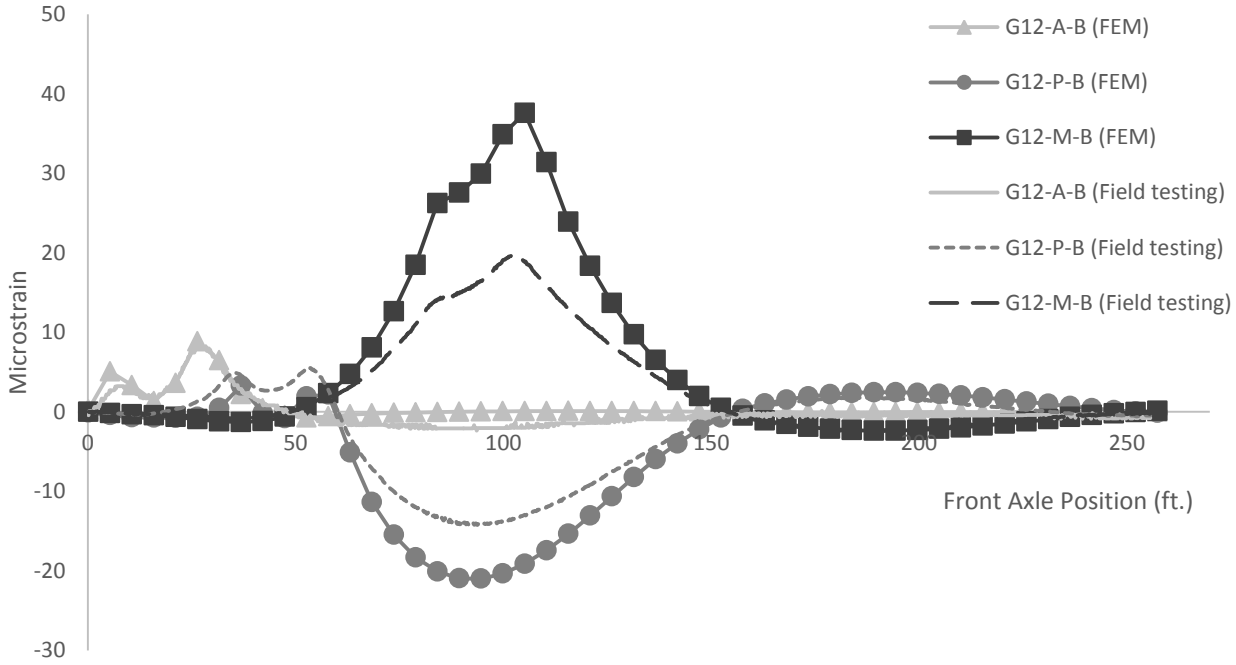

Figure 59. Comparison at the bottom flange of the exterior girder in LC1 (Original *E*)

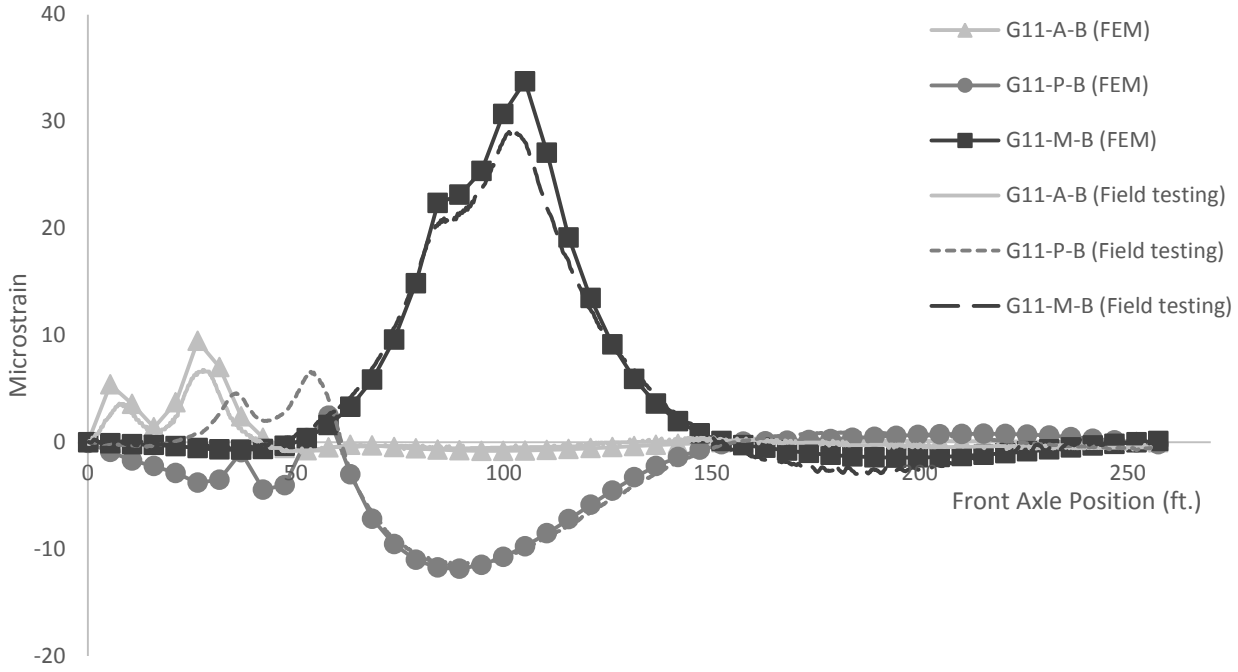

Figure 60. Comparison at the bottom flange of the first interior girder in LC1 (Original *E*)

Generally, the FEM provided a higher strain value than the field testing results. Hence, the Young's Modulus was altered to calibrate the FEM. For the deck, the Young's Modulus was increased from 3,400 ksi to 4,000 ksi. For the pre-stressed concrete girder, three Young's Modulus values (4,000 ksi, 5,100 ksi, and 7,000 ksi) were evaluated. The increase in the Young's Modulus is justified because it is very likely that the concrete strength (and thus Young's Modulus) is higher than the minimum specified in the plans.

The percentage difference between the peak strains was calculated using Equation (3) to compare the results from the field testing and the FEM.

$$Percentage\ difference\ = \frac{\varepsilon_{FEM} - \varepsilon_{field\ testing}}{\varepsilon_{field\ testing}} \times 100\% \quad (3)$$

The average percentage difference of each of the abutment, pier, and mid-span sections was calculated for the first three girders on the east side of the bridge because these three girders provide relatively high strain values. The average percentage difference of the whole bridge is the average value of these three sections, as listed in Table 5 for LC1.

Table 5. Summary of average percentage difference on each section and the whole bridge

Young's Modulus of the girder (ksi)	Abutment Section	Pier Section	Mid-Span Section	Whole Bridge
4000	14.7	23.9	33.6	24.1
5100	9.2	10.8	30.8	16.9
7000	18.6	31.3	33	27.6

The 5,100 ksi Young's Modulus for the pre-stressed girder together with a 4,000 ksi Young's Modulus for the deck provided the minimum average percentage difference (16.9%) for LC1.

The FEM with updated Young's Modulus values was used to analyze all five load cases. The strain versus position plots at each gauge location of the two girders under the truck in LC1, LC2, and LC5 with the increased Young's Modulus are shown in Figure 61 through Figure 66.

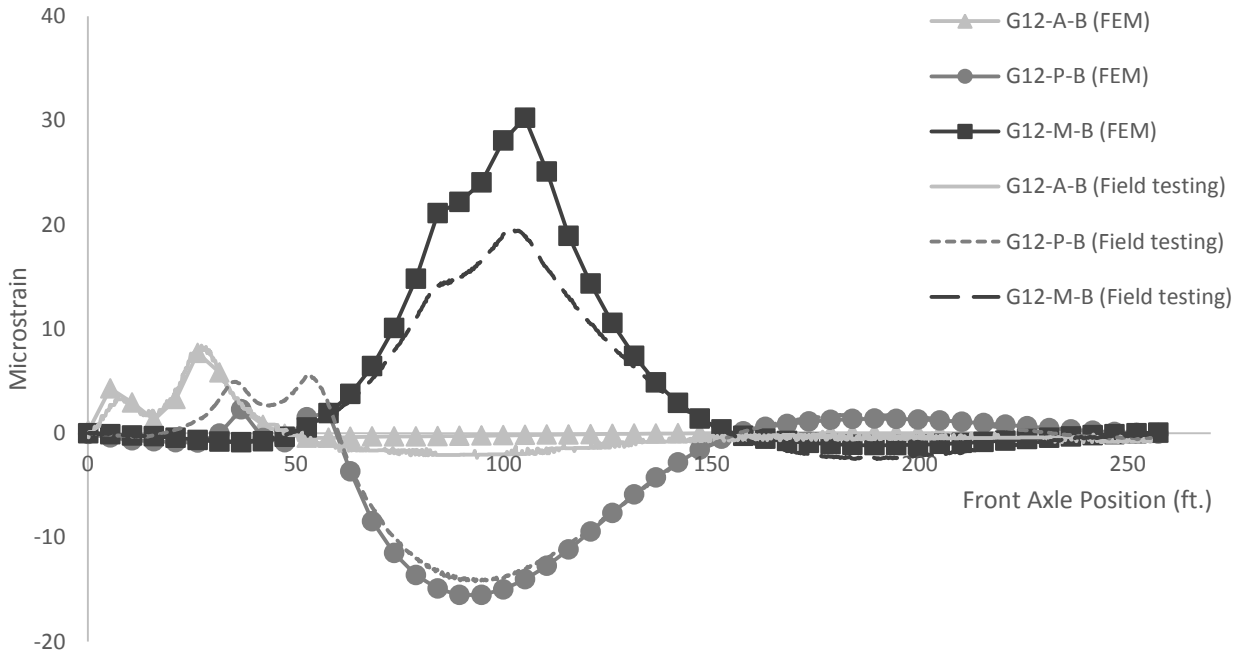

Figure 61. Comparison at the bottom flange of the exterior girder in LC1

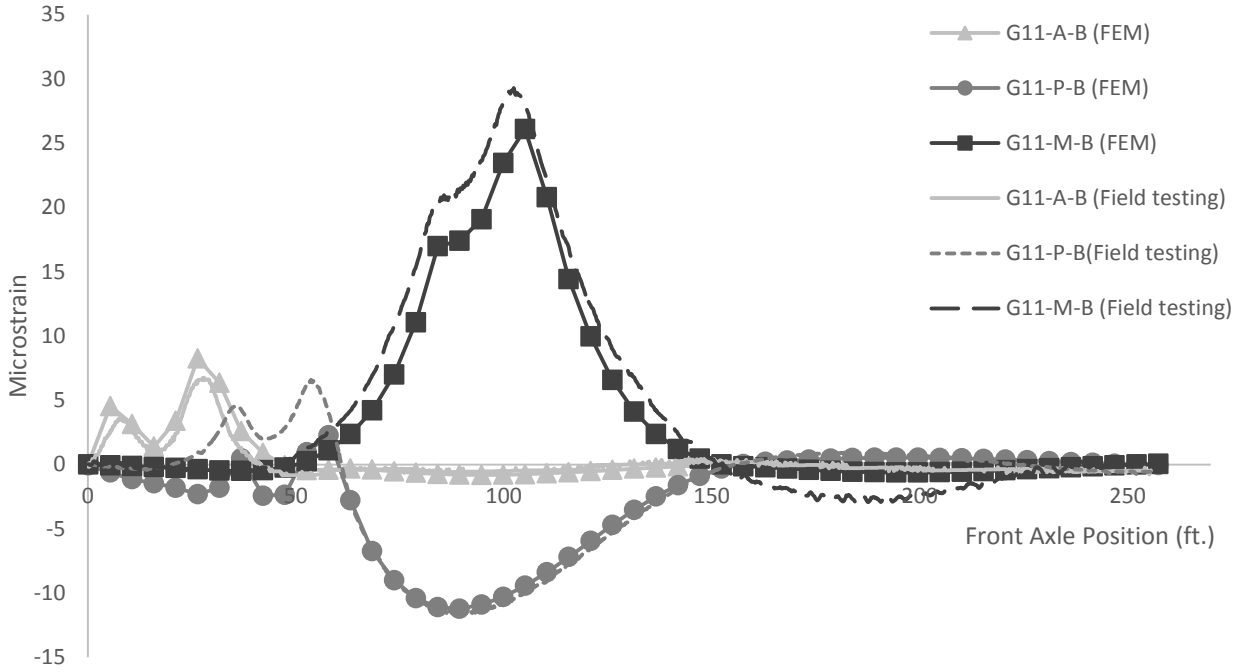

Figure 62. Comparison at the bottom flange of the first interior girder in LC1

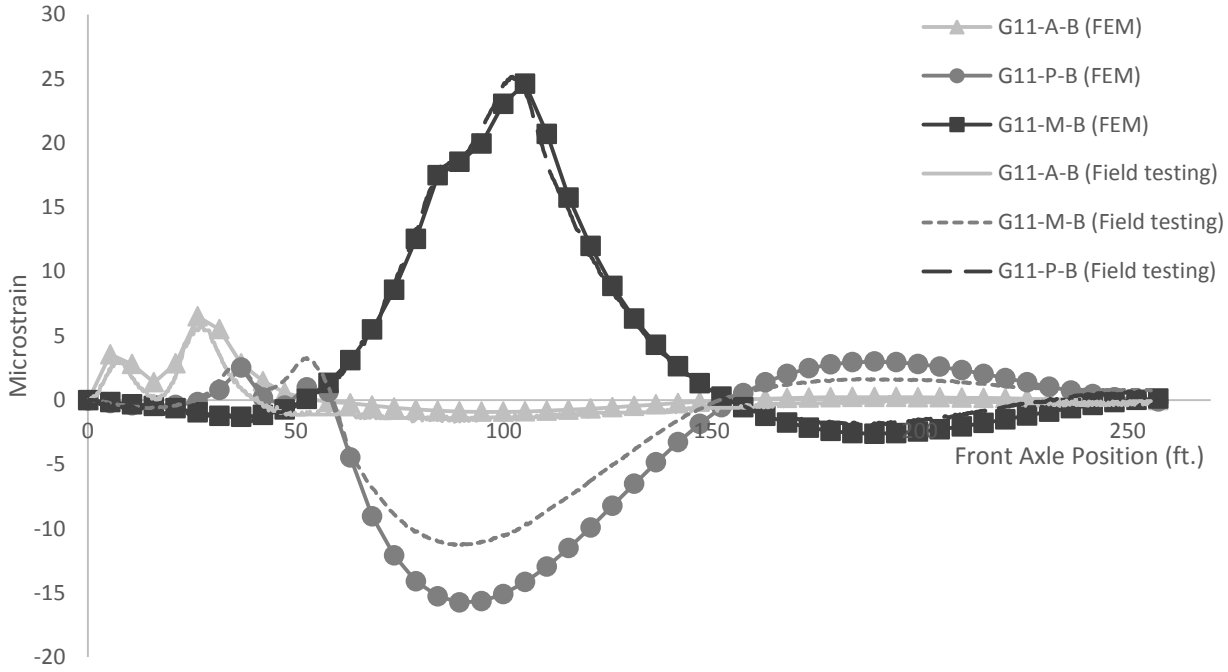

Figure 63. Comparison at the bottom flange of the first interior girder in LC2

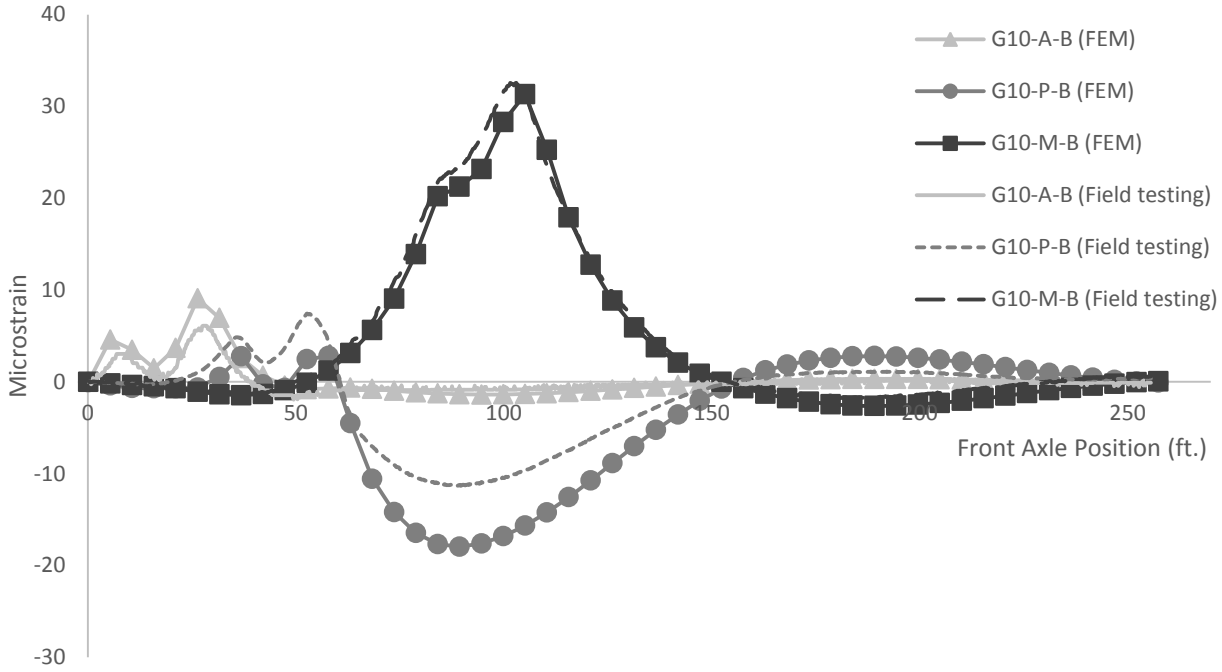

Figure 64. Comparison at the bottom flange of the second interior girder in LC2

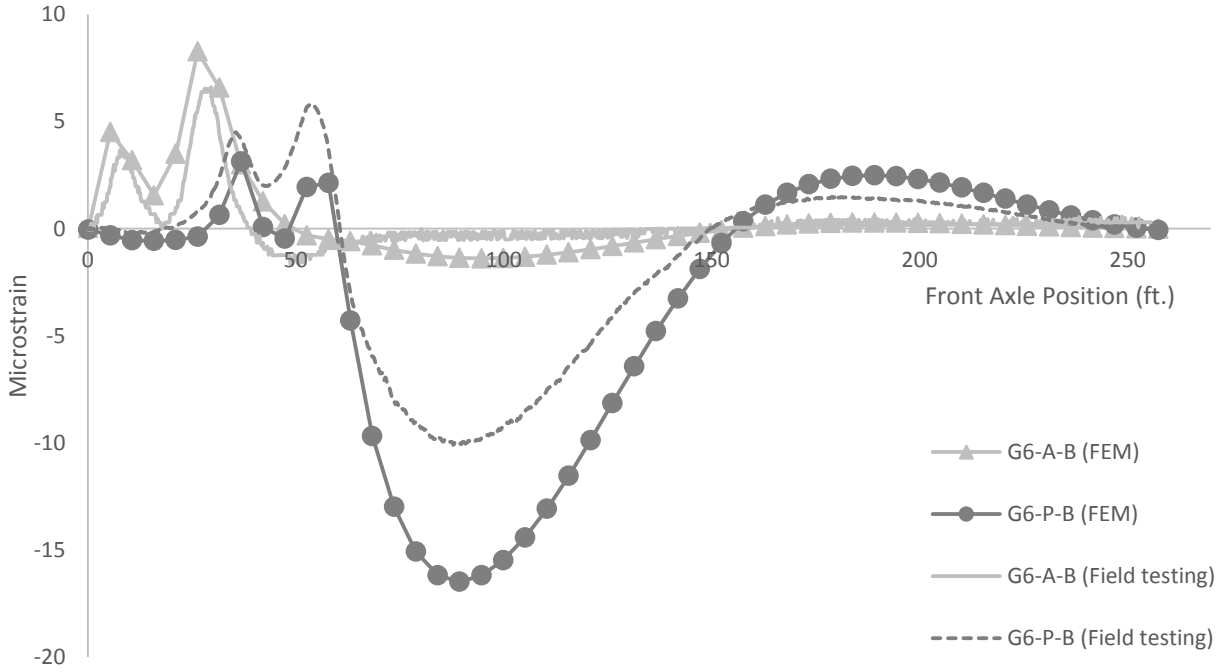

Figure 65. Comparison at the bottom flange of the sixth girder from the west side in LC5

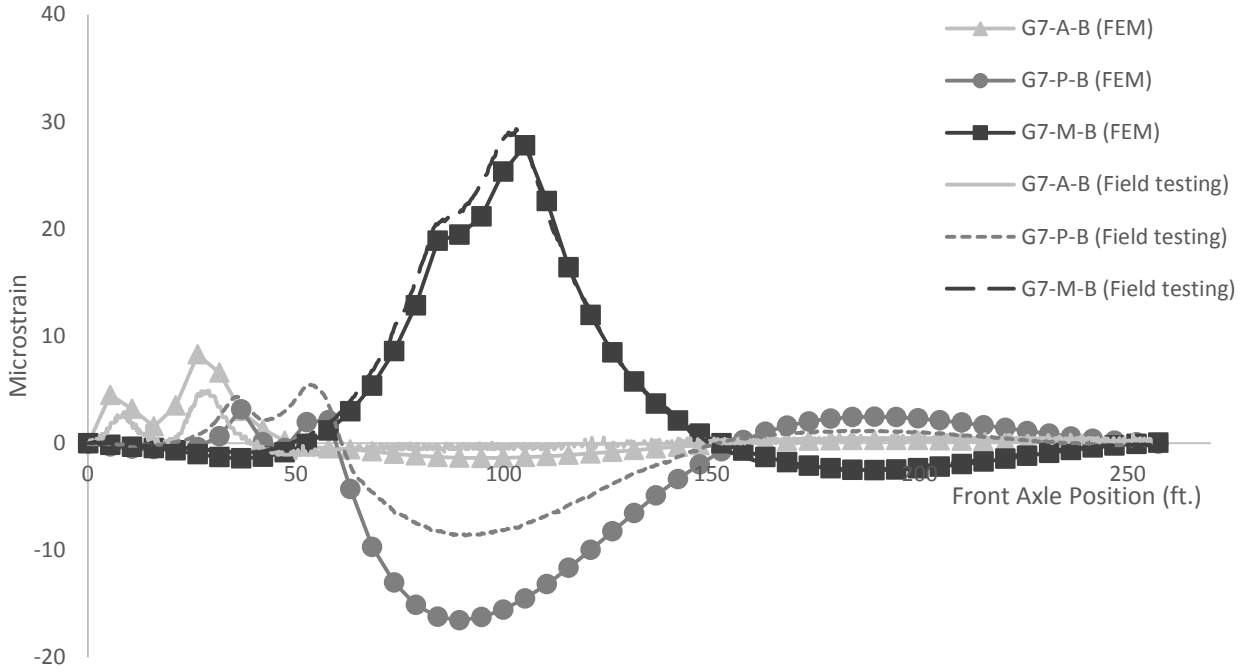

Figure 66. Comparison at the bottom flange of the sixth girder from the east side in LC5

A further comparison between the field testing results and the FEM results in LC1 (shown in Figure 61 and Figure 62) revealed that, from the FEM, the strain value in the exterior girder in the mid-span sections was higher than that of the first interior girder, while field testing results from the first interior girder gave a higher strain value than the exterior girder. The observed behavior difference is likely due to the complex interaction of the barrier rail with the superstructure.

5.5.2 Validation for Long-term Behavior

5.5.2.1 Temperature Loading

For the FEM thermal loadings, two types of temperature changes were considered (see Section 4.2). The first is a temperature difference between the deck and the abutment. When the temperature of the deck is lower than the abutment, the deck contracts relative to the abutment; thus, tensile forces are induced in the deck near the abutment region. Additionally, the temperature gradient through the thickness of the deck would also produce tensile stress at the bottom of the deck on a sunny day. For example, when the bridge is exposed to sunshine, the temperature at the top surface of the deck would be 20° F to 30° F higher than the temperature at the bottom of the deck. As a consequence, the top surface of the deck would expand and generate tensile stress at the bottom of the deck.

The temperature changes input into the FEM are shown in Figure 67 and are based on the temperature measurement results discussed in Chapter 4.

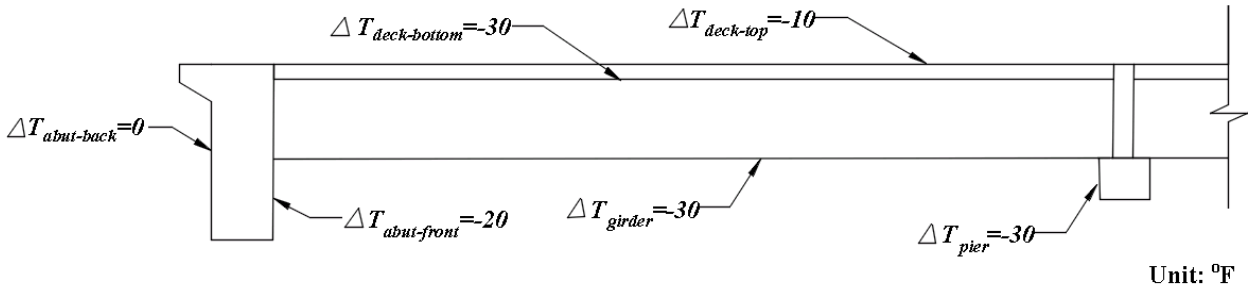

Figure 67. Temperature changes input into the FEM (reference temperature 38 °F)

Specifically, the temperature change at the bottom of deck was set to -30° F, and the temperature change on the front surface of the abutment was set to -20° F. Similarly, the temperature change at the top surface of the deck on a sunny day was -10° F, assuming a 20° F temperature gradient through the deck thickness. The temperature changes for the girder, diaphragm, and pier cap were assumed to be -30° F, similar to the deck bottom temperature change.

During long-term testing, the temperature on the soil side of the abutment was unknown, but it is probably stable and changes very slowly. Thus, zero temperature change was assumed to have occurred in that region (shown in Figure 67).

5.5.2.2 Validation

With the temperature changes, the strain change at each strain gauge location at the bottom of the deck was extracted to compare with the field test results. Note that because the temperature values input into the FEM represent the temperature changes from 38° F, the calculated strain value represents the corresponding strain changes. In Figure 68 through Figure 79, the black lines represent the results from the FEM simulation.

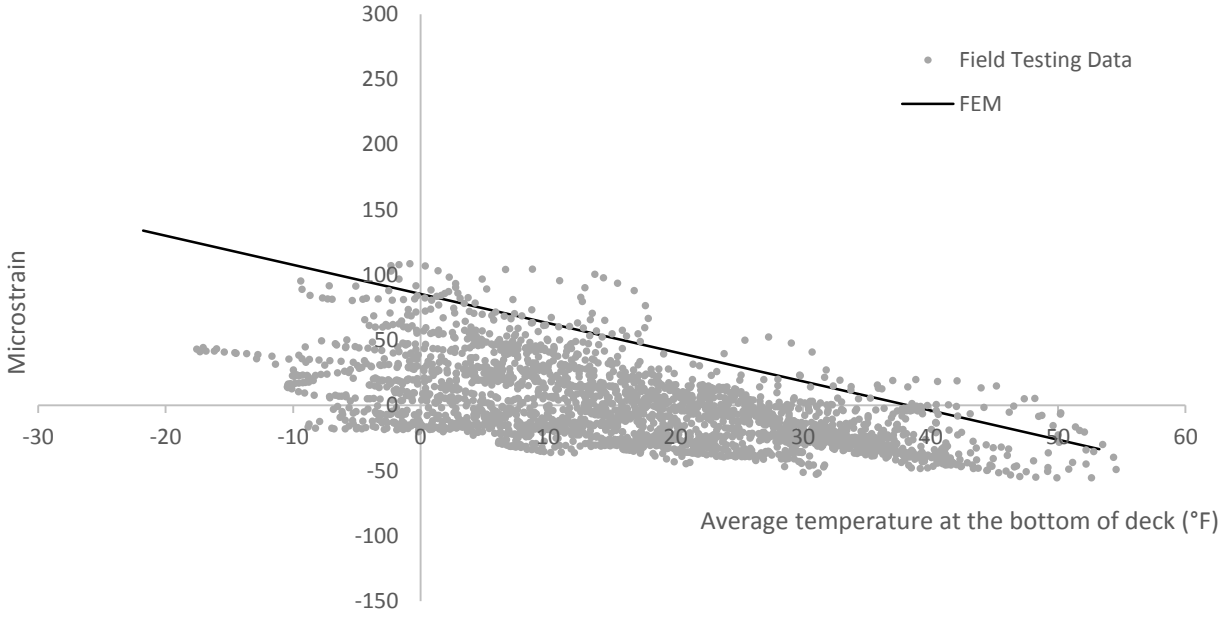

Figure 68. Results comparison for the gauge in the first bay near the abutment

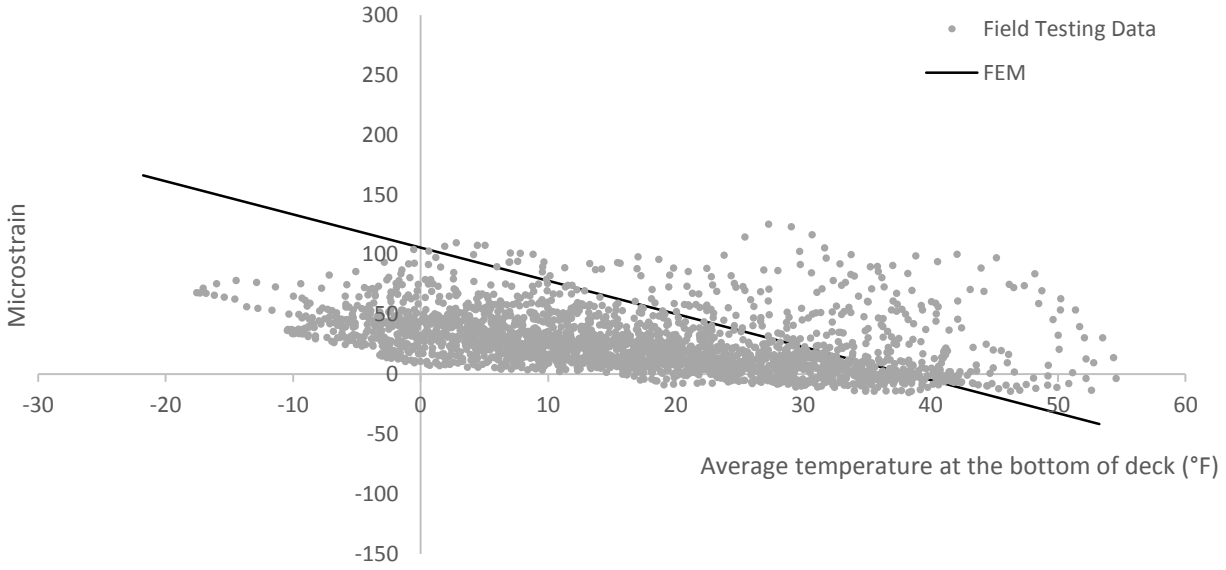

Figure 69. Results comparison for the gauge in the second bay near the abutment

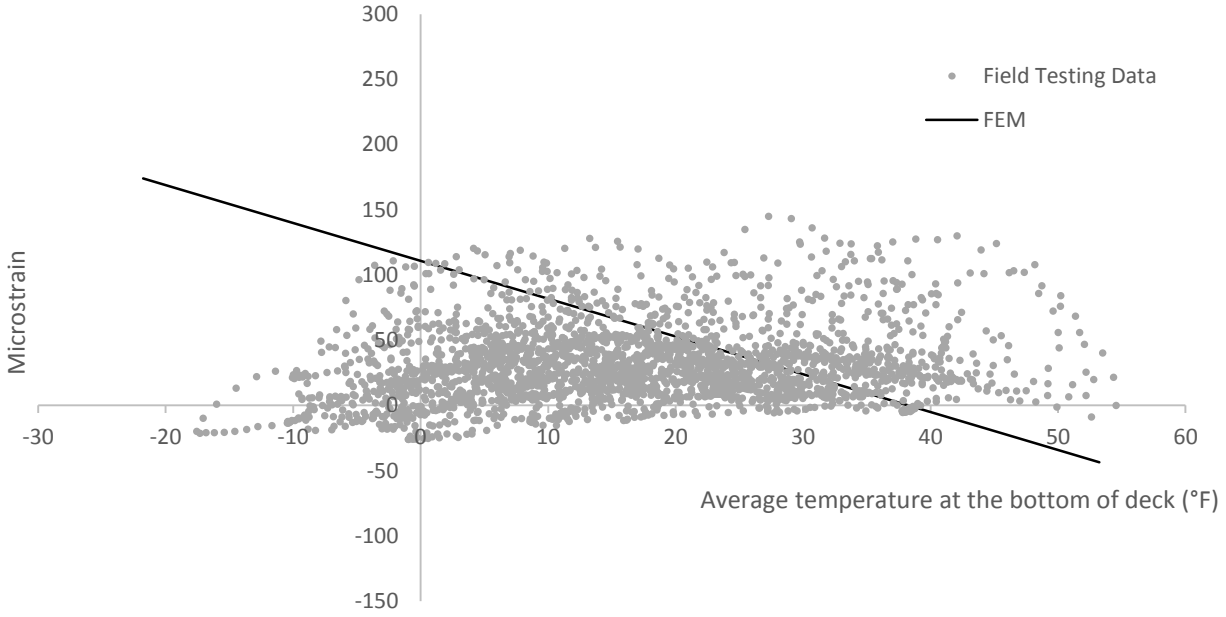

Figure 70. Results comparison for the gauge in the third bay near the abutment

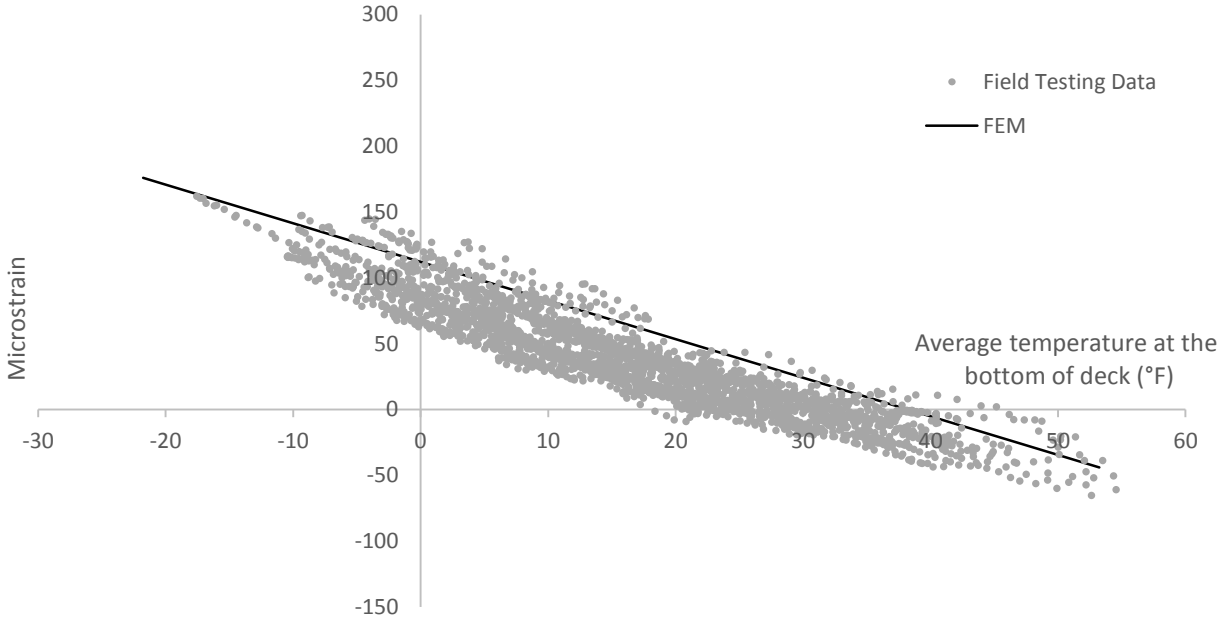

Figure 71. Results comparison for the gauge in the fourth bay near the abutment

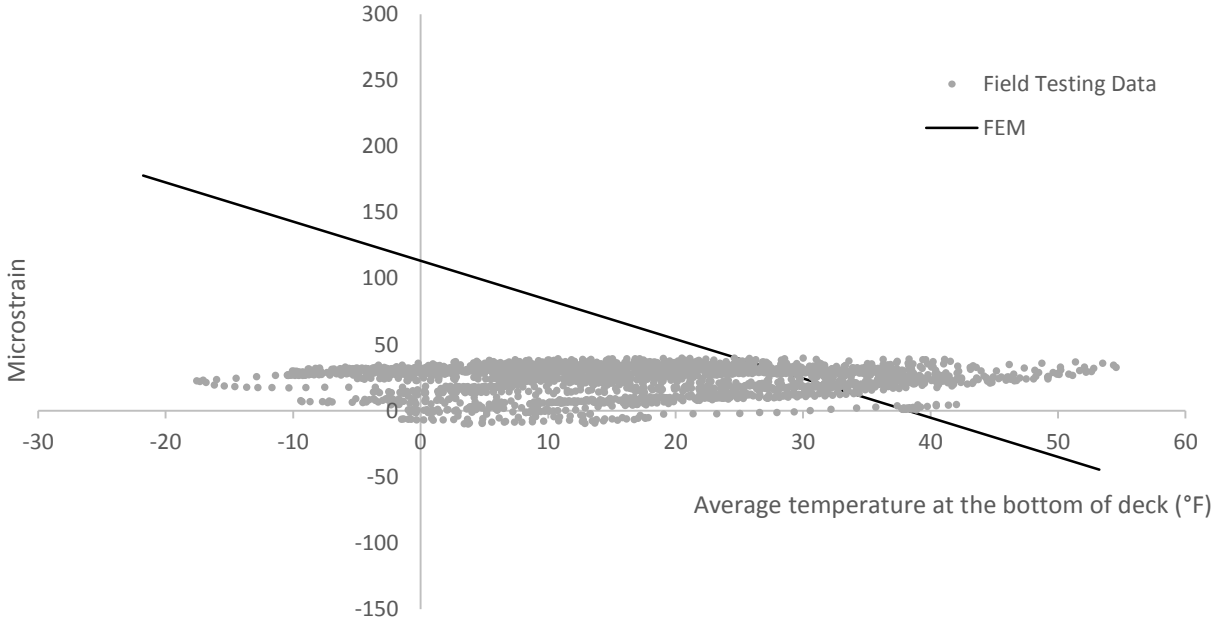

Figure 72. Results comparison for the gauge in the fifth bay near the abutment

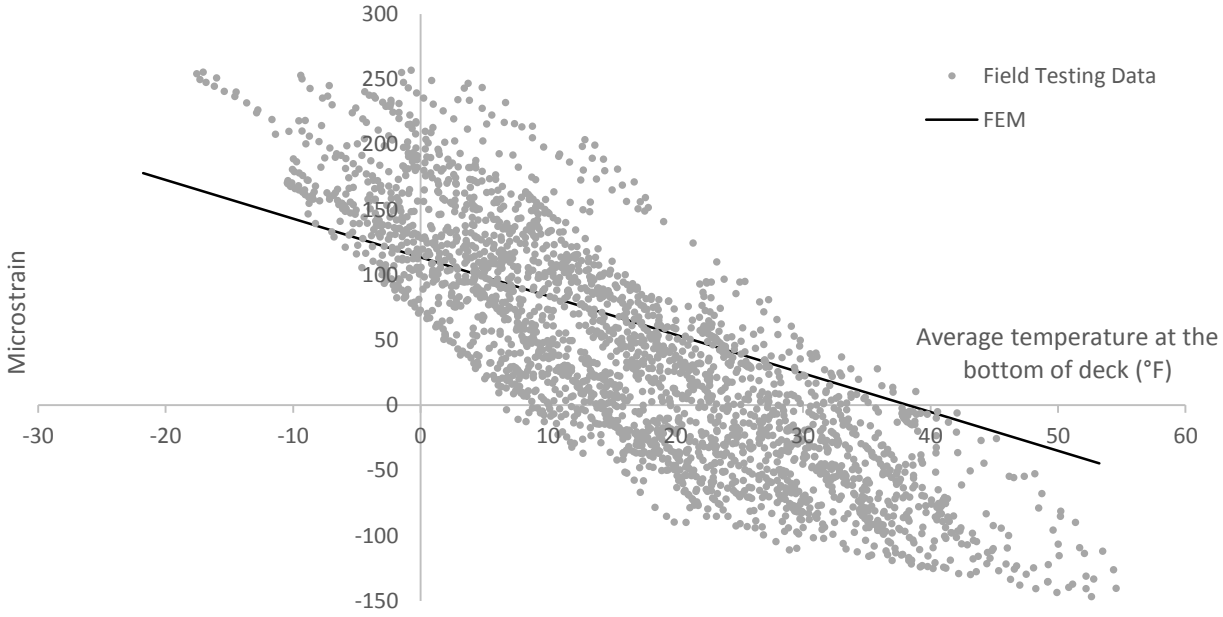

Figure 73. Results comparison for the gauge in the sixth bay near the abutment

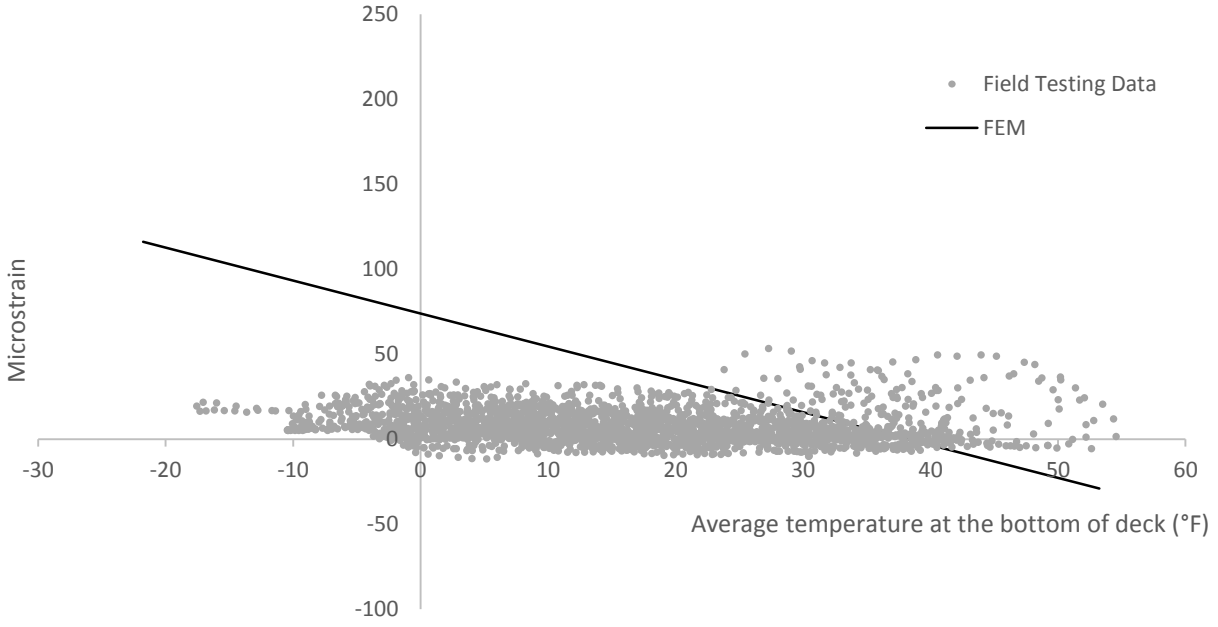

Figure 74. Results comparison for the gauge in the first bay in the middle span

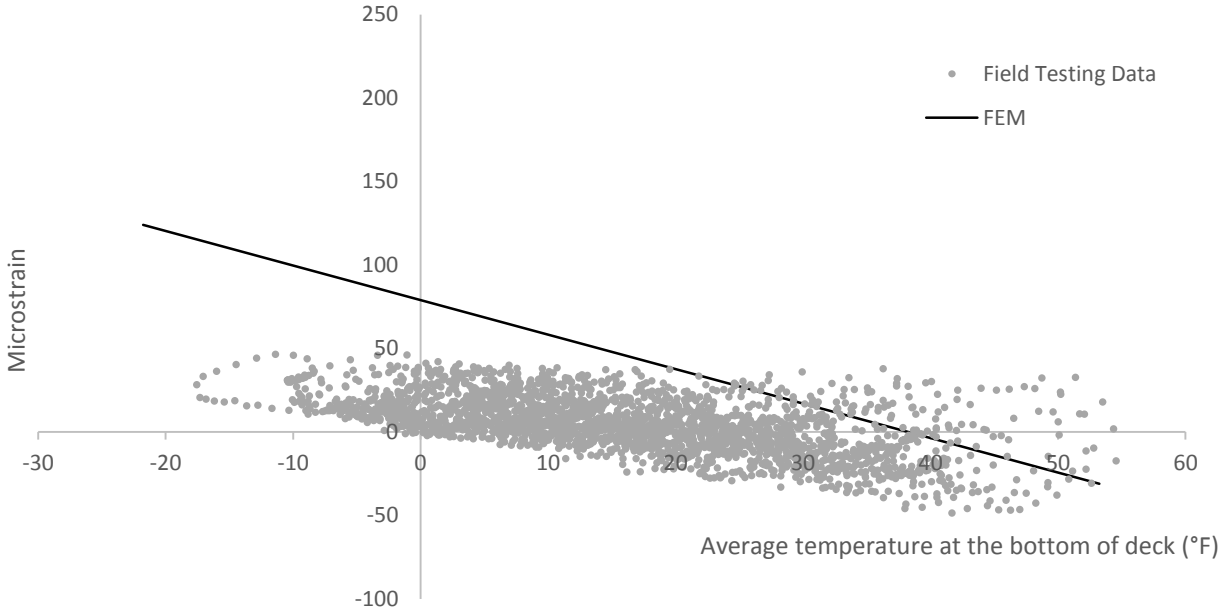

Figure 75. Results comparison for the gauge in the third bay in the middle span

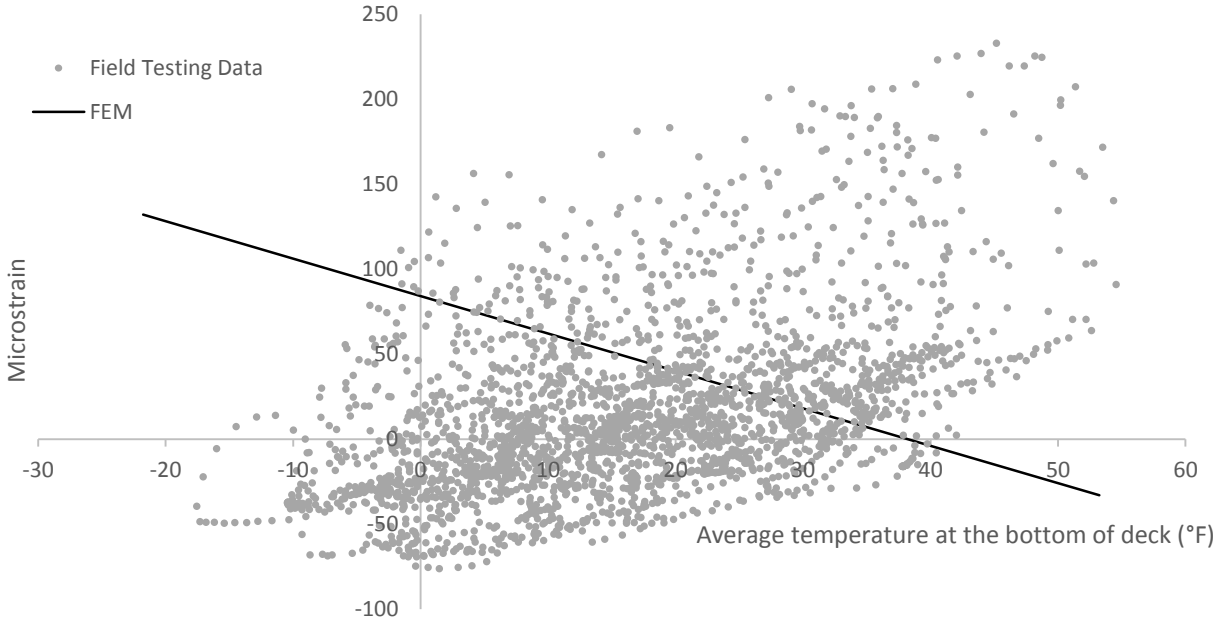

Figure 76. Results comparison for the gauge in the fifth bay in the middle span

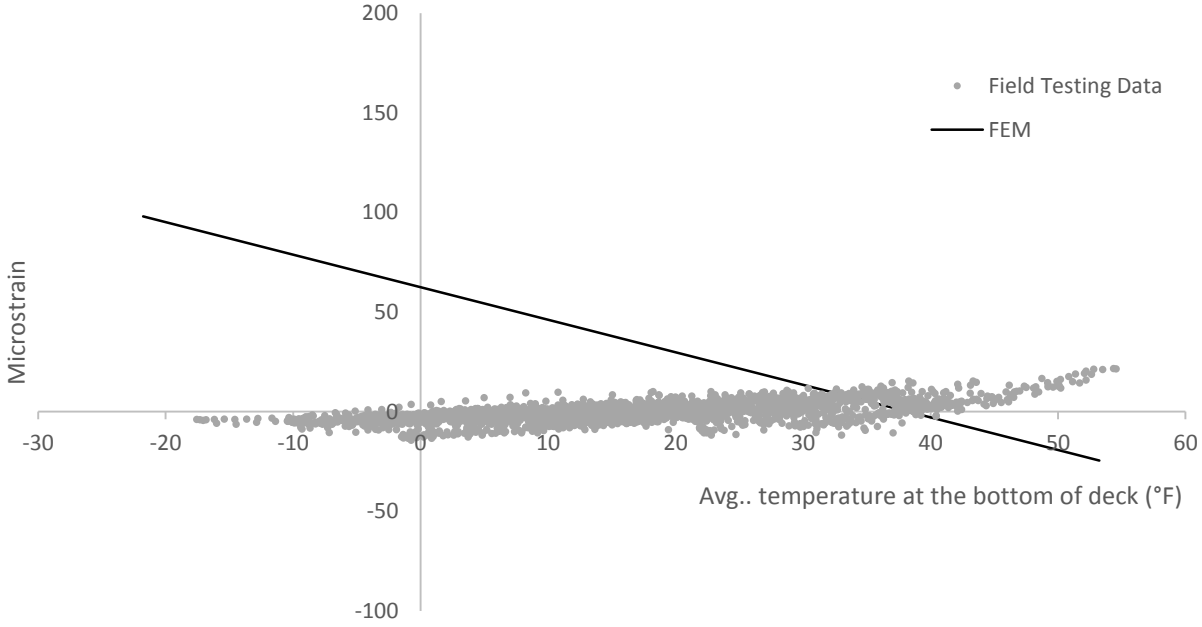

Figure 77. Results comparison for the gauge in the first bay near the pier

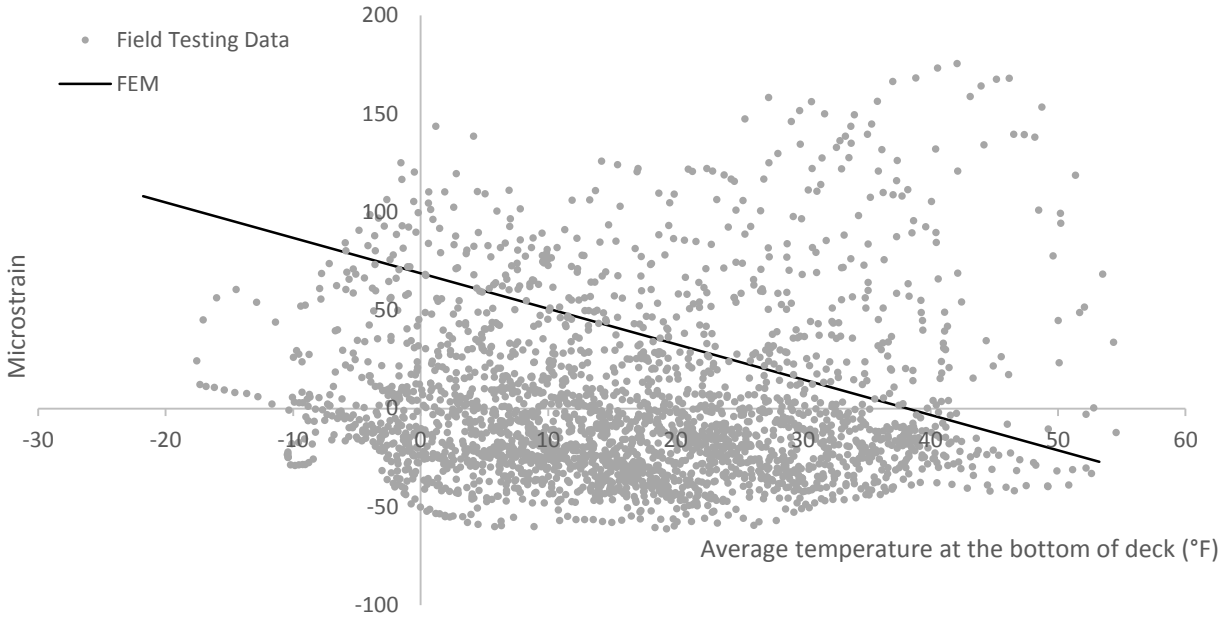

Figure 78. Results comparison for the gauge in the third bay near the pier

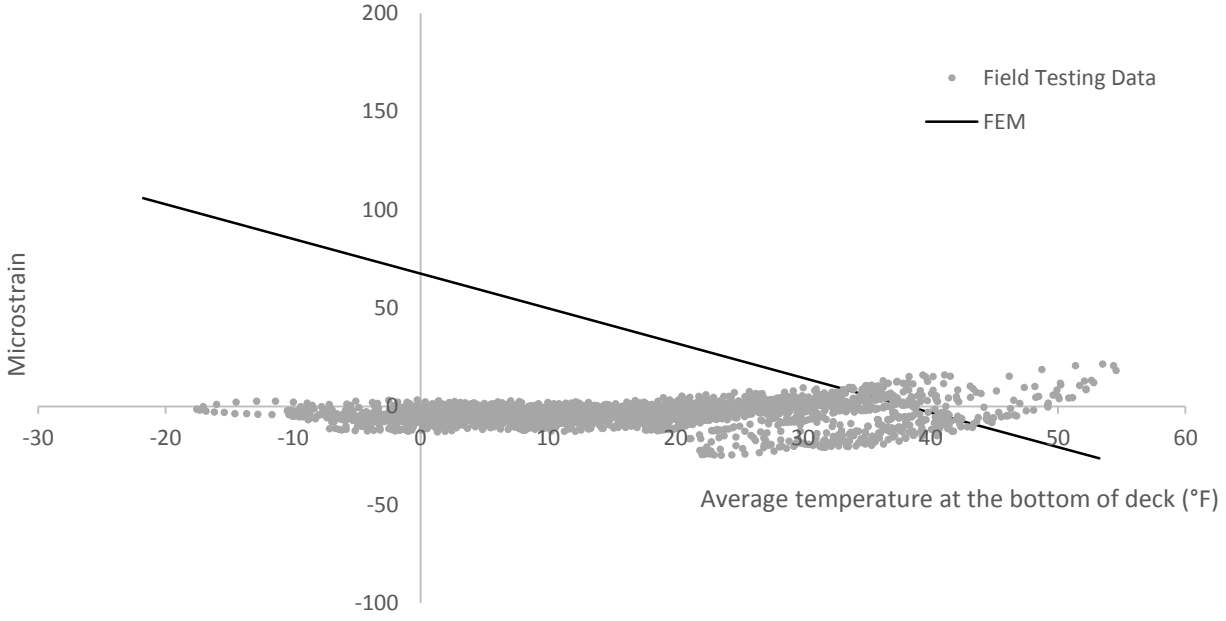

Figure 79. Results comparison for the gauge in the fifth bay near the pier

For convenience in plotting, the initial temperature for the FEM was set to 38° F, the same as the initial temperature of the field testing. The black lines in Figure 68 through Figure 79 therefore represent the change from the condition at 38° F.

For the abutment section, the results from field testing reasonably match the results from the FEM, except in the third, fifth, and sixth bays. As described in Section 4.2, the strain gauges in the third and fifth bays were installed close to the edge of a crack, which altered the strain pattern by reducing the strain readings. In the sixth bay, the strain gauge was placed near the end of a crack, and it is likely that high strain values due to stress concentration were measured. The comparison of displacement results between the FEM and the field testing is shown in Figure 80 through Figure 82.

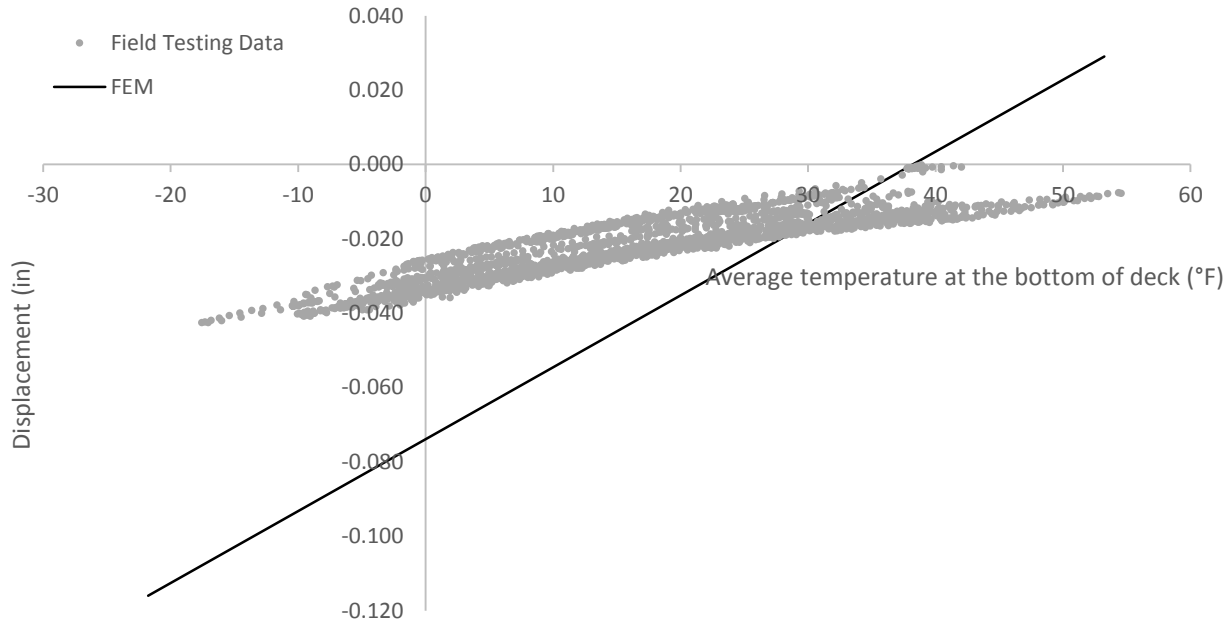

Figure 80. Results comparison for DS-2

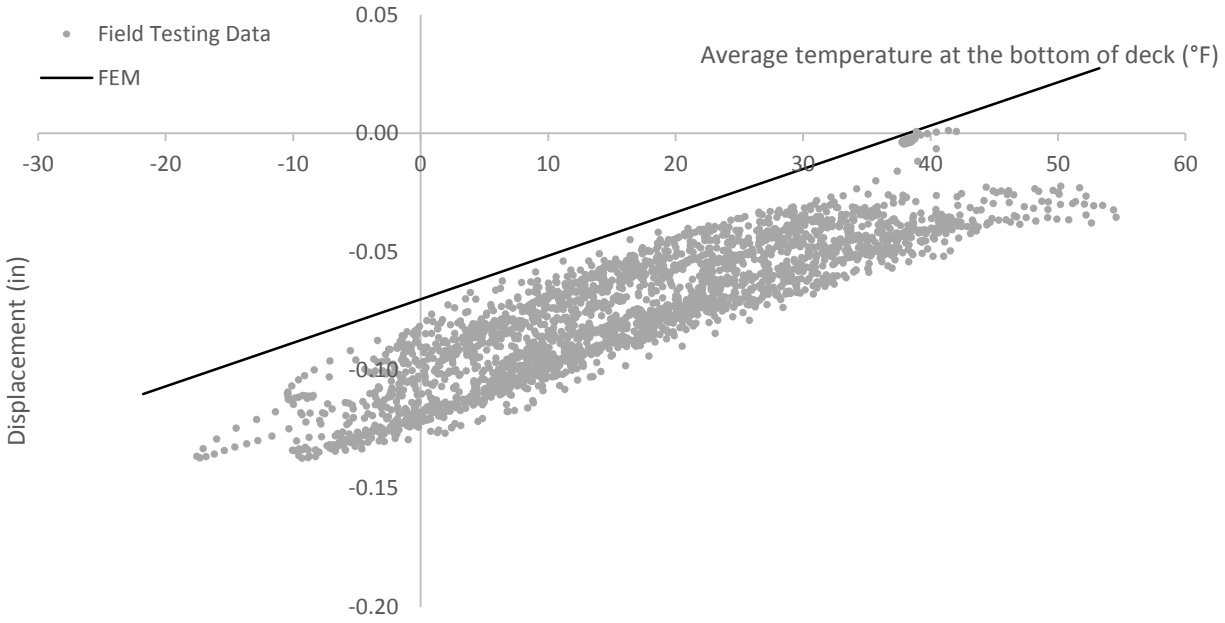

Figure 81. Results comparison for DS-3

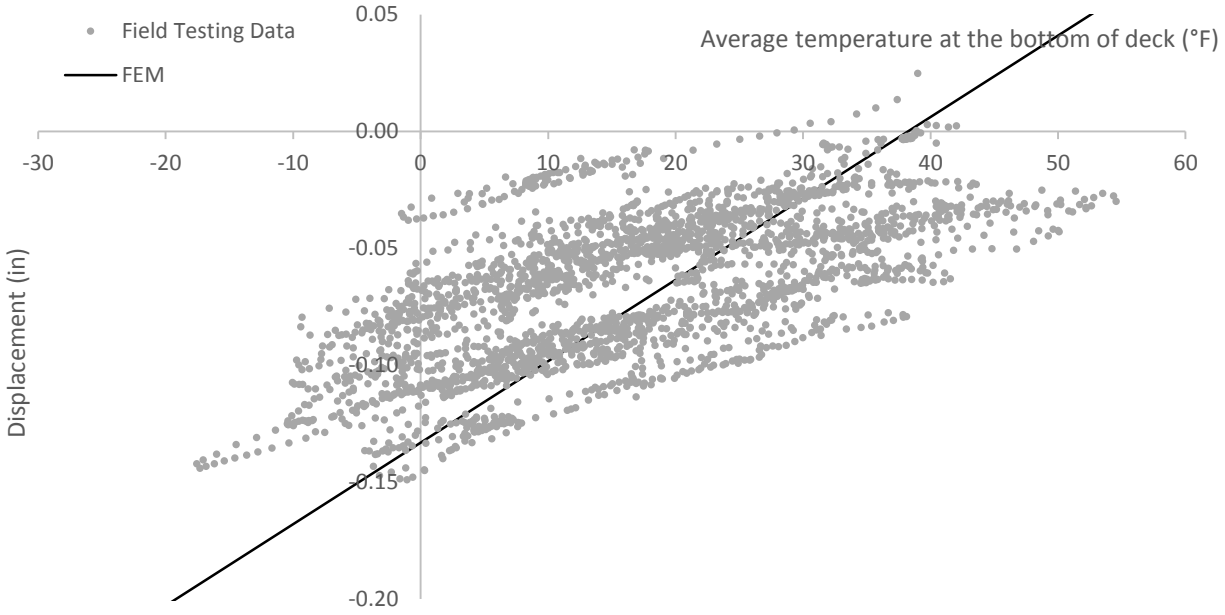

Figure 82. Results comparison for DS-4

DS-2 measured the longitudinal displacement on the east side of the bridge. The FEM results are between the field testing results and 0.08 in. calculated using a conventional $\alpha \times \Delta T \times L$ calculation.

DS-3 measured the displacement in the transverse direction near the abutment. Because both the FEM and field testing results have very similar slopes, no further calibration related to this behavior was required.

DS-4 measured the displacement in the transverse direction near the pier. The FEM overestimates the rate of change of displacement in the transverse direction near the pier, which could be explained by two reasons:

1. An idealized support condition was used to replace the pier column. A further FEM study altering the support condition at the bottom of the pier cap, from a vertical roller to a pin support, revealed that the pier boundary condition is not the reason.

2. The assumed temperature changes at the pier diaphragm were regarded as the main reason that the FEM overestimated the displacement change near the pier. Because the support conditions at the pier have little effect on the behavior of the deck near the abutment, only the vertical support boundary condition was used.

5.5.3 Validation for Crack Pattern

5.5.3.1 Annual Temperature Loading

An annual temperature change was used in the FEM to study the crack pattern that might result. The annual temperature change was calculated as the difference between a very cold day temperature and an assumed construction day. Within this methodology, a uniform temperature of 80°F was used as the construction temperature.

Based on the historical temperature records for Iowa, the minimum temperature was -47° F in 1996. The lowest temperature in the Waterloo region was -35° F in 2009. A minimum temperature of -40° F, between both extreme temperatures, was selected as the cold day air temperature and also as the deck temperature. The temperature at the front side of the abutment was calculated based on the 2/3 relationship between the abutment temperature changes and the deck bottom temperature changes. (See Section 4.2 for more detailed information.)

The temperature at the soil side of the abutment was unknown. Fortunately, temperature records at the soil side of an abutment were available in the research report *Field Monitoring of Curved Girder Bridges with Integral Abutments* (Greimann et al. 2014). These records indicated that the temperature at the top of the steel piles remains about 35° F for the entire year.

The temperatures at different parts of the bridge on the cold day are shown in Figure 83. The temperature changes from the construction temperatures are shown in Figure 84.

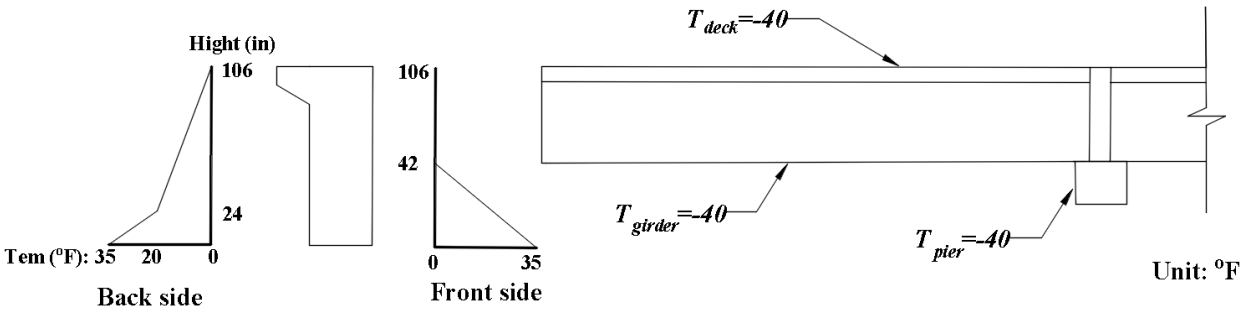

Figure 83. Assumed temperatures for the cold day calibration of crack pattern

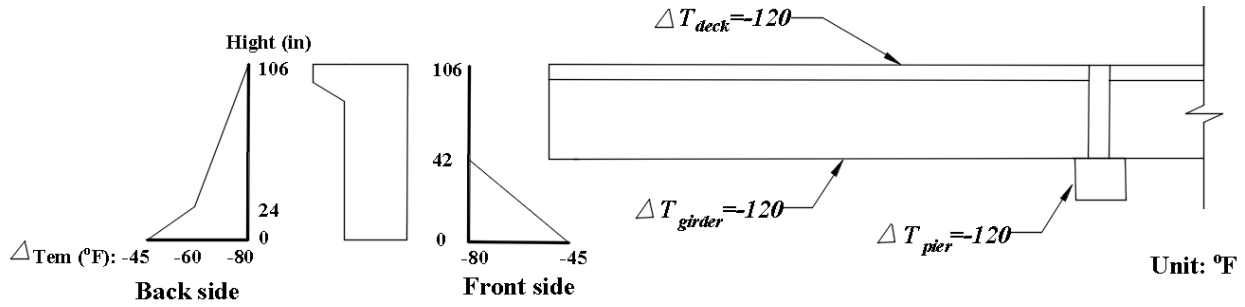

Figure 84. Temperature changes used for calibration of crack pattern

5.5.3.2 Validation

The first principal strain distributions and directions on the top surface of the bridge deck from the FEM were compared to the observed crack pattern (see Figure 7 and Figure 8). Based on the bridge inspection results, most of the cracks on the top surface of the deck were found to start above a girder, with a higher density of cracks at the corner of the bridge. The first principal strain direction is expected to be perpendicular to the crack direction. As shown in Figure 85, the maximum strain at the bridge corner is 129~146 microstrain, which is higher than the estimated crack strain of 132 microstrain calculated by $7.5\sqrt{f_c'}/57000\sqrt{f_c'}$. The arrows in Figure 85 indicate the strain directions in the region. The FEM matched the expectation for the first principal strain direction.

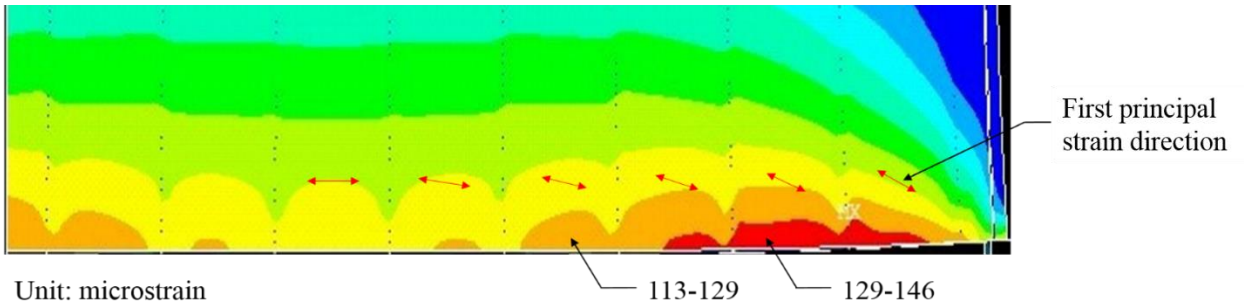

Figure 85. First principal strain contour on the top surface of the deck (calibration for crack pattern)

5.5.4 Validation for Shrinkage

5.5.4.1 Shrinkage Loading

Shrinkage strain was calculated using the relationship given by the AASHTO (2004) specification and shown in Equation (4).

$$(\varepsilon_{sh})_t = -k_s k_h \left(\frac{t}{35+t}\right) 0.51 \times 10^{-3} \quad (4)$$

where,
$(\varepsilon_{sh})_t$ = Free strain due to shrinkage at time *t*,
t = Drying time,
k_s = Size factor related to volume-to-area ratio (k_s= 0.54 for the abutment and pier diaphragm; k_s= 0.71 for the deck)
k_h = Humidity factor (humidity was selected as 30% in this research, or k_h=1.57)

To simulate the maximum shrinkage strain, an infinite number of drying days (*t*) was assumed for each bridge component, as shown in Figure 86.

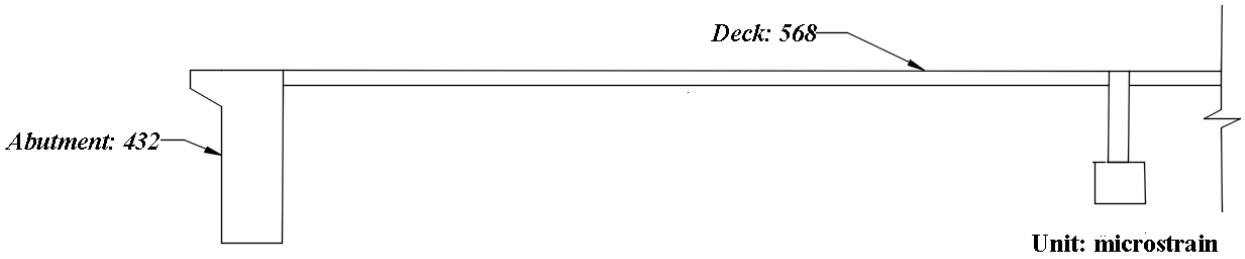

Figure 86. Shrinkage strain on each component of the bridge

Shrinkage loading was applied in the FEM by an "equivalent temperature method," by which a temperature change resulted in the same strain change as the shrinkage strain. This method has been verified and used by Strainge and Burgueno (2012) to simulate shrinkage loading on a

bridge to study cracking. Free shrinkage strain was applied to the bridge through temperature loading, with the equivalent temperature calculated by Equation (5).

$$\Delta T = -\frac{(\varepsilon_{sh})_t}{\alpha} \quad (5)$$

Because the girders were pre-stressed concrete and the majority of the shrinkage had occurred before they were shipped to the field, the girder shrinkage strain was taken as zero.

5.5.4.2 Validation

Crack maps (see Figure 7 and Figure 8 in Chapter 3) were used to compare the first principal strain distribution and direction predicted by the FEM under shrinkage loading (Figure 87). The arrows in Figure 87 represent the first principal strain vector in the region.

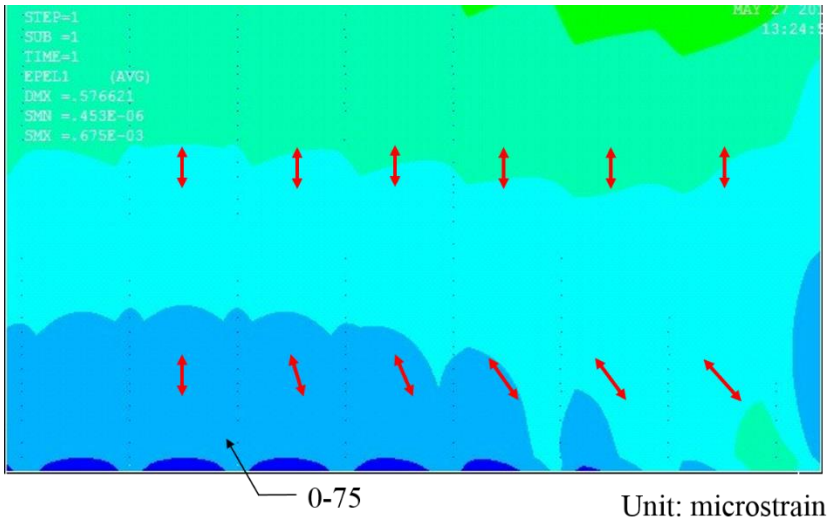

Figure 87. First principal strain contour plot with strain vector under shrinkage loading

The strain vectors at the corner of the bridge deck are normal to the diagonal cracks, which indicates that the shrinkage loading may contribute to the diagonal cracks at the deck corner. However, based on the strain contour plot, transverse shrinkage cracks are expected to occur away from the abutment. At the middle of the deck near the abutment, transverse cracks would dominate. This phenomenon does not correspond to the bridge inspection results. Hence, the shrinkage was not considered to be a primary loading for the deck end cracks and was not used during the parametric study.

CHAPTER 6. PARAMATRIC STUDY ON FULL BRIDGE MODEL

6.1 Introduction

In this chapter, a parametric study performed to investigate the effect of bridge width on the tensile strain in the deck is described. This work also includes a detailed study of the factors that may impact the level of tensile strain in the deck, such as bridge skew, bridge width, abutment type, pier type, girder type, girder spacing, and number of spans. The annual temperature change (see Section 5.5.3 for additional details) was used as the primary loading for this parametric study.

6.2 Bridge Width and Skew

In this section, the impact of two geometric features on deck strain are described. In total, six different bridge models were developed to study the influence of bridge skew and bridge deck width.

6.2.1 Bridge Width Influence on Integral Abutment Bridge with Zero Skew

6.2.1.1 Strain in the Deck

Figure 88 shows the first principal strain magnitude and direction on the top surface of the deck for the zero skew condition for three variable bridge widths.

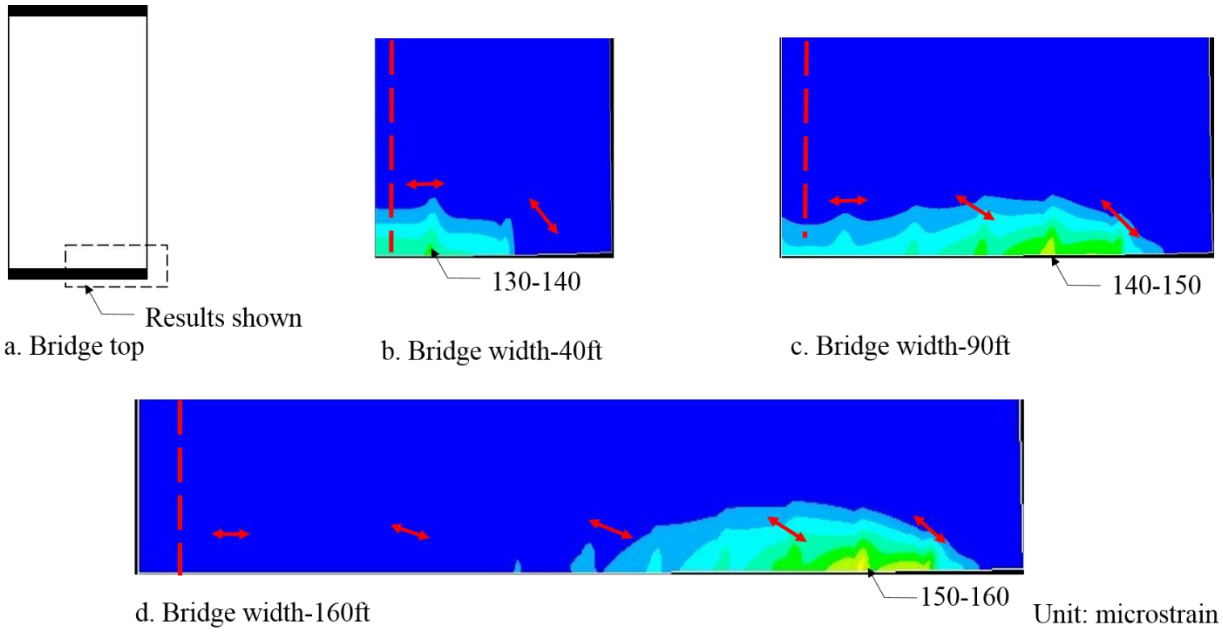

Figure 88. First principal strain on the top surface of the deck

Similarly, Figure 89 shows the first principal strain magnitude and direction on the bottom surface of the deck.

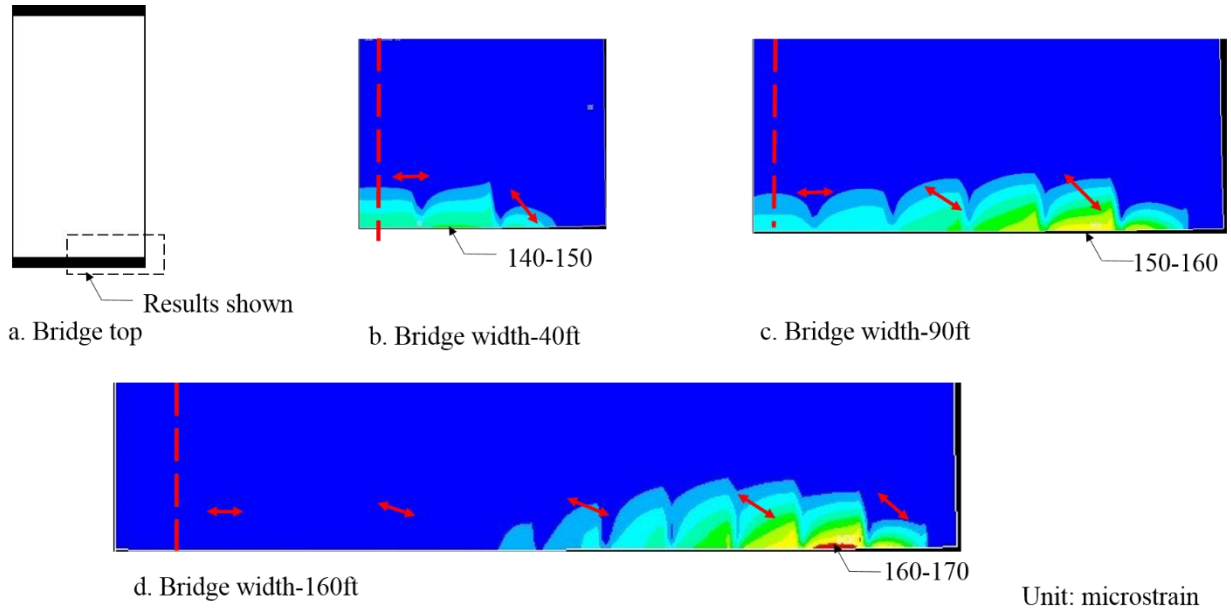

Figure 89. First principal strain on the bottom surface of the deck

Regardless of bridge width, the highest stress on both the top surface and the bottom surface of the deck occurred near the abutment, and the highest stress concentration point was always 10–20 ft from the side of the bridge.

The maximum principal strain in the deck increases by 20 to 30 microstrain when the bridge width increases from 40 ft to 160 ft The tensile strain from all three models exceeds the estimated cracking strain of the concrete.

6.2.1.2 Strain in Other Bridge Components

Besides the strain in the bridge deck, the strain in other bridge components, such as the abutment and girders, were also examined. Figure 90 and Figure 91 show the strain distributions on the soil and front sides of the abutment, respectively.

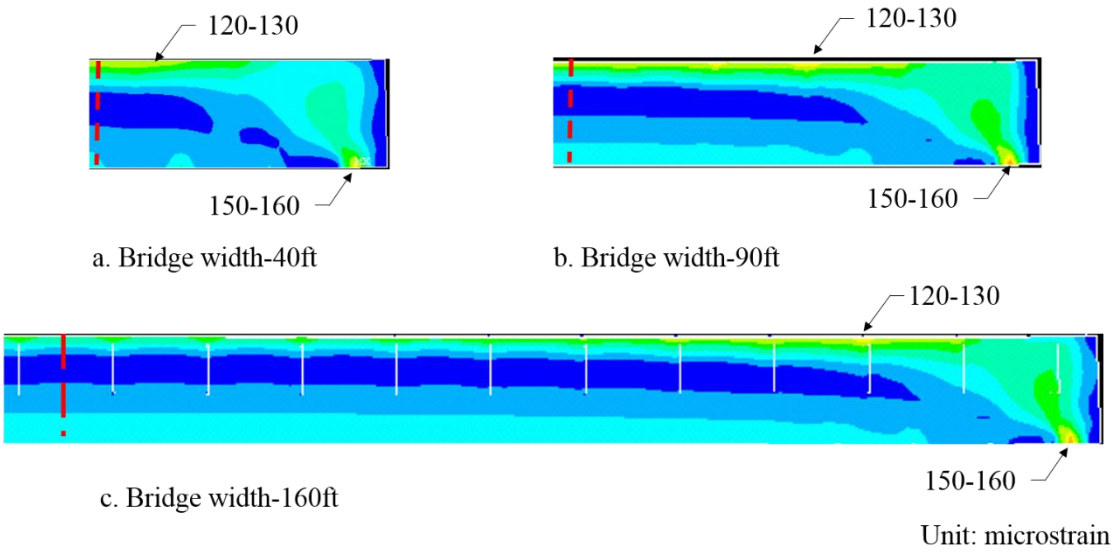

Figure 90. First principal strain distribution on the soil side of the abutment

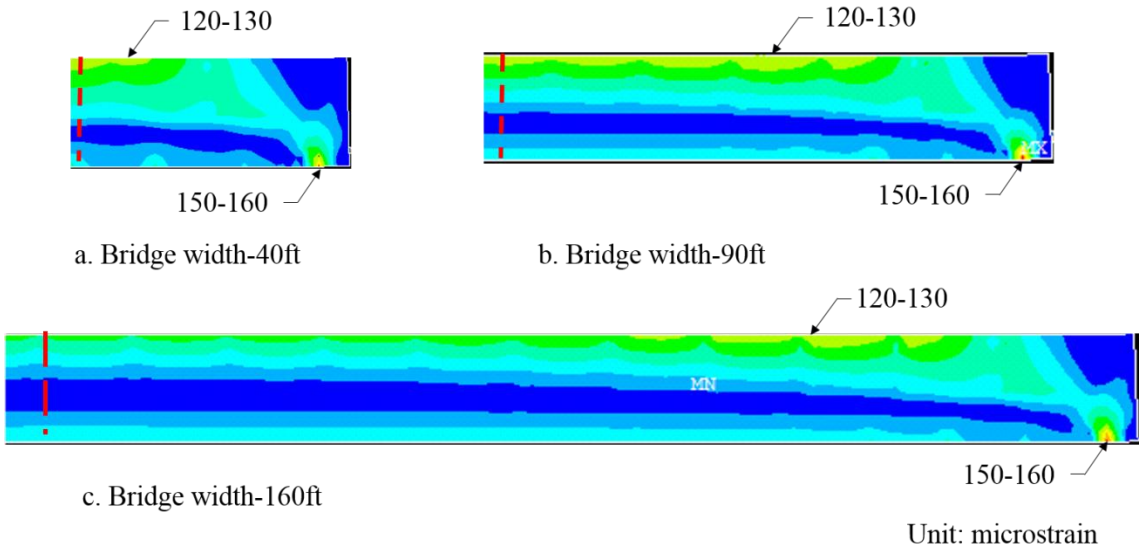

Figure 91. First principal strain distribution on the front side of the abutment

On both sides of the abutment, high strain concentrations occur at the bottom corners of the abutments in all three bridge models. These strain concentrations were not regarded as a significant issue affecting the strain distribution in the deck, because the idealized support conditions at the piles are believed to be the source. The next highest strain on the abutment occurred at the top of the abutment near the deck, with the same strain magnitudes. There is no significant relationship between the strain magnitude in the abutment and bridge width.

6.2.2 Bridge Width Influence on Integral Abutment Bridge with 45 Degree Skew

Figure 92 shows the strain distribution on a 40 ft width bridge model that has a 45 degree skew.

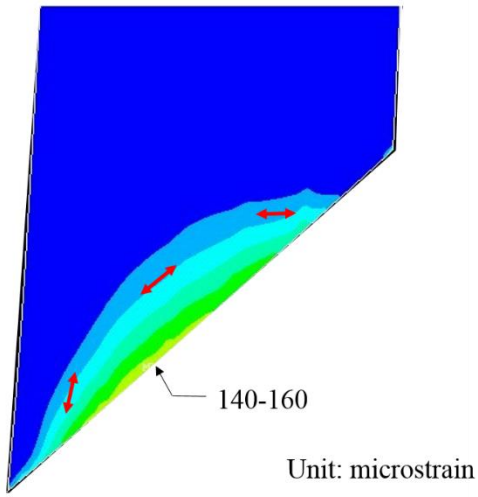

Figure 92. First principal strain distribution on a 40 ft bridge with a 45 degree skew

As in previous figures, the arrows represent the tensile strain direction. Because the bridge, which is the primary focus of this study, had essentially zero skew, the crack map of Bridge #49661 shown in Figure 93 was used to provide some validation that the skewed bridge model was realistic.

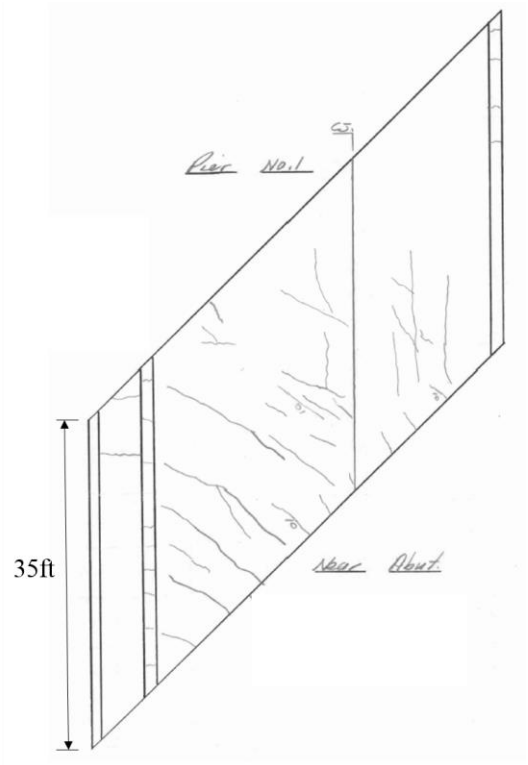

Figure 93. Crack map of Bridge #49661

Bridge #49661 was specifically selected because it is 40 ft wide with a 45 degree skew. There is a good correlation between the direction of maximum tensile strain and the orientation of cracking.

Figure 94 shows three first principal strain contour plots for the 45 degree skewed bridges with different bridge widths.

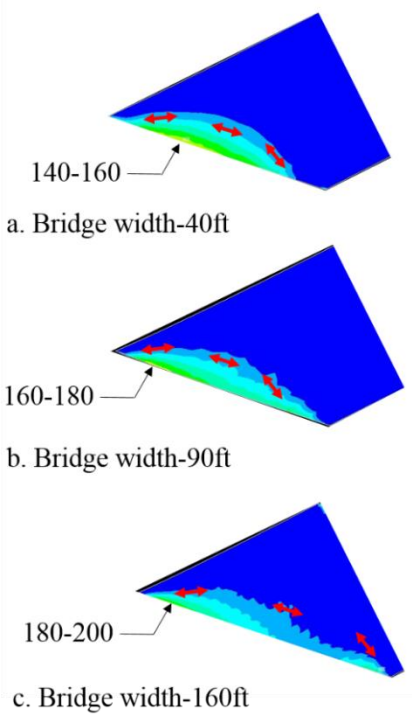

Figure 94. First principal strain contour plots of three skew models

Regardless of the bridge width, the maximum tensile strain is concentrated at the acute angle corners. The maximum strain increases from 156 to 193 microstrain as the bridge width increases from 40 ft to 160 ft.

6.2.3 Summary

Table 6 summarizes the maximum strain on the deck's top surface for the skew and non-skew models. There does seem to be a relationship between peak thermally induced strain and both bridge width and skew.

Table 6. Maximum tensile strain on non-skew and skew bridge models

Bridge Width	Non-Skew	Skew-45º
40 ft	140~150	140~160
90 ft	150~160	160~180
160 ft	160~170	180~200

6.3 Abutment Type

To study the influence the abutment type has on the strain in the bridge deck, two non-skew bridge models with 90 ft widths were modeled and compared. One bridge model had integral abutments, while the other had stub abutments. Figure 95 compares the deck strain distributions.

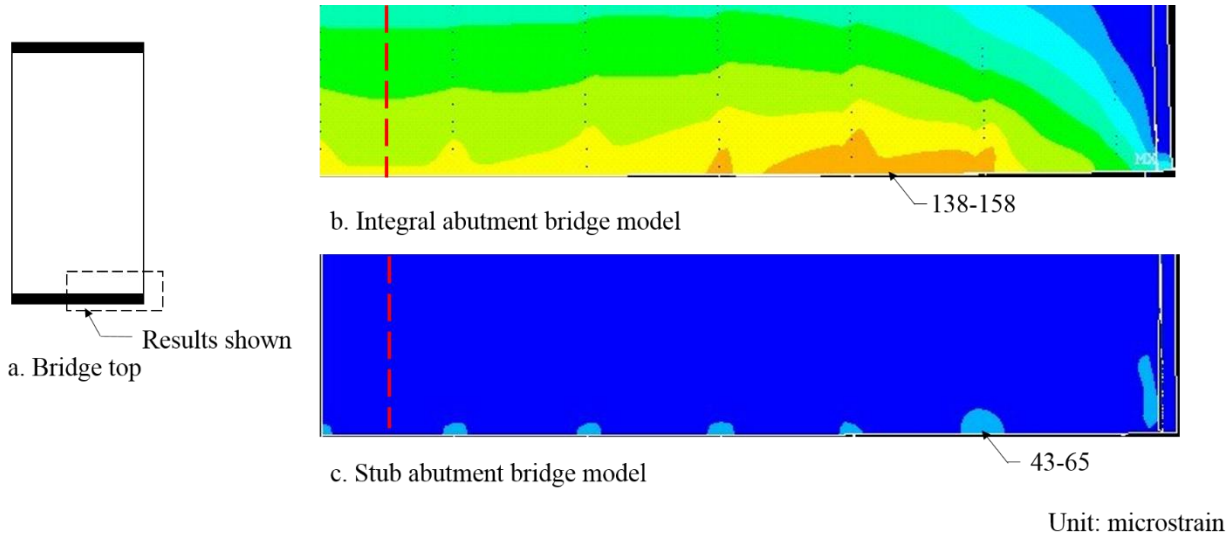

Figure 95. First principal strain contour plots of an integral abutment bridge model and a stub abutment bridge model

The maximum tensile strain in the deck of the integral abutment bridge model was 130~148 microstrain, while on the stub abutment bridge model the maximum tensile strain in the deck was 43~65 microstrain. Clearly from this result, one might expect fewer cracks associated with the stub abutment. The topic is further addressed later.

6.4 Pier Type

The influence of two different pier types on strain was studied: fixed pier and expansion pier. Based on details commonly utilized by the Iowa DOT, the major behavioral difference between these types of pier is that the expansion pier releases the translations in transverse and longitudinal directions between the girder and pier cap, while in the fixed pier the girder and pier cap move together transversely and longitudinally.

Figure 96 shows the first principal strain contour plots on the top surface of the deck for the expansion pier bridge model and the fixed pier bridge model.

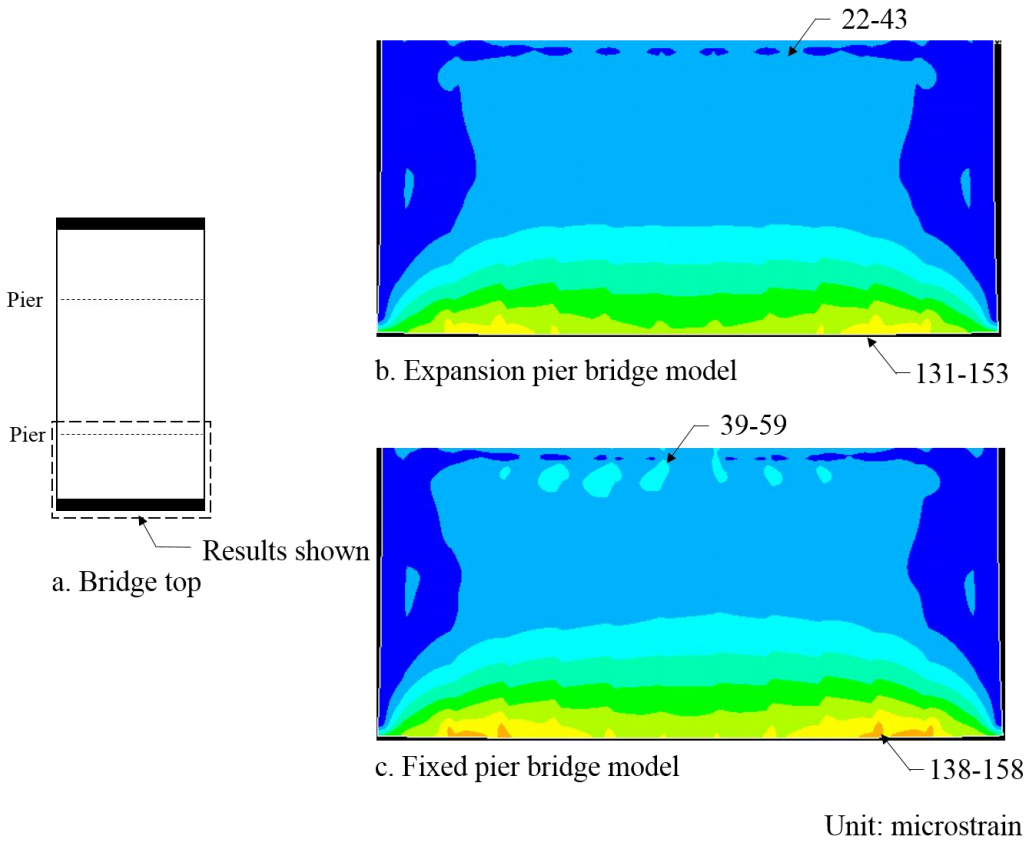

Figure 96. First principal strain contour plots of an expansion pier bridge model and a fixed pier bridge model

Pier type has no significant influence on the strain in the deck near the abutment.

6.5 Span

To study the influence of the number of spans on strain, a one-span bridge model and a three-span bridge model were developed and compared. Figure 97 presents the first principal strain contour plots for the one-span model and for the first span of the three-span bridge model.

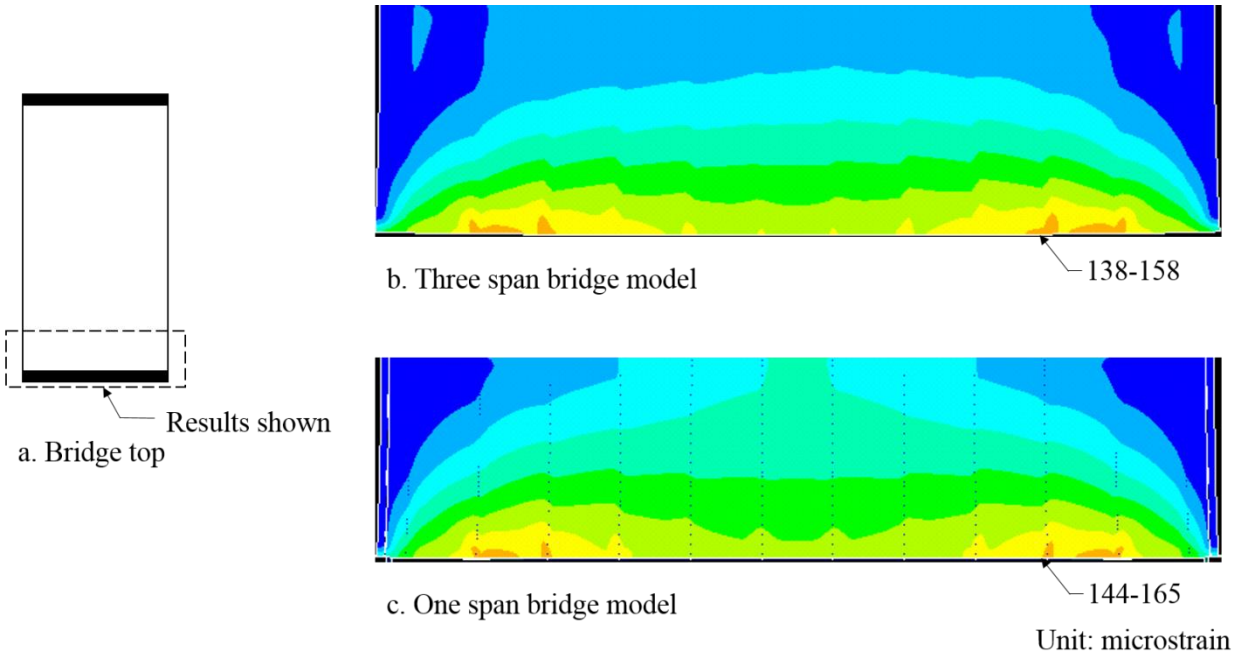

Figure 97. First principal strain contour plots of the deck of a one-span bridge model and a three-span bridge model

As shown in Figure 97, the one-span bridge model has a somewhat higher deck strain than the three-span bridge model. However, the strain difference is insignificant.

6.6 Girder Type

With help from the Iowa DOT, an equivalent steel girder design (shown in Figure 98) was established such that the concrete girder on Bridge #605220 could be replaced with a structurally equivalent steel beam.

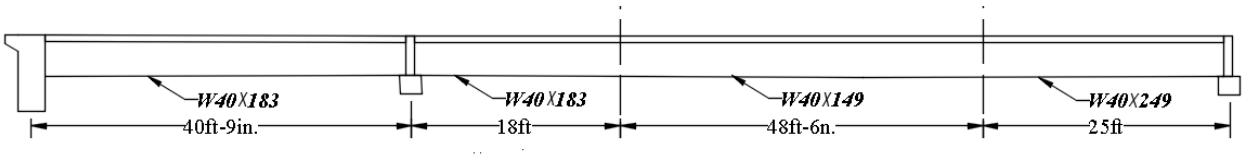

Figure 98. Equivalent steel girder design

Figure 99 compares the first principal strain distributions on the deck of the steel girder bridge model and concrete girder bridge model.

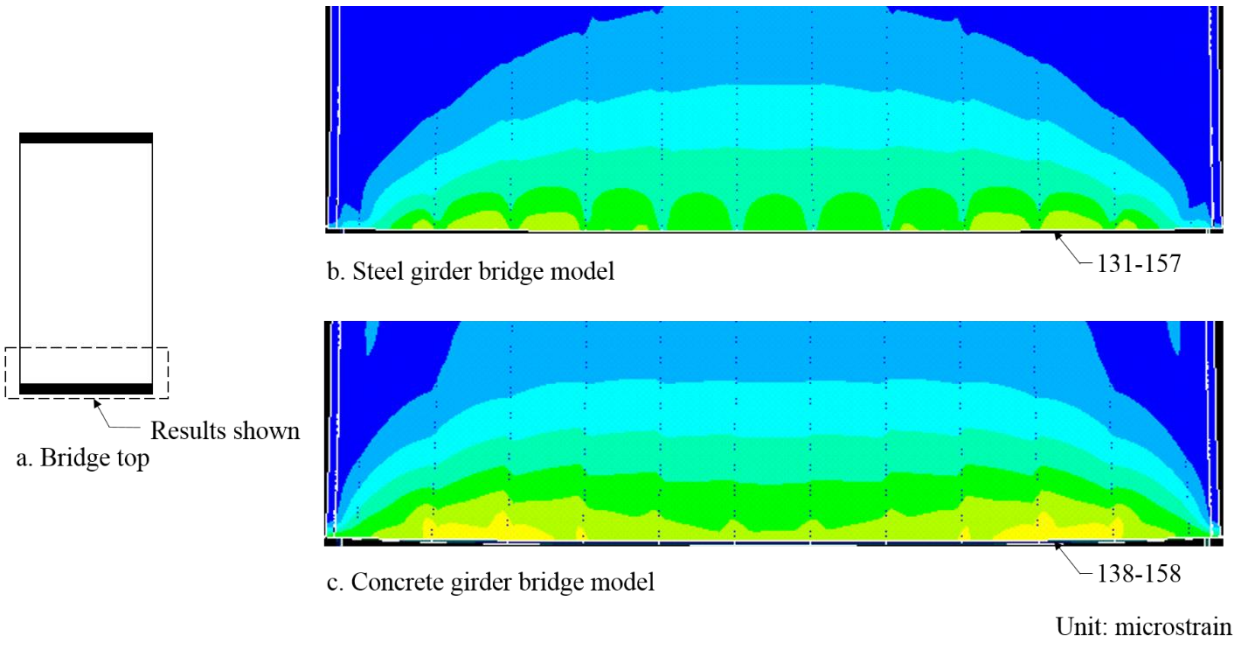

Figure 99. First principal strain contour plots of the deck of a steel girder bridge model and a concrete girder bridge model

There is virtually no difference between the two models.

6.7 Girder Spacing

Two different girder spacings were analytically studied to evaluate the influence of girder spacing on deck strain. One girder spacing was the original girder spacing of 88.375 in., and the other girder spacing (176.75 in.) was twice that. No other changes were made to account for the increased girder spacing (e.g., required girder size). Figure 100 shows the first principal strain contour plots for both the one-girder-spacing model and the double-girder-spacing model.

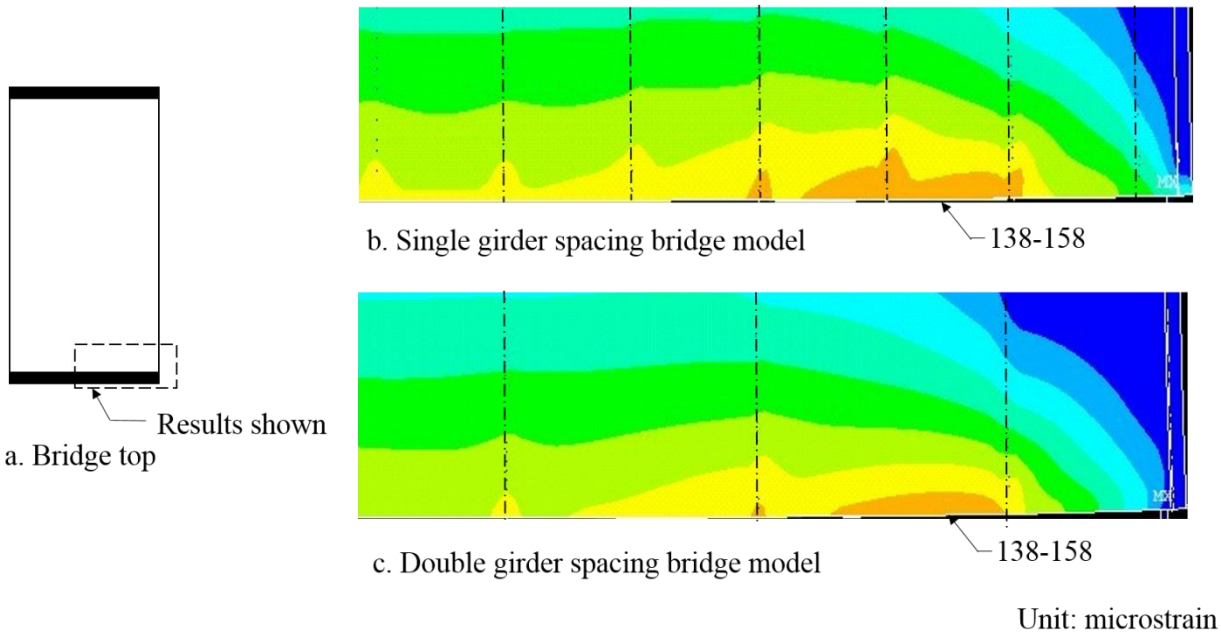

Figure 100. First principal strain contour plots of the deck of a one-girder-spacing bridge model and a double-girder-spacing bridge model

For both models, the maximum tensile strain on the top surface of the deck was around 140 microstrain. No significant difference in strain between the two bridge models was observed.

CHAPTER 7. RESULTS, VALIDATIONS, AND POTENTIAL SOLUTIONS

A search of deck crack conditions for in-place bridges was conducted to validate the parametric study results. Three potential solutions that may reduce the tensile strain in the deck were also preliminarily investigated. Both of these activities are described in this chapter.

7.1 Deck Cracking of In-Place Bridges

7.1.1 Search on 40 Bridges with Single Type of Abutment

To further validate the parametric study results in Section 6.2, a search of bridge inspection reports from the Iowa DOT Structure Inventory and Inspection Management System (SIIMS) was conducted. The bridge search resulted in 40 case study bridges in Iowa: 20 integral abutment bridges and 20 stub abutment bridges. For each type of bridge, 10 narrow bridges (around 40 ft) and 10 wide bridges (around 80 ft) were selected. For each bridge width, five skewed bridges and five non-skewed bridges were selected. However, only three wide stub abutment bridges with high skew were found. Relevant bridge inspection parameters are shown in Table 7 and Table 8.

Table 7. Bridge inspection results for integral abutment bridges

No.	FHWA No.	Deck Width (ft)	Skew	Rating	Comments
1	14281	40	0	3	
2	606905	40	0	3	3-6 longitudinal cracks
3	606685	40	0	2	7-10 longitudinal and diagonal cracks
4	16331	40	0	5	No cracks
5	19421	40	0	1	Extensive longitudinal and diagonal cracks
6	32581	40	45	4	1-3 longitudinal and diagonal cracks
7	43241	40	45	3	2-4 longitudinal and diagonal cracks
8	49661	40	45	1	Extensive longitudinal and diagonal cracks
9	609575	40	45	4	1-3 longitudinal and diagonal cracks
10	609565	40	45	5	No cracks
11	20841	75	1	1	Extensive longitudinal and diagonal cracks
12	47051	68	0	2	4-8 longitudinal and diagonal cracks
13	42391	86	0	5	No cracks
14	605220	87.2	2	1	Extensive longitudinal and diagonal cracks
15	609165	71	10	3	5-10 longitudinal and diagonal cracks
16	607530	83	45	3	3-5 diagonal cracks
17	609160	83	45	3	1-6 diagonal cracks with leaching
18	700060	113	35	3	3-5 diagonal cracks
19	504510	92.5	20	4	2-3 diagonal cracks
20	607635	73	27	2	7-10 longitudinal and diagonal cracks

Table 8. Bridge inspection results for stub abutment bridges

No.	FHWA No.	Deck Width (ft)	Skew	Rating	Comments
1	601235	40	0	5	No crack
2	48231	40	0	5	No crack map included report was found
3	21841	40	0	4	1 longitudinal crack
4	605830	40	0	4	1-2 longitudinal cracks
5	211161	40	0	5	No crack
6	30121	40	45	4	1-2 diagonal cracks
7	30091	40	45	5	No crack
8	51311	40	45	3	3-4 cracks at obtuse angle corner
9	51301	40	45	5	No crack
10	607730	40	47	4	2-3 longitudinal cracks
11	044691	82	0	5	No cracks
12	041141	70	0	5	No cracks
13	044691	82	0	5	No cracks
14	043131	60.25	0	5	No cracks
15	700145	54	0	5	No longitudinal or diagonal cracks
16	032021	66	45	4	1-3 diagonal cracks
17	609260	59	58	5	No cracks
18	042061	68	23.5	5	No cracks
19	032100	66	15	4	1 longitudinal crack
20	604440	72	25	5	No cracks

Crack maps from some of the bridge inspection reports were used to qualitatively evaluate deck cracking. The deck top crack condition related to longitudinal and diagonal cracks near the abutment were rated on a scale from 1 to 5 as follows:

1 – Large areas with extensive cracks
2 – Small areas with extensive cracks
3 – Three to seven cracks
4 – One to three cracks
5 – No cracks

For all the bridges, there was no observed significant relationship between bridge width and deck cracking and no apparent relationship between bridge skew and deck cracking. Comparison of the bridge abutment types indicated that seven of the 20 integral abutment bridges have a rating lower than 3, while all 20 bridges with stub abutments have a rating higher than 3. Nineteen of

the 20 stub abutment bridges rate above 3 and 13 have no cracks, while only nine of 20 integral abutment bridges are above 3 and three show no cracks.

These results appear to match the FEM results in Section 6.2. The results are also consistent with the literature review results in Chapter 2. This search provides additional information pointing to the fact that the predominant factor influencing deck strain and, therefore, deck cracking is the type of abutment. Integral abutments result in greater deck strain because of the restraint afforded by the structural details and the temperature difference between the deck/superstructure and substructure.

7.1.2 Deck Crack Condition on a Bridge with Two Different Abutment Types

While conducting the search of bridges with different abutment types, the research team located a bridge with both an integral and a stub abutment. Bridge #608585, located northwest of Mount Pleasant, Iowa, is a 220 ft long three-span bridge with a 36 degree skew. The traffic on the bridge is in the east-west direction. The east abutment is an integral abutment, and the west abutment is a stub abutment. Figure 101 shows the deck top crack condition near the abutments.

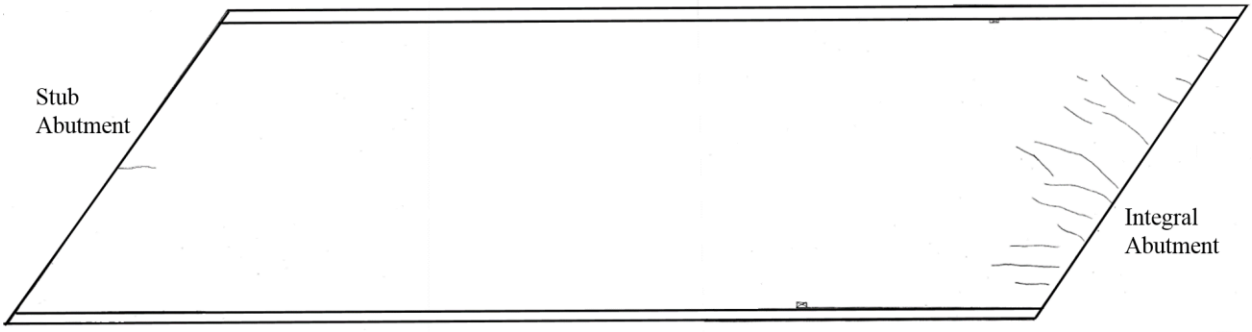

Figure 101. Deck top crack map of Bridge #608585

On the integral abutment side, more cracks were visually observed than at the other end of the bridge. This matches the parametric study results in Section 6.3, indicating that high strain in the deck occurs with integral abutments.

7.2 Potential Solutions to Reduce Longitudinal Cracks

After the parametric study, a preliminary study of various means of reducing strain (cracking) in the deck was conducted utilizing the bridge FEM.

7.2.1 Isolation of Abutment from Soil

Because the large strain in the deck near the abutment is due to a combination of abutment restraint and the temperature difference between the abutment and the deck, the conceptual

temperature isolation pad shown in Figure 102 might prevent heat transfer from the soil to the abutment.

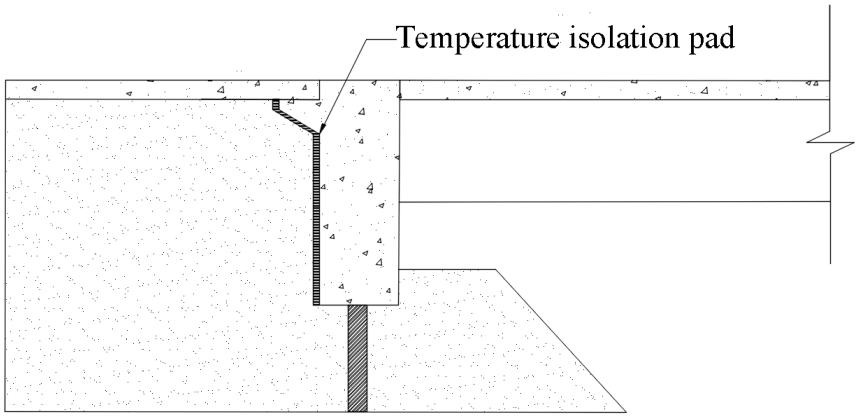

Figure 102. Temperature isolation pad configuration and position

If the temperature isolation pad is fully functional, the temperatures in the abutment and the deck will be similar. In this case, the whole bridge will be under the same temperature change. To study this, an extreme uniform temperature change (-113° F) from summer to winter was applied in the FEM.

Figure 103 shows the first principal strain distribution on the top surface of the deck.

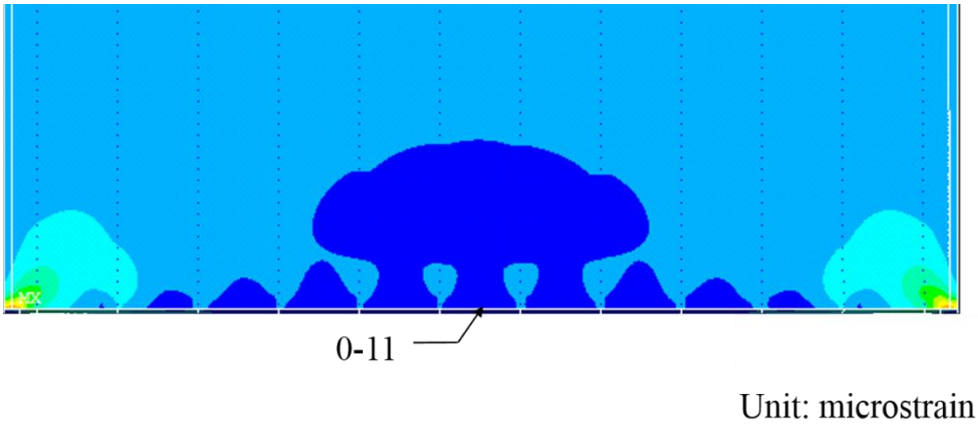

Figure 103. First principal strain distribution plot on a deck due to a uniform temperature change of -113°F

As the plot shows, the strain in the deck near the abutment remote from the stress concentration point is greatly reduced from 150 microstrain (shown in Figure 88) to 10 microstrain (shown in Figure 103). The strain concentration at the corner of the deck is not considered significant because for this preliminary study no temperature isolation pad was placed at the wing wall.

7.2.2 Vertical Expansion Joints on Abutment

To release the high strain in the deck, the addition of vertical expansion joints in the abutment was theoretically considered. In the analytical model, two expansion joints with three different spacings were considered. To accomplish this, the nodes at the expansion joint locations were separated to simulate the expansion joint. The top node at the expansion joint was connected to the deck (shown in Figure 104).

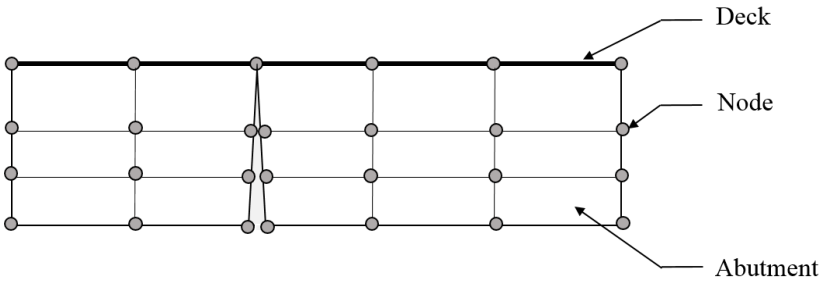

Figure 104. Separation of the abutment in the FEM

Three different arrangements were studied, with the distance between the expansion joints being 24 ft, 39 ft, and 53 ft (shown in Figure 105 through Figure 107).

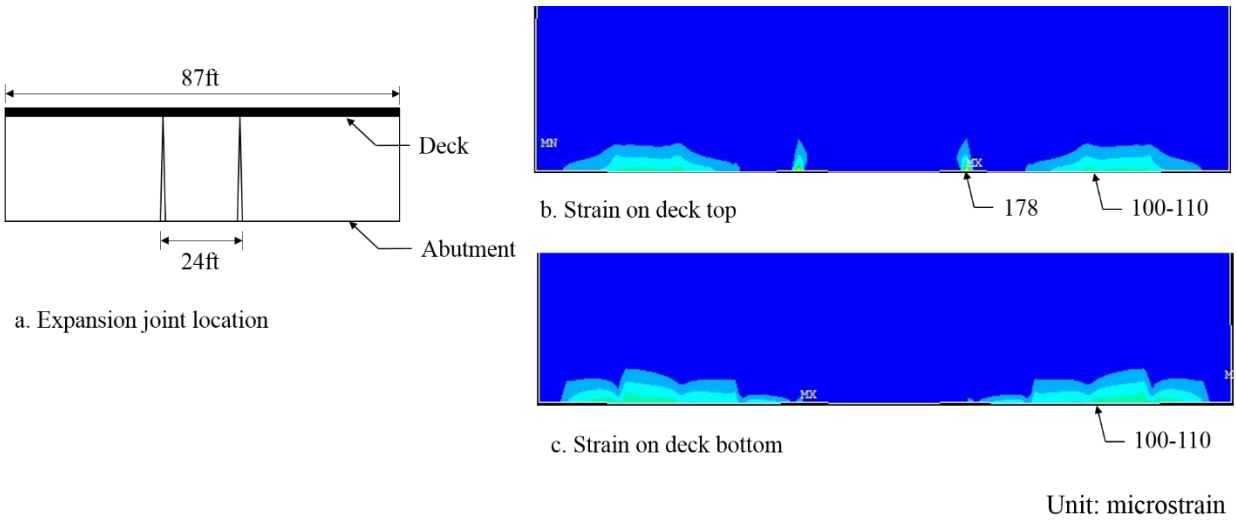

Figure 105. First principal strain plots for the model with 24 ft expansion joint spacing

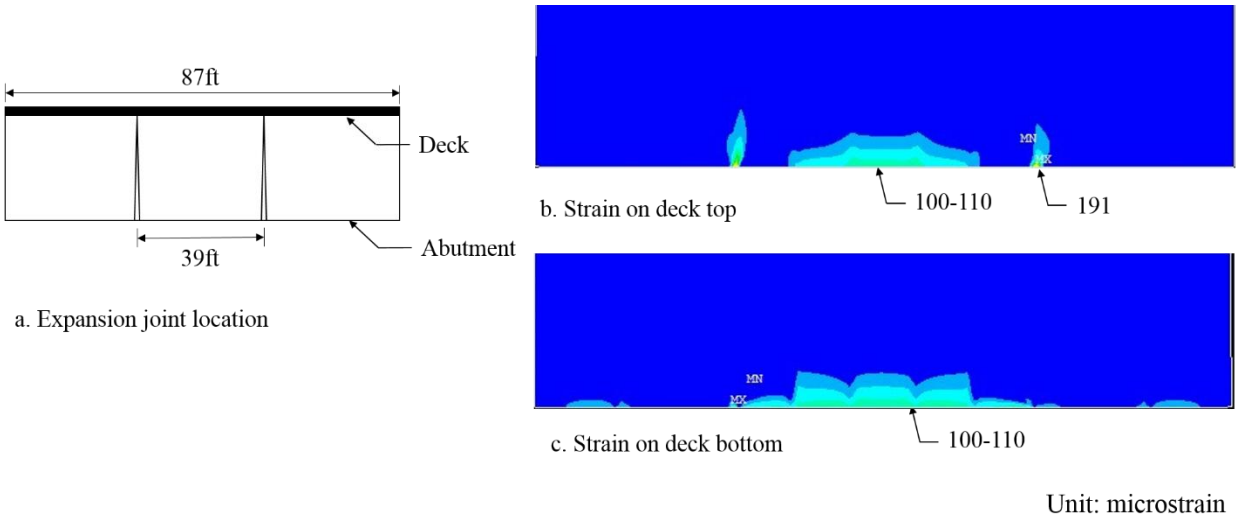

Figure 106. First principal strain plots for the model with 39 ft expansion joint spacing

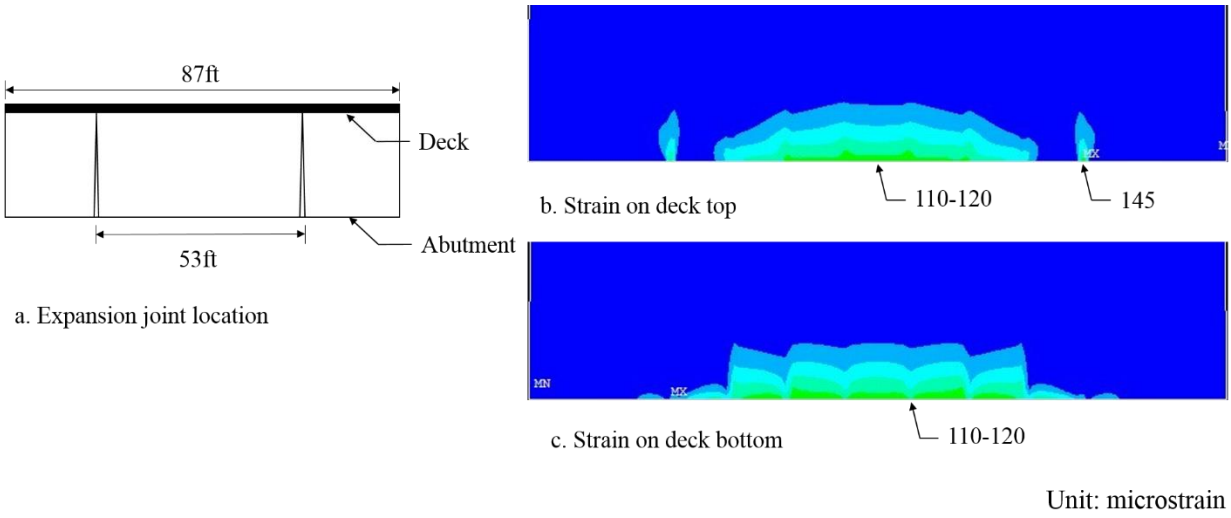

Figure 107 First principal strain plots for the model width 53 ft expansion joint spacing

Figure 105 to Figure 107 show the first principal strain contour plots on the top and bottom surfaces of the deck resulting from the conceptual case of a bridge with an expansion joint in the abutment. On the top surface of the deck, stress concentrations were observed at the top of the expansion joint caused by the connection between the vertical expansion joint and the deck at the top node. Beyond these stress concentrations, the strain was lower than the strain in the model without the expansion joint. By comparing the first principal strain contour plots from the three different models, it is evident that placement of the expansion joints affects the locations of the maximum strains in the deck. More study would be required to determine how to actually implement such a solution.

7.2.3 Increasing the Amount of Temperature and Shrinkage Steel in the Deck

Gilbert (1992) indicated that the shrinkage and temperature reinforcement required for a fully restrained slab could be double that required by ACI 318. The author showed that the Australian specification (1988) requires two to three times more shrinkage and temperature reinforcement than the minimum required by ACI 318 (Gilbert 1992). Hence, further increasing the temperature steel in the deck may be a solution to reducing those cracks.

According to the AASHTO (2004) specification, the area of temperature reinforcement per foot required for this concrete bridge deck is 0.142 in.^{2}/ft (0.135 percent). The reinforcement percentage for this bridge deck specified by the ACI specification is 0.2 percent. The Australian specification gives a minimum steel reinforcement percentage of 0.945 percent, and Gilbert (1992) suggests using at least 0.284 in.^{2}/ft (0.27 percent) for a fully restrained slab.

Figure 108 and Figure 109 show the transverse and longitudinal reinforcement steel arrangement in the deck provided by the Iowa DOT.

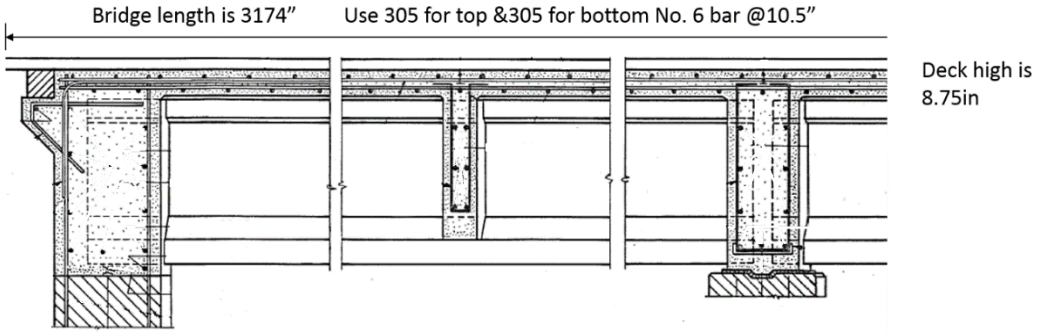

Figure 108. Transverse reinforcement steel arrangement in the deck

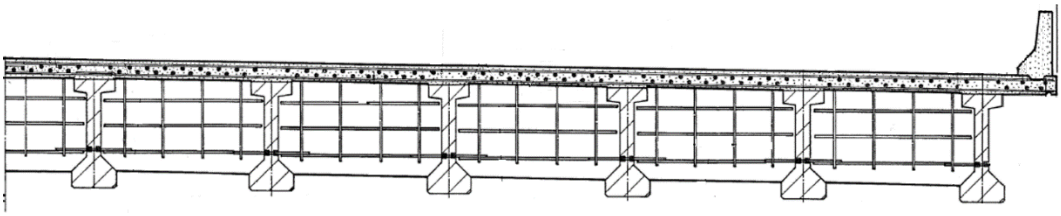

Figure 109. Longitudinal reinforcement steel arrangement in the deck

The reinforcement percentage for the transverse steel is one percent (1.01 in.^{2}/ft). In the longitudinal direction, the reinforcement steel percentage is 0.8 percent (0.81 in.^{2}/ft).

Comparing the reinforcement ratio with the minimum recommendations from ACI 318, AASHTO (2004), the Australian specification (1988), and Gilbert (1992), it appears that Bridge #620550 has a sufficient steel temperature in both the transverse and longitudinal directions. Hence, further increasing the amount of steel was not studied.

CHAPTER 8. CONCLUSIONS AND RECOMMENDATIONS

8.1 Summary

8.1.1 Summary of Field Testing

Field testing, which included both short-term live-load and long-term testing, was conducted on Bridge #605220, which is located near Waterloo, Iowa, to provide general behavior information and data for the calibration of an analytical model that would be the focal point of much of the research. The bridge was selected based upon an examination of detailed bridge inspection results for five candidate bridges and other factors (including traffic, location, etc.). Bridge #605220 is a 264.5 ft long four-span bridge with a 1.5 degree skew. The bridge consists of an integral abutment and 12 pre-stressed concrete girders.

8.1.1.1 Live-Load Testing

In total, 60 BDI strain transducers were installed on Bridge #605220 during live-load testing. Twenty-four transducers were placed near the south abutment and south pier, and twelve transducers were placed at the mid-span of the second span. At each instrumented location, one transducer was attached to the side of the top flange, and a second transducer was attached to the bottom surface of the bottom flange.

During live-load testing, a three-axle Iowa DOT snooper truck was driven across the bridge at a crawl speed (approximately 3 mph) to induce a pseudo-static load on the bridge. In total, five load cases with different transverse vehicle positions were utilized to obtain the needed strain data. The live-load testing demonstrated that the bridge effectively acted in a symmetric manner. Only those gauges on the three to four girders nearest the truck path had significant readings, which were then used for the calibration of the FEM.

8.1.1.2 Long-Term Testing

Long-term testing focused on studying the behavior of the bridge deck near the abutment during temperature changes, because previous bridge inspection results and the technical literature indicated that most longitudinal and diagonal cracks occurred in that region. The long-term monitoring plan provided strain, displacement, and temperature data for further calibration and validation of the FEM.

Vibrating wire strain gauges were used to measure the load-induced strain at the bottom of the deck resulting from restrained temperature changes at three cross-sections. Four vibrating wire long-range displacement meters were used to measure the relative longitudinal and transverse displacement due to thermal changes in the first span of the bridge. Two were installed in the exterior bays to measure the relative longitudinal displacement in the first span. The other two displacement meters were used to measure the relative displacement in the transverse direction.

The temperature at the bottom of the deck was measured by the thermistors housed within each vibrating wire strain gauge. The temperature at the mid-depth of the deck and within the abutment were also measured.

The long-term testing results showed that the temperature at the bottom of the deck is generally very uniform and that changes that occur at the mid-depth of the deck are the same as those at the bottom of the deck. The front abutment average temperature change was about 2/3 of the temperature change on the bottom of the deck.

8.1.2 Summary of Bridge Model Development

8.1.2.1 Bridge Model Development

The bridge FEM included discrete idealizations of the deck, girder, diaphragm, abutment, and pier cap. Piles under the abutment and pier columns were idealized by assuming proper support conditions. Beam 4 elements were used to model the girder flanges, pier cap, and steel diaphragm; Shell 181 elements were used to model the deck, concrete diaphragm, abutment, and girder web. The deck reinforcing steel was smeared into the concrete and represented by effective material properties.

8.1.2.2 Calibration for Live-load Behavior

Comparisons of the girder strains initially indicated that the FEM predicted higher strain values than the field testing results. The Young's Modulus of the girders was increased to minimize the percentage difference.

8.1.2.3 Validation for Long-term Behavior

For the FEM thermal loadings, two temperature changes were considered: (1) a temperature difference between the deck and the abutment and (2) a temperature gradient through the thickness of the deck.

The strain comparisons near the abutment showed that the FEM results from those bays without visible cracks are very close to the field testing results, which means that the FEM can be used to simulate deck behavior before cracks occur. Comparison of the strains near the abutment and the transverse displacement supported the conclusion that the FEM is sufficiently accurate to be used in a parametric study.

8.1.2.4 Validation for Crack Pattern

To validate the ability of the model to predict cracking in the deck, an annual bridge temperature change was estimated based on the long-term testing measurements and historical temperature

records. The first principal strain distribution was large enough to crack the concrete, and the orientation matched the cracking observed at the bridge.

8.1.2.5 Validation for Shrinkage

The strain induced by shrinkage was calculated using the relationship given by the AASHTO (2004) specification. The first principal strain distribution and direction did not match with the crack maps from the bridge inspection results, and low strain was observed in the crack near the abutment in the FEM. Hence, shrinkage loading was not considered to be the cause of the observed cracks.

8.1.3 Summary of Parametric Study

A parametric study was performed to investigate the effect of bridge width on deck cracking. Other parameters such as bridge skew, girder spacing, girder type, abutment type, pier type, and the number of bridge spans were also studied.

The bridge width influence study was performed on both a skewed model and a non-skewed model. For both the non-skewed and skewed models, increasing the bridge width increased the maximum strain in the deck by 20–30 microstrain. However, this increase is not significant compared to the magnitude of the deck strain values because even for the narrowest bridge width the maximum strain exceeded the cracking strain. This result was consistent with results of the bridge inspections and literature review.

To study the influence of abutment type on strain, two non-skewed bridge FEMs, an integral abutment bridge model and a stub abutment bridge model, were developed. The maximum tensile strain in the deck of the integral abutment bridge model was two to three times higher than the strain in the stub abutment model. The study of the other factors—pier type, girder type, girder spacing, and number of spans—showed that these factors had little effect on the strain in the deck near the abutment.

8.1.4 Summary of Potential Solutions

To reduce the tensile strain in the deck, three solutions were preliminarily evaluated using the calibrated FEM. Use of a temperature isolation pad was regarded as the most effective solution to reduce the strain in the deck, if such a system could actually prevent heat transfer from the soil to the abutment. Adding an expansion joint within the abutment was also observed to reduce the strain in the deck. However, to put these expansion joints into practice, more consideration would be required. Increasing the amount of reinforcement steel in the deck was also considered as a potential solution, but this was not studied further because the subject bridge has sufficient temperature steel in the longitudinal and transverse directions according to ACI 318, AASHTO (2004), and the Australian specification (1988).

8.2 Conclusions

Based on the results of the literature review, field observations, and the FEM study, the following conclusions can be made:

- Longitudinal and diagonal cracking in the deck on an integral abutment bridge is due to the restraint of the abutment and the temperature differences between the abutment and the deck. Although not likely to induce cracking, shrinkage of the deck concrete may further exacerbate cracks developed from thermal effects.
- Based upon a limited review of bridges in the Iowa DOT inventory and the FEM study, it appears that, regardless of bridge width, longitudinal and diagonal cracks are prevalent in integral abutment bridges but not as prevalent in bridges with stub abutments.
- The FEM parametric study results show that bridge width and skew have minimal effect on the strain in the bridge deck resulting from restrained thermal expansion.
- Pier type, girder type, girder spacing, and number of spans also appear to have no influence on the level of restrained thermal expansion strain in the deck near the abutment.
- Based upon the literature review results and research experience, adding more transverse temperature steel in the deck near the abutment will not likely be effective in reducing the strain in the deck.

8.3 Recommendations

In general, no practical solution to eliminate deck cracking was found during the research. The following items are suggested to reduce deck cracking, though more research work is required before putting some of these into practice:

- If deck cracking is a major concern in certain situations, the use of a stub abutment is recommended.
- To obtain a better understanding of bridge deck behavior, a bridge with both integral and stub abutments is recommended to be monitored for long-term behavior and performance.
- Based upon the FEM results, an effective solution to reduce cracking in the deck might be to place an isolation pad between the soil and back side of the abutment.
- Vertical expansion joints in the abutment do theoretically help to reduce the strain in the deck and control the maximum strain location in the deck. However, implementation presents several problems.

REFERENCES

AASHTO. 1999. *AASHTO LRFD Bridge Design Specifications, 3rd ed.* Washington, DC, 2004.

Burke, Martin, Jr. Cracking of Concrete Decks and Other Problems with Integral-Type Bridges. *Transportation Research Record Transportation Research Record: Journal of the Transportation Research Board*. No. 1688, pp. 131-138.

Frosch, R., D. Blackman, and R., Radabaugh. 2003. *Investigation of Bridge Deck Cracking in Various Bridge Superstructure System.* Federal Highway Administration-Joint Transportation Research Program.

Fu, G., Feng, J., Dimaria, J., and Zhuang, Y. 2007. *Bridge Deck Corner Cracking on Skewed Structures.* Michigan Department of Transportation.

Gilbert, R. I. 1992. Shrinkage Cracking in Fully Restrained Concrete Members. *ACI Structure Journal*. pp. 141-149.

Greimann, Lowell, Brent M. Phares, Yaohua Deng, Gus Shryack, and Jerad Hoffman. 2014. *Field Monitoring of Curved Girder Bridges with Integral Abutments.* Ames,IA: Bridge Engineering Center, Iowa State University.

Illinois DOT. 2012. *Bridge Manual.* Bureau of Bridge and Structures, Division of Highways.

Iowa DOT. 2012. *LRFD Bridge Design Manual.* Ames, Iowa: Iowa DOT Office of Bridge and Structures.

Kunin, J. K., and Alampalli, S. 2000. Integral Abutment Bridges: Current Practice in United States and Canada. *Journal of Performance of Constructed Facilities*. Vol.14, No.3.

MnDOT. 2012. *LRFD Bridge Desiogn Manual.* Minnesota DOT Bridge Office.

—. 2011. *Bridge Deck Cracking Transportation Research Synthesis.* Minnesota Department of Transportation Office of Policy Analysis, Research & Innovation.

Montana DOT. 2002. *Montana Structures Manual.*

Nevada DOT. *NDOT Structures Manual.* 2008.

Paul, M., Laman, A. J., and Linzell, D. G. 2005. Thermally Induced Superstructure Stress in Prestressed Girder Integral Abutment Bridges. *Transportation Research Record: Journal of the Transportation Research Board.* CD 11-S. pp. 287-297.

Purvis, R. 2003. *NCHRP Synthesis 319: Bridge Deck Joint Performance.* Washington, DC: Transportation Research Board.

Russel, H. G., and Gerken, L. J. 1994. Jointless Bridges - the Knowns and the Unknowns. *ACI Concrete International*. 16(4),44-48.

Standards Association of Australia. 1988 *Australian Standard of Concrete Structures (AS 3600-1988).* Sydney, Australia.

Strainge, D. J., and Burgueno, R. 2012. Identification of Causes and Solution Strategies for Deck Cracking in Jointless Bridges. *Final report to Michigan Department of Transportantion, Michigan State University, Lansing, Michigan*.

Washington D.C. DOT. 2009. *Design and Engineering Manual.*